



OLLSCOIL NA GAILLIMHE
UNIVERSITY OF GALWAY

Elucidating the Drivers of Butyric Acid Degradation and Production in Anaerobic Digestion Systems

Xiaoxiao Shi

Civil Engineering, College of Science and Engineering, University of Galway,

Galway, Ireland

Research Supervisor:

Prof. Xinmin Zhan, Civil Engineering, University of Galway

Dr. Yuansheng Hu, Civil Engineering, University College Dublin

A dissertation submitted to the University of Galway in fulfilment of the
requirements for the degree of Doctor of Philosophy.

April 2025

Abstract

Butyric acid is a highly valuable chemical due to its wide range of applications. Its production and recovery from organic waste offers greater economic benefits and reduced environmental impacts, as it is currently mainly derived from fossil fuels. Although the accumulation of butyrate is a recurrent phenomenon in anaerobic digestion, there has been limited research on the optimal conditions for butyrate accumulation and the underlying accumulation mechanisms. This thesis aimed to investigate the factors influencing butyric acid degradation and production, with the goal of identifying the optimal conditions for its accumulation in anaerobic digestion systems. The specific objectives of this PhD research were: 1) to elucidate the effects of ammonia (TAN) concentration and pH on butyrate degradation; 2) to investigate the influence of butyrate concentration and temperature on butyrate degradation and its associated metabolic pathway; 3) to identify the best conditions (pH, temperature, and inoculum to substrate ratio) for maximizing butyric acid yields and to explore the underlying mechanisms governing volatile fatty acid (VFA) distribution under varying conditions.

The results showed that at pH 7.5, butyrate degradation experienced remarkable inhibition when TAN exceeded 8.0 g N/L, while no discernible impacts were observed at pH 7.0–8.0 and 4.0 g TAN/L. Additionally, the lag phase for butyrate degradation extended with increasing TAN concentration. NH_4^+ contributed more to inhibition than NH_3 at TAN concentrations of 2.0–20.0 g N/L. Notably, the activity of butyrate-degrading bacteria was able to be fully recovered from severe ammonia inhibition (TAN of 20 g N/L or NH_3 of 779.2 mg N/L), provided a prolonged adaption time.

Complete butyrate degradation occurred in the range of 2.0 to 20.0 g COD/L, regardless of temperature (37 °C or 55 °C); however, degradation kinetics differed in the two temperature conditions. At 37 °C, iso-butyrate production was observed with butyrate concentrations from 2.0 to 20.0 g COD/L, while it only occurred with 20 g COD/L butyrate at 55 °C. The kinetic analysis of butyrate oxidation showed that the production of iso-butyrate was important for butyrate degradation. Metagenomic analysis revealed that the key enzymes such as enoyl-CoA hydratase (EC 4.2.1.17) and 3-hydroxyacyl-CoA dehydrogenase (EC 1.1.1.35) involved in iso-butyrate metabolism correlated positively with efficient butyrate degradation.

The optimal condition for efficient butyrate accumulation from glucose was pH 5.5, a temperature of 37°C, and an ISR of 1:3. Different experimental conditions significantly shaped the microbial community dynamics. The genera playing significant roles in butyrate production included *Clostridium*, *Caproicibacter*, *Caproicibacterium*, *Sporolactobacillus*, and *Ethanoligenens*. The relative abundance of genes encoding key enzymes involved in reverse β -oxidation significantly increased under optimal conditions, suggesting that the enhancement of butyrate production was driven by carbon chain elongation, using intermediate metabolites like ethanol or lactate as electron donors and acetate as the electron acceptor. These findings demonstrate that chain elongation can be sustained without the need for external electron donors or additional chemicals, effectively promoting both the yield and purity of butyrate.

This PhD research provides deeper insights into the biochemical and microbial mechanisms of butyrate accumulation in anaerobic digestion, and provides practical solutions for enhancing butyrate production from wastes, thereby supporting sustainable resource recovery and advancing biorefinery technologies.

Table of contents

Abstract.....	i
Table of contents.....	iii
List of tables.....	vii
List of figures.....	viii
Declarations	xi
Acknowledgements.....	xii
List of Abbreviations	xiii
List of Equations.....	xv
Chapter 1 Introduction.....	1
1.1 Background	2
1.2 Research aims and objectives	5
1.3 Procedures	6
1.4 Structure of thesis	7
1.5 Research outputs.....	8
Chapter 2 Literature review	10
2.1 Introduction.....	11
2.2 Metabolic pathway of butyric acid production and degradation in anaerobic digestion.....	11
2.2.1 Butyric acid production metabolic pathway	11
2.2.2 Butyric acid degradation metabolic pathway.....	14
2.3 Butyric acid conversion in anaerobic digestion systems	16
2.3.1 Factors influencing butyric acid production.....	16
2.3.2 Butyric acid degradation.....	27

2.4	Summary.....	30
Chapter 3 Ammonia-induced constraints on butyrate degradation in anaerobic digestion: Impact of ammonia levels and pH conditions, and recovery behaviour		
3.1	Introduction.....	32
3.2	Materials and methods	34
3.2.1	Anaerobic inoculum.....	34
3.2.2	Experimental operation.....	34
3.2.3	Model analysis	36
3.2.4	Analytical method	37
3.2.5	Data statistical analysis.....	39
3.3	Results and discussion	39
3.3.1	Anaerobic digestion performance	39
3.3.2	Thermodynamics and kinetics of butyrate degradation	44
3.3.3	Inhibition model.....	47
3.3.4	Recovery after ammonia removal	49
3.4	Conclusions.....	50
Chapter 4 Microbial transitions and degradation pathways driven by butyrate concentration in mesophilic and thermophilic anaerobic digestion under low hydrogen partial pressure		
4.1	Introduction.....	52
4.2	Materials and methods	54
4.2.1	Anaerobic inoculum.....	54
4.2.2	Experimental operation.....	54
4.2.3	Kinetic models	55
4.2.4	Analytical analysis	57

4.2.5	DNA extraction and metagenomic sequencing.....	57
4.2.6	Data analysis.....	58
4.3	Results and discussion	58
4.3.1	Methane production and butyrate degradation.....	58
4.3.2	Kinetics of butyrate degradation and methane production.....	61
4.3.3	Analysis of the microbial community structure.....	63
4.3.4	Metabolic pathways	68
4.4	Conclusions.....	72
Chapter 5 Decoding butyrate fermentation: Parameter optimization and metagenomic insights with glucose as a model substrate.....		
73		
5.1	Introduction.....	74
5.2	Material and Method.....	74
5.2.1	Anaerobic inoculum.....	76
5.2.2	Experiment operation.....	76
5.2.3	Analytical methods.....	77
5.3	Results and discussion	80
5.3.1	Anaerobic digestion performance	80
5.3.2	Microbial community	86
5.3.3	Metabolic pathway.....	92
5.4	Conclusion	101
Chapter 6 Conclusions and Recommendations.....		
102		
6.1	Overview	103
6.2	Main conclusions.....	103
6.2.1	Inhibition of ammonia on butyrate degradation.....	103

6.2.2	Effect of temperature and butyrate concentration on butyrate degradation	103
6.2.3	Optimal conditions for butyrate selective production	104
6.2.4	Summary	104
6.3	Recommendations for future research.....	105
	Bibliography	108

List of tables

Table 1.1 Characteristics and global market of typical VFAs.....	5
Table 2.1 Standard Gibbs energy of main fermentation reaction from glucose.....	12
Table 3.1 Reactions of butyrate and propionate degradation	32
Table 3.2 Experimental conditions for inhibition and recovery experiments	36
Table 3.3 Kinetic parameters of first order and modified Gompertz models.....	47
Table 3.4 Model parameters of simple and modified Monod model	49
Table 4.1 Samples and reactors	58
Table 4.2 Spearman’s correlation between the methane yield and butyrate concentration at different temperatures.....	60
Table 4.3 Kinetic parameters of the butyrate degradation model.....	61
Table 4.4 Correlation between the metabolic pathway and butyrate degradation rate.....	71
Table 5.1 Experimental condition for pH, temperature and ISR experiments	77
Table 5.2 Concentration and efficiency of products from glucose at the end of anaerobic fermentation	83
Table 5.3 Diversity and richness indices of the microbial community of samples under different conditions	87
Table 5.4 Keystone species in Zi-Pi analysis	92
Table 5.5 The names of enzymes in metabolic pathways	96
Table 5.6 Pearson’s correlation analysis between VFAs concentrations and the relative abundance of genes encoding key enzymes involved in metabolic pathways.....	100

List of figures

Figure 1.1 Global primary energy consumption by source based on the substitution method and measure in terawatt – hours (Ritchie et al., 2023)	2
Figure 1.2 Main stages in anaerobic digestion process (Adapted from Wang et al. (2023))	3
Figure 1.3 An overview of the research	7
Figure 2.1 Metabolic pathway for VFAs production	13
Figure 2.2 Biochemical pathways of butyric acid oxidation. The $\Delta G\theta$ and $\Delta G'$ (at 1 Pa hydrogen) of each step is indicated (KJ/mol) (adapted from Stams and Plugge, 2009, Luo et al., 2019)	15
Figure 3.1 Effects of ammonia concentration and pH on anaerobic butyrate degradation and methane production: (a) butyrate degradation, (b) methane production at different TAN concentrations (0.18 – 20.0 g N/L); (c) butyrate degradation, (d) methane production at pH levels (7.0, 7.5 and 8.0)	41
Figure 3.2 VFAs composition change in the entire process at different ammonia concentrations.....	42
Figure 3.3 EPS concentration (a) and ETS activity (b) of substrate with different ammonia concentration. P: protein. C: carbohydrate.....	44
Figure 3.4 Gibbs energy of butyrate oxidation.....	45
Figure 3.5 Butyrate degradation concentration under different ammonia concentration with different models. (a): Gompertz model; (b): modified first-order kinetic model.	46
Figure 3.6 Variation in C_{max} , μ_m and λ at different ammonia concentrations	47
Figure 3.7 $INH_4 + /INH_3$ ratios for butyrate degradation under different ammonia concentrations.....	49
Figure 3.8 Recovery of methane production and butyrate degradation after severe ammonia inhibition	50

Figure 4.1 Simplified reaction scheme of butyrate degradation.....	56
Figure 4.2 Cumulative methane yield (a), butyrate degradation efficiency (b), rate of butyrate degradation and methane production (c), and VFAs evolution (d) in the reactors	59
Figure 4.3 Fitting of the kinetic model of butyrate degradation in different reactors	63
Figure 4.4 Comparisons of genus diversity under different conditions. (a): Shannon index at the genus level; (b) Simpson index at the genus level; (c) PCA (Principal Components Analysis) revealing the similarity of samples by analysing the top 12 most abundant genera in each sample; (d) PCoA (Principal Coordinates Analysis) revealing the separation of microbial communities based on Bray-Curtis distance .	64
Figure 4.5 Comparisons of microbial diversity of different groups. (a) Shannon index; (b) Simpson index	65
Figure 4.6 Composition of microbial communities in different reactors, showing bacterial (a) and archaeal (b) communities and Pearson’s correlation analysis between bacterial genera and reactor performance (c).....	67
Figure 4.7 Schematic diagram of iso-butyrate metabolic pathway	69
Figure 4.8 Analyses of metabolic pathways: (a) schematic diagram of butyrate metabolic pathway, including butyrate oxidation and methanogenesis; (b) names of enzymes involved in the metabolic pathways; (c) relative abundance of enzymes involved in butyrate oxidation; and (d) relative abundance of enzymes involved in methanogenesis present in different reactors	70
Figure 5.1 pH values at the end of the reaction in the ISR experiment.....	78
Figure 5.2 Percentage and concentration of butyrate in all reactors	81
Figure 5.3 Mass balance of VFAs, ethanol, lactate and H ₂ under the following conditions (a) pH range of 4.5 – 7.0 at 37 °C and 55 °C, (b) pH range of 8.5 – 11.0 at 37 °C and 55 °C, (c) various ISRs (1:3, 1:2, 1:1, 2:1, and 3:1) at 37 °C with uncontrolled pH.	86

Figure 5.4 Microbial community structure, (a) top 10 phyla; (b) relationships between phyla and environmental variables; (c) top 30 genus; (d) co-occurrence network analysis of critical genus and reactor performance; (e) co-occurrence network analysis of top 30 genus with the red edges representing the positive associations and the green edges representing the negative associations; (f) identification of keystone species on their topological roles in networks with module hubs being identified as $Z_i \geq 2.5$, $P_i \leq 0.62$, connectors being identified as $Z_i < 2.5$, $P_i \geq 0.62$ and network hubs being identified as $Z_i \geq 2.5$, $P_i \geq 0.62$; (g) Relative abundance of 29 keystones presented in module hubs, connectors and network hubs.91

Figure 5.5 Electron transfer and NADH concentrations under different conditions: (a) ETS activity and the ratio of NADH/ NAD⁺; (b) abundance of functional genes involved in electron transfer (hycB: FeS-containing electron transfer protein; fixC: electron transfer flavoprotein-quinone oxidoreductase; fixB: electron transfer flavoprotein alpha subunit; fixA: electron transfer flavoprotein beta subunit); (c) relative abundance of NADH dehydrogenases94

Figure 5.6 Analyses of metabolic pathways: (a) schematic diagram of the hydrolysis metabolic pathway; (b) schematic diagram of the acidogenesis metabolic pathway, including propionate, butyrate, acetate and ethanol production; (c) relative abundance of enzymes involved in the glycolysis process; and (d) relative abundance of enzymes involved in the acidogenesis process 100

Declarations

This thesis or any part thereof, has not been, or is not currently being submitted for any degree at any other university.

The work reported herein is as a result of my own investigations, except where acknowledged and referenced.

Acknowledgements

As I stand at the end of this PhD journey, my heart is filled with profound gratitude for the many people who have been my steadfast pillars of support, guidance, and encouragement throughout this incredible journey.

First and foremost, I want to express my heartfelt thanks to my supervisor, Xinmin Zhan. Your guidance, patience, and unwavering belief in me have been invaluable. You have been more than a mentor—you've been a source of constant inspiration, and I am truly grateful for all the time and effort you have invested in my growth.

I would also like to extend my sincere thanks to my Graduate Research Committee members, Guangxue Wu, Mark Healy and Bryan McCabe. Your insightful feedback and encouragement have significantly shaped this work, and I am deeply appreciative of your support.

To my amazing colleagues at NEO GREEN research group, thank you for creating a vibrant, supportive, and intellectually stimulating environment. The camaraderie we shared, the countless discussions, the shared frustrations and triumphs, have all been integral to my experience.

To my family, words cannot express the depth of my gratitude. To my parents, Zhongtao Shi and Lian Wang, thank you for your endless love, encouragement, and sacrifices. Your unwavering faith in me has been my anchor through this long journey.

Finally, I would like to thank the funding agencies, China Scholarship Council, whose financial support made this research possible. This dissertation is a testament to the collective effort of everyone who has been part of my journey. Each of you has left an indelible mark on my life, and I carry your contributions with me as I move forward. From the bottom of my heart, thank you.

List of Abbreviations

AD: anaerobic digestion

AF: anaerobic fermentation

BCCT: butyryl-CoA-acetyl CoA transferase

BK: butyrate kinase

COD: chemical oxygen demand

EPS: extracellular polymeric substances

FAN/ NH₃: free ammonia

FID: flame ionization detector

GHG: greenhouse gases

H₂: hydrogen gas

INT-ETS: 2-(p-iodophenyl)-3-(p-nitrophenyl)-5-phenyltetrazolium chloride-electron transport system

ISR: the ratio of inoculum to substrate

MLSS: mixed liquor suspended solids

NAD⁺: β-nicotinamide adenine dinucleotide

NADH: 1,4,β - dihydronicotinamide adenine dinucleotide

NH₄⁺: ammonium ions

OFMSW: organic fraction of municipal solid waste

OLR: organic loading rate

ORF: open reading frame

ORP: oxidation-reduction potential

PBS: phosphate buffer solution

PCA: principal components analysis

PCoA: principal coordinates analysis

PTB: phosphotransbutyrylase

RDA: redundancy analysis

SBOB: syntrophic butyrate oxidizing bacteria

TAN: total ammonia

TS: total solids

VFAs: volatile fatty acids

VS: volatile solids

VTS: volatile total solids

List of Equations

Equation. (2-1): The thermodynamic stoichiometric equation for the conversion of butyric acid to acetic acid

Equation. (2-2): The thermodynamic stoichiometric equation for the conversion of butyric acid to iso-butyric acid

Equation. (2-3), (2-4) and (2-5): The thermodynamic stoichiometric equation for the conversion of butyric acid to methane

Equation. (2-6): The calculation equation of free ammonia

Equation. (3-1): The first order kinetic model describing the butyrate degradation

Equation. (3-2): The modified Gompertz kinetic model describing the butyrate degradation

Equation. (3-3), (3-4) and (3-5): The inhibition model describing the inhibition degree from different ammonium species

Equation. (3-6): The calculation method of CH₄ volume at standard conditions

Equation. (4-1), (4-2), (4-3), (4-4) and (4-5): The Monod-type kinetic equation describing the degradation reaction of butyrate, iso-butyrate, acetate, and CH₄ production

Equation. (4-6), (4-7), (4-8), and (4-9): The rate equations for the simultaneous degradation of butyrate, iso-butyrate, acetate, and CH₄ production

Equation. (5-1): The calculation equation of VFA production efficiency

Equation. (5-2), (5-3), (5-4), (5-5), (5-6) and (5-7): Biochemical reactions in the glucose degradation process

Chapter 1

Introduction

1.1 Background

As the global population continues to grow, there is a corresponding increase in the demand for energy resources, as illustrated in Fig. 1.1, with a remarkable rise of consumption of fossil fuels. However, the finite fossil fuel reserves and the constantly rising fossil fuel prices have exacerbated the energy shortage. Additionally, the environmental impacts associated with fossil fuel combustion, such as water, air and soil pollution and greenhouse gas emissions, have further intensified the severe energy crisis and environmental challenges associated with the burning of fossil fuels (Mu et al., 2023). Concurrently, the volume of waste generated by human activities is also escalating (Feng et al., 2022). This dual trend underscores the mounting pressure on both energy systems and waste management infrastructure, emphasizing the need for more sustainable approaches to address these interlinks.

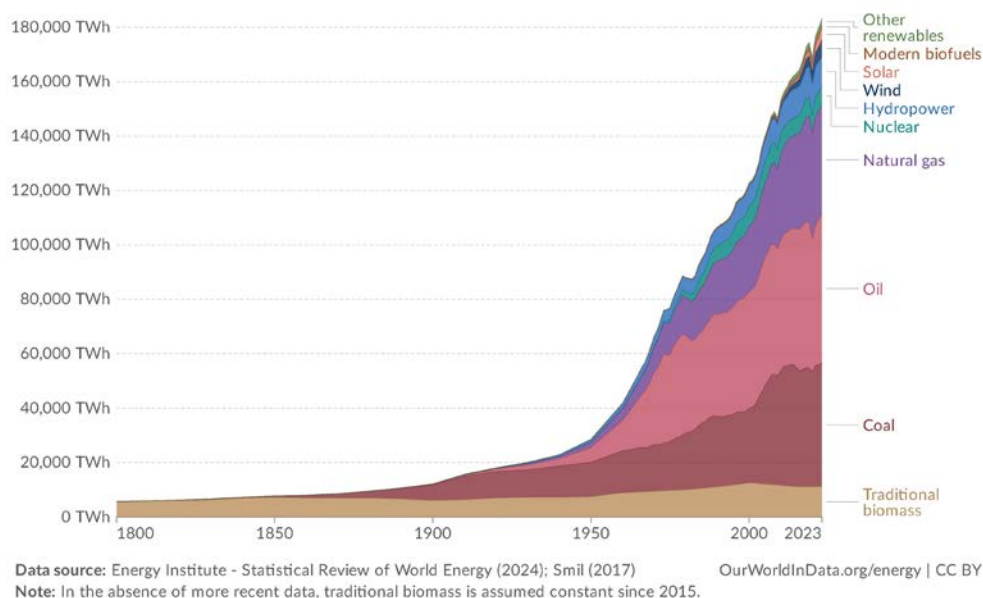


Figure 1.1 Global primary energy consumption by source based on the substitution method and measure in terawatt – hours (Ritchie et al., 2023)

Anaerobic digestion (AD) is a promising treatment method, which not only effectively manages organic waste such as food waste, animal manure, wastewater and sludge (Carlsson et al., 2012), but also generates renewable energy in the form of biogas. The digestate of AD can be used as soil amendment and organic fertilizer. AD offers several benefits over other organic waste treatment methods, including effective odor control, reduction of greenhouse gas (GHG) emissions, pathogen removal, and versatility with different types of substrates

(Chiappero et al., 2020). The AD process consists of four sequential and parallel processes that decomposes organic waste in the absence of oxygen: hydrolysis, acidogenesis, acetogenesis, and methanogenesis (Fig. 1.2) (Fakkaew and Polprasert, 2021; Wang et al., 2023c).

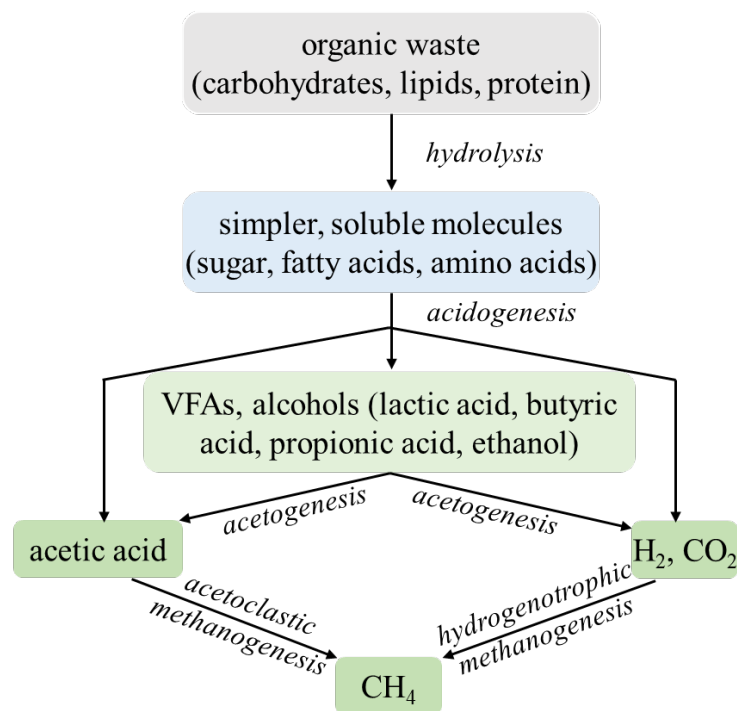


Figure 1.2 Main stages in anaerobic digestion process (Adapted from Wang et al. (2023))

In the hydrolysis stage, complex organic compounds such as carbohydrates, proteins, and fats are broken down into simpler, soluble molecules like sugars, amino acids, and fatty acids by hydrolytic bacteria. These soluble molecules are then converted by acidogenic bacteria into volatile fatty acids (VFAs), alcohols, hydrogen, and carbon dioxide, producing various intermediate products such as lactic acid, butyric acid, and propionic acid. The next stage, acetogenesis, involves further breakdown of the VFAs and alcohols into acetic acid, hydrogen, and carbon dioxide by acetogenic bacteria. This prepares the substrates for the methane generation, in which methanogenic archaea convert acetic acid, hydrogen, and carbon dioxide into methane and carbon dioxide, resulting in biogas. While the primary goal of AD is often seen as biogas production, it is equally important to recognize the substantial value of the intermediate products generated during the process, particularly VFAs (Strazzer et al., 2018). In order to enhance the production of VFAs and H₂, methanogenesis is suppressed through various inoculum pre-treatment strategies (Dahiya et al., 2018). This

process, referred to as anaerobic fermentation (AF), is primarily aimed at producing specific products like ethanol, lactic acid, and VFAs, rather than CH₄ (Venkata Mohan et al., 2016). Generation of VFAs from biowaste is promising since VFAs production requires significantly shorter retention time, smaller reactor units, and nearly all substrates can be converted into VFAs (Feng et al., 2022). In addition, VFAs hold greater value than biogas due to their versatile applications as chemicals, higher economic potential and easier storage and transportation (Zhou et al., 2018).

VFAs refer to carboxylate with 2 to 6 carbon atoms including acetic, propionic, butyric, valeric and caproic acid, which are typically produced in the acidogenesis and acetogenesis stages in AD. VFAs are widely used in many industries such as food, pharmaceuticals, and are cost-effective precursors for the production of bioplastics (Al Battashi et al., 2020), biodiesel (Zhang et al., 2021a) and other high value products (Strazzera et al., 2018). These acids are conventionally derived from fossil fuels, leading to negative environmental impacts such as GHG emissions and non-renewable petrochemical utilization (Atasoy et al., 2018). The bioproduction of VFAs from organic waste is a sustainable alternative for waste management and resource recovery, contributing to environmental protection and economic growth. However, the high cost of recovery and purification of a specific VFA from mixed VFAs production hinders the subsequent reuse. Therefore, production of selective VFAs instead of producing a mixture of VFAs is a promising strategy.

Butyric acid is considered highly valuable due to its huge application potential and is widely used in many fields including chemical industry, perfume, medicine and animal feed (Jiang et al., 2018). As shown in Table 1.1, the solubility of butyric acid is 60 g/L at 25 °C, which is lower than that of propionic and acetic acids. The low solubility of butyric acid reduces the recovery cost from the fermentation broth. The global market price for butyric acid ranges from \$2000 to 2500 per ton, which is higher compared to propionic acid (\$1500 – 2000 per ton) and acetic acid (\$400 – 800 per ton) (Duong and Nga, 2024). But the global market of butyric acid value (\$317 million in 2022) is lower than that of propionic and acetic acid due to its production limitations. The demand of butyric acid is growing at a higher compound annual growth rate of 9.2% between 2022 and 2027 compared to other VFAs (<https://www.marketsandmarkets.com/Market-Reports/butyric-acid-market-76962011.html>). Although valeric acid also holds significant market potential, it can be naturally extracted by boiling water or soda from the roots of plants like *Angelica archangelica* and *Valeriana*

officinali (Goldberg and Rokem, 2009). Therefore, the production and recovery of butyric acid from organic waste can generate higher economic benefits and reduce the environmental impacts. Notably, butyric acid recovered from organic waste streams has applications in bio-based material, bioenergy, and green chemistry as a valuable platform chemical. However, its direct reuse in food and pharmaceutical industries is typically not intended, as such applications are governed by strict regulatory frameworks ensuring purity, safety, and consumer acceptance (EFSA, 2025). Consequently, this study focuses on optimizing butyric acid recovery, contributing to the development of bio-based materials and renewable chemical production.

Table 1.1 Characteristics and global market of typical VFAs

VFAs	Solubility (g/L, 25 oC)	Energy density (KJ/mol)	Global market value (\$ million)	Reference
acetic acid	1000	874.2	8080	(Feng et al.,
propionic acid	1000	1527.3	1100	2022; Hunter et
butyric acid	60	2183.6	818	al., 2021;
valeric acid	24	2837.8	16401	PubChem, 2024)

The accumulation of butyric acid in AD is a dynamic process that requires simultaneous consideration of both its production and degradation. Despite its importance, there is a noticeable gap in research specifically focused on the factors that affect butyric acid degradation. Furthermore, the optimal conditions for butyric acid production are inconsistent due to the variability in experimental conditions in the literatures. Therefore, to better understand the mechanisms behind butyric acid accumulation, it is essential to explore these two processes in detail, especially the factors that affect butyric acid degradation and production in anaerobic conditions.

1.2 Research aims and objectives

The primary aim of this PhD research was to investigate the factors influencing butyric acid degradation and production, as well as to elucidate the mechanisms of butyric acid conversion.

For elucidating the effect of ammonia concentration and pH on butyric acid degradation and inhibition mechanism of ammonia, the specific objectives were:

- 1) to investigate butyric acid degradation under different ammonia concentrations.
- 2) to assess the individual inhibitory effects of NH_4^+ and free ammonia (NH_3) on butyrate degradation.
- 3) to examine the potential reversibility of butyrate degradation following severe ammonia inhibition.

For exploring the effect of temperature and butyric acid concentration on butyric acid degradation, the specific objectives were:

- 1) to investigate the effects of butyrate concentration and temperature on butyrate degradation and methane production.
- 2) to analyse the microbial community structure and butyrate degradation pathways in both mesophilic and thermophilic environments.

For exploring the optimal conditions and mechanisms of butyric acid production in anaerobic fermentation (AF), the specific objectives were:

- 1) to investigate butyric acid production and VFAs distribution under different conditions (pH, temperature, the ratio of inoculum to substrate (ISR)).
- 2) to investigate the microbial community succession and interactive correlation with butyric acid production.
- 3) to explore the butyric acid production metabolic pathway under optimal conditions.

1.3 Procedures

The PhD research consisted of a series of batch experiments as shown in Fig. 1.3. The procedures are briefed here and will be detailed in individual chapters. The study investigated the factors influencing butyric acid accumulation, focusing on both degradation and production processes. On the degradation part, variables like pH, ammonia, temperature, and butyric acid concentration were analysed to understand how they affected butyrate degradation. On the other hand, butyrate production was examined by considering the effects

of pH, temperature, and ISR. By evaluating these parameters, the research would identify optimal conditions for promoting butyric acid accumulation.

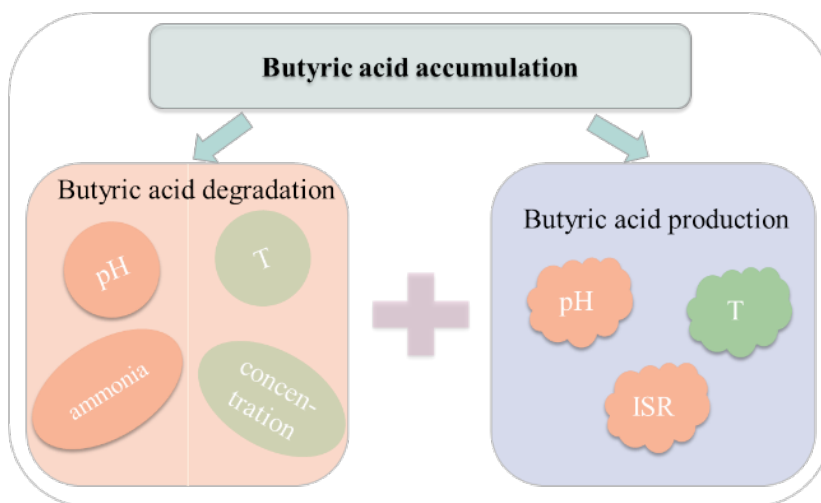


Figure 1.3 An overview of the research

1.4 Structure of thesis

This dissertation comprises 6 chapters:

Chapter 1 is the introduction. The background of this research, main objectives, procedures and the structure of thesis are presented.

Chapter 2 reviews the metabolic pathways involved in the production and degradation of butyric acid, as well as the factors influencing these processes.

Chapter 3 investigates the impact of ammonia levels and pH conditions on butyric acid degradation in AD process.

Chapter 4 studies microbial transition and degradation pathway driven by butyric acid concentration in mesophilic and thermophilic anaerobic digestion.

Chapter 5 explores the optimal conditions for butyric acid production and presents the microbial community structure and the shifts in the metabolic pathway under varying conditions.

Finally, Chapter 6 presents the conclusions drawn from all the lab studies described in Chapters 3–5. Recommendations for further research are also put forward.

1.5 Research outputs

Published article:

Chapter 3: Shi, X., Wang, S., Wang, Z., Wu, G., Hu, Z., & Zhan, X. (2024). Ammonia-induced constraints on butyrate degradation in anaerobic digestion: Impact of ammonia levels and pH conditions, and recovery behaviour. *International Biodeterioration & Biodegradation*, 193, 105847. DOI: 10.1016/j.ibiod.2024.105847.

Chapter 4: Shi, X., Yasuda, S., Wang, Z., Hu, Y., Wu, G., Lens., P., & Zhan, X. (2024). Microbial transitions and degradation pathways driven by butyrate concentration in mesophilic and thermophilic anaerobic digestion under low hydrogen partial pressure. *Bioresource Technology*, 419, 132012. DOI: 10.1016/j.biortech.2024.132012.

Manuscripts under review or in preparation :

Chapter 5: Shi, X., Yasuda, S., Tuohy, M., Wang, Z., Hu, Y., Wu, G., & Zhan, X. Decoding butyrate fermentation: Parameter optimization and metagenomic insights with glucose as a model substrate (in preparation).

Chapter 2: Shi, X., Hu, Y., Wang, Z., & Zhan, X. A comprehensive review on current status and future perspectives of butyrate accumulation in anaerobic digestion. (in preparation)

Conference presentations:

Oral: Enhancing selective butyric acid production by controlling fermentation conditions. 11th International Conference on Sustainable Solid Waste Management, Rhodes, Greece, 19-22 June 2024.

Oral: The factors that affect butyrate degradation: ammonia, pH, temperature and butyrate concentration. 11th International Conference on Environment, Resources & Energy, Galway, Ireland, 24-25 June 2024.

Oral: Butyrate degradation and methane production with different butyrate concentration in mesophilic and thermophilic anaerobic digestion. The 2nd Forum for Chinese PhD Students in Ireland 2023, Cork, Ireland, 4-5 November 2023.

Poster: Effect of ammonia concentration and pH on anaerobic butyric acid degradation. The 10th International Conference on Sustainable Solid Waste Management, Chania, Greece, 21-24 June 2023.

Poster: Effect of temperature and butyrate concentration on butyrate degradation and methane production during anaerobic digestion. Istanbul, Turkey, 13-15 September 2023.

Chapter 2

Literature review

2.1 Introduction

Butyric acid is a key intermediate in AD process and a high-value product with broad applications in the food manufacturing, chemical, and pharmaceutical industries (Zhang et al., 2009; Zigová, 2000). It has been found to consistently accumulate in anaerobic digesters. This phenomenon has been particularly observed in some AD process (Dennehy et al., 2016; Peng et al., 2018). This chapter provides a comprehensive review of the existing literature concerning the production and degradation of butyric acid, with a particular focus on the factors and mechanisms influencing its accumulation.

This literature review is structured to first provide an overview of the metabolic pathways involved in butyric acid production and degradation. Through the analysis of metabolic pathways, a better understanding of the mechanisms of butyric acid production and degradation can be gained, which facilitates the optimization of parameters to regulate butyric acid accumulation. Following this, the chapter investigates the influence of various operational parameters, such as pH, temperature, ammonia concentration, on butyric acid production and degradation. Finally, the review synthesizes the findings to identify current gaps in knowledge and potential areas for future research. By drawing connections between different studies, this chapter aims to provide a clearer understanding of the optimal conditions for butyric acid accumulation and of the complex dynamics of butyric acid accumulation.

2.2 Metabolic pathway of butyric acid production and degradation in anaerobic digestion

In AD process, there are specific metabolic pathways for each type of VFA production and degradation. The specific pathways can be changed under different conditions. Therefore, the review of microbial activities and underlying metabolic pathways is better to tap full potential of butyric acid production and conversion in anaerobic digestion.

2.2.1 Butyric acid production metabolic pathway

Organic matter can be converted into various VFAs via anaerobic fermentation. Table 2.1 presents the primary chemical equations derived from glucose, highlighting the production of

acetic acid, propionic acid, butyric acid, lactic acid, and ethanol. The metabolic pathways involved in acidogenesis are illustrated in Fig. 2.1 (Feng et al., 2022; Li et al., 2022c; Liu et al., 2012b; Yadav et al., 2022; Zhou et al., 2018). According to Fig. 2.1, butyric acid is synthesized through the reduction and decarboxylation of pyruvate (Zhou et al., 2018). Various enzymes and microbial communities are involved in butyric acid production during the AF process. The pathway begins with the conversion of pyruvate to acetyl-CoA by pyruvate-ferredoxin oxidoreductase. Acetyl-CoA is then transformed into acetoacetyl-CoA by thiolase. Acetoacetyl-CoA is subsequently converted into butyryl-CoA through the intermediates 3-hydroxybutyryl-CoA and crotonyl-CoA, catalyzed sequentially by 3-hydroxybutyryl-CoA dehydrogenase, crotonase, and butyryl-CoA dehydrogenase. Finally, there are two distinct pathways to convert butyryl-CoA to butyrate: one involves the direct transformation of butyryl-CoA to butyrate by butyryl-CoA-acetyl CoA transferase (BCCT) (Lim et al., 2014), and the other involves the phosphorylation of butyryl-CoA (Butyryl-P) followed by its conversion to butyrate through the catalytic actions of phosphotransbutyrylase (PTB) and butyrate kinase (BK) (Chaganti et al., 2011; Vital et al., 2014).

Table 2.1 Standard Gibbs energy of main fermentation reaction from glucose

Reaction	ΔG° (KJ/mol)	References
$C_6H_{12}O_6 + 2H_2O \rightarrow 2CH_3COOH + 2CO_2 + 4H_2$	-206.0	
$C_6H_{12}O_6 + 2H_2 \rightarrow 2CH_3CH_2COOH + 2H_2O$	-279.4	(Fuess et al., 2018)
$C_6H_{12}O_6 \rightarrow CH_3CH_2CH_2COOH + 2CO_2 + 2H_2$	-254.0	
$C_6H_{12}O_6 \rightarrow 2CH_3CHOHCOOH$	-188.6	(Xie et al., 2018)
$C_6H_{12}O_6 \rightarrow 2CH_3CH_2OH + 2CO_2$	-164.8	(Fuess et al., 2018)

BCCT, PTB and BK are directly involved in butyric acid production, while the varying contributions of these enzymes to butyric acid production have been reported. Some studies have highlighted that BCCT has more contribution for butyric acid production in human bacterial flora (Morrison, 2006; Pryde, 2002). Similarly, research on anaerobic co-digestion of brown water and food waste found that the high butyric acid accumulation was related to the BCCT pathway (Lim et al., 2014). Conversely, other studies have indicated that the butyric acid production is consistent with the activity and concentration of BK and PTB (Luo et al., 2020; Zhu and Yang, 2003; Zhu and Yang, 2004). Lu et al. (2020) reported that butyric acid accumulation was correlated with the increasing activity of BK. The different key

functional enzymes in butyric acid production were due to different butyric acid production pathways. Previous studies illustrated that the microorganisms utilizing acetic acid and hydrogen tend to prefer the BCCT pathway for the production of butyric acid (Barcenilla et al., 2000). Therefore, a high concentration of butyric acid and low concentration of acetic acid can be achieved by controlling the contribution of BCCT and PTB/BK.

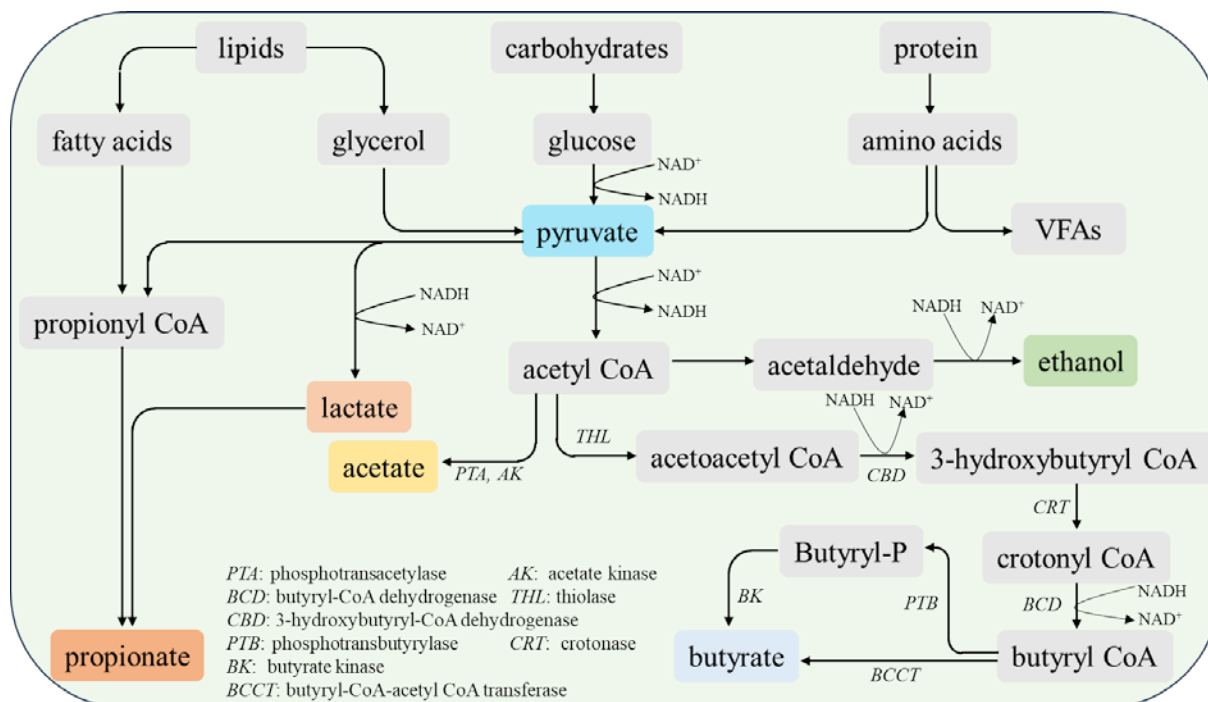


Figure 2.1 Metabolic pathway for VFAs production

Microbial communities play a crucial role in butyric acid production. At the phylum level, *Proteobacteria*, *Kosmotoga*, *Enterobacteriaceae*, *Fimicutes* are related to butyric acid generation (Kong et al., 2018b; Li et al., 2020d). At the genus level, the increased relative abundance of *Butyriolbrio*, *Butyribacterium*, *Clostridium*, *Eubacterium*, *Fusobacterium*, *Megasphaera*, *Lactobacillus*, *Saccharomyces* and *Caproiciproducens* was evidently associated with butyric acid production (Chen et al., 2015; Feng et al., 2018; Fuess et al., 2018; Luo et al., 2020). Among these genera, *Clostridium* is widely studied for butyric acid fermentation due to its high production and simple growth medium requirements (Liu et al., 2021; Suo et al., 2019). In addition, many species of this genus can produce butyric acid as the dominant VFAs product, such as *Clostridium tyrobutyricum*, *Clostridium acetobutylicum*, *Clostridium thermobutyricum*, *Clostridium populeti*, *Clostridium sp*, *Clostridium perfringens* and *Clostridium butyricum*. Metabolic engineering of *Clostridium* has been applied to increase the production of butyric acid, as will be elaborated in the following sections.

However, the bioaugmentation using *Clostridium* species for butyric acid production in AD has not been extensively studied.

As shown in Fig. 2.1, the balance of 1,4, β - dihydronicotinamide adenine dinucleotide/ β -nicotinamide adenine dinucleotide (NADH/NAD⁺) is also a key co-factor affecting enzyme activities and metabolic processes (Su et al., 2017; Zhu and Yang, 2004). The oxidation and reoxidation of NADH regulate the metabolic pathways and products. Pyruvate and acetic acid generation process result in the accumulation of NADH (Paiano et al., 2019). In acetic acid metabolic pathway, only ATP is produced from acetyl-CoA to acetic acid, without NADH consumption. To meet the balance of NADH and NAD⁺, the reoxidation of NADH is necessary by reducing other organic compounds or producing more reduced compounds, such as propionic acid and butyric acid. Compared to acetic acid production, two more NADH are consumed for butyric acid production. Therefore, butyric acid metabolic is favorable in reduced conditions. Since butyric acid production can be enhanced by altering the NADH/NAD⁺ level, a series of measures have been introduced to improve NADH level or enhance NADH availability (Chen et al., 2022; Zhang et al., 2021c; Zhao et al., 2022).

2.2.2 Butyric acid degradation metabolic pathway

Butyric acid as an important intermediate can not be directly utilized by methanogens, which must be firstly converted to acetic acid and hydrogen as shown in Fig. 1.2. Fig. 2.2 illustrates the butyric acid degradation metabolic pathway. Eq. (2-1) and Fig. 2.2 show that the degradation of butyric acid is thermodynamically unfavorable. Therefore, butyric acid degradation is the most challenging process with energy input, called reverse electron transfer.

During the butyric acid degradation process, butyric acid is firstly oxidized to butyryl-CoA. Then butyryl-CoA is subsequently converted to crotonyl-CoA. Crotonyl-CoA is catalyzed to acetyl-CoA with 3-hydroxybutyryl-CoA and acetoacetyl-CoA as intermediates. Finally, acetyl-CoA is converted to acetic acid. The processes require an energy investment to release electrons as hydrogen or formate. Except the pathway from butyric acid to acetic acid, the production of iso-butyric acid, propionic acid and methyl compounds is other potential metabolism pathway of butyric acid degradation. Meng et al. (2022) explored the enrichment of syntrophic butyrate-oxidizing methanogenesis in a high butyrate loading based on 16S

rRNA genes and metagenome and found the production of propionic acid and methyl compounds. In addition, the isomerization of butyric acid is thermodynamically favorable as shown in Eq. (2-2). The isomerization may be a detoxifying mechanism by converting butyric acid to its less toxic equivalent (Petrognani et al., 2020). The biochemistry of butyric acid degradation process and the relevant bacteria are still not fully understood, especially if the β -oxidation is reversible.

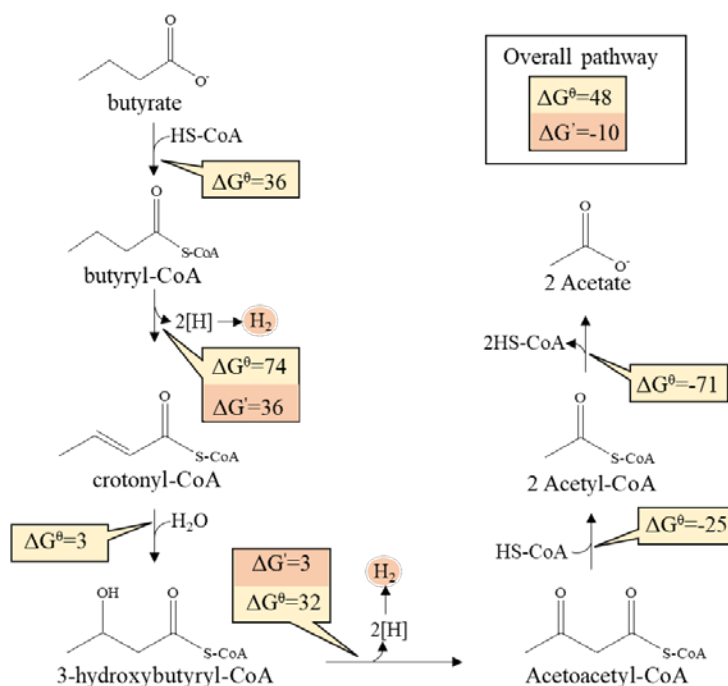
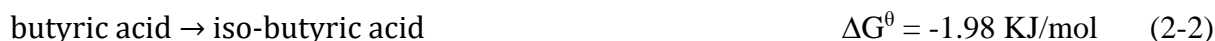
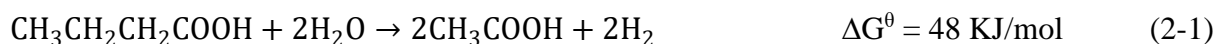


Figure 2.2 Biochemical pathways of butyric acid oxidation. The ΔG^θ and $\Delta G'$ (at 1 Pa hydrogen) of each step is indicated (KJ/mol) (adapted from Stams and Plugge, 2009, Luo et al., 2019)

The genera of *Mesotoga*, *Aminivibrio*, *Acetivibrio*, *Desulfovibrio*, *Petrimonas*, *Proteobacteria* and *Anaerolineae* are contributed to butyric acid oxidation (Luo et al., 2020; Meng et al., 2022; Yi et al., 2020). As shown in Fig 2.2, hydrogen production from butyryl-CoA and 3-hydroxybutyryl-CoA are involved in butyric acid metabolism. Hydrogen and acetic acid accumulation will affect butyric acid oxidation. Therefore, the syntrophic species, other major bacteria, are involved in butyric acid degradation and methanogenesis. Syntrophic butyric acid oxidizers are known as the family *Syntrophomonadaceae* and the order *Syntrophobacterales* (Zhang et al., 2023b). The species of *Syntrophomonadaceae* for butyric acid oxidation includes: *Syntrophomonas wolfei*, *Syntrophospora bryantii*, *Syntrophomonas erecta*, *Syntrophomonas curvata*, *Syntrophomonas zehnderi* and

Thermosyntropha lipolytica (Muller et al., 2010). The syntrophic bacteria make butyric acid degradation possible and thermodynamically feasible. But the syntrophic mechanism still needs to be further studied.



2.3 Butyric acid conversion in anaerobic digestion systems

2.3.1 Factors influencing butyric acid production

Butyric acid is produced from glucose, accompanied by hydrogen and acetic acid production, as shown in Table 2.1. The simultaneous production of acetic acid can reduce the butyric acid yield and increase purification costs. Therefore, understanding the factors that influence butyric acid production in anaerobic fermentation is crucial to enhance butyric acid percentage in anaerobic fermentation broth.

2.3.1.1 pH

In AD system, pH can affect the structure and activity of the microbial community because the hydrolytic and acidogenic bacteria can't survive in extremely acidic or alkaline conditions (Liu et al., 2012a). pH not only influences both hydrolytic and acidogenic process, but also regulates the fermentation type. Controlling pH for the selective production of VFAs is a widely used method (Zhou et al., 2018), and thus, finding optimal pH is important for butyric acid production.

As shown in Table 2.2, many studies have observed that pH can change the metabolic pathway in acidogenic fermentation and affect the distribution of products. However, there is no consistent conclusion about the influence of pH on the composition of products. It is found that butyric acid production could be improved at alkaline pH. Atasoy et al. (2019) found that butyric acid was the primary product under alkaline condition (pH was 8 and 10). Stein et al. (2017) found that when pH was controlled at 9.0, butyric acid concentration rose sharply compared to pH 5.5 in food waste fermentation. Similarly, the concentration of butyric acid was higher at alkaline pH 11 than at acidic pH 5.5 in Begum et al.'s research (2018). Alkaline

pH contributes to butyric acid accumulation as it promotes the macromolecule destruction, inhibits methanogenesis and enhances VFAs production.

While butyric acid is also found to be the primary product under acidic conditions. This is essentially due to the fact that acidic condition can decrease the NADH/NAD⁺ ratio in the fermenter. As shown in Fig. 2.1, NADH is consumed to reduce acetoacetyl-CoA to 3-hydroxybutyryl-CoA and crotonyl-CoA to butyryl-CoA in butyric acid production process. Hence, butyric acid production is influenced by the ratio of NADH/NAD⁺. As shown in Table 2.2, the optimal pH for butyric acid production under acidic conditions varies from 4.7 to 7.0. Jin et al. (2019) found that butyric acid concentration was higher at pH 6.5 in AD of saccharification residue from food waste. In AD of potato peel waste, the highest proportion of butyric acid was obtained at pH 5 (Lu et al., 2020). However, under the optimal pH range of 4.7 to 7.0, butyric acid may not always be the only primary product, as the type of fermentation can shift with slight changes in pH. For instance, butyric acid was the dominant product at pH 4.7 and 5.0, whereas lactic acid and valeric acid were the dominant products at pH 4.5 and 6.0, respectively (Feng et al., 2020).

These inconsistent research findings suggest that the pH is not the only factor that affects butyric acid production. The optimal pH for butyric acid production is related to the types of substrates (Garcia-Aguirre et al., 2017), organic loading rate (OLR) (Jiang et al., 2013), the ratio of carbon to nitrogen (Fu et al., 2012), and the dominated microbial community (Dwidar, 2013; He et al., 2005) and so on. Therefore, the optimal pH for butyric production in AD process needs to be explored further.

Table 2.2 Production and composition of VFA under different pH

Operational conditions				High VFA production		
pH	Substrate	inoculum	Temperature (°C)	Optimized condition*	composition	References
5, 6, 7, 8	glucose	anaerobic digested sludge	37	Not decided	71.7% butyric acid at pH 5	(Horiuchi et al., 2002)
5, 6, 7, 8, 10, 12	glucose	anaerobic sludge	22	pH 7	66% acetic acid, 23% propionic acid, 10% butyric acid; Highest butyric acid percentage (47%) was at pH 12	(Khan et al., 2019)
5, 6, 7	food waste	anaerobic digested sludge	35	pH 6	53.27% butyric acid, 23.75% acetic acid, 13.46% propionic acid	(Jiang et al., 2013)
4, 5, 6	food waste	anaerobic activated sludge	30	pH 6	over 70% butyric acid. Highest percentage of butyric acid was achieved at pH 5	(Wang et al., 2014)
5.5, 7, 9	food waste	anaerobic sludge	37	pH 9	48.3% butyric acid, 39.0% acetic acid, 12.7% propionic acid	(Stein et al., 2017)
3.2, 4, 4.2, 4.5, 4.7, 5	food waste	anaerobic digested sludge	35	pH 4.7	61.1% butyric acid, 24.8% acetic acid	(Feng et al., 2020)

4, 5, 6	food waste	anaerobic digested sludge	37	pH 4 and 5	almost no butyric acid accumulation	(Lukitawesa et al., 2020)
5, 10	food waste	anaerobic digested sludge	35	pH 10	Acetic acid, propionic acid and butyric acid were the three major products accounting 86%-89%. The percentage of butyric acid was higher at pH 5	(Khatami et al., 2021)
4.5, 5.5, 6.5	food waste	-	50	pH 6.5	52.9% butyric acid	(Yu et al., 2021)
4, 6, 7.5, 9, 10, 11	food waste	anaerobic digested sludge	35	pH 9	60.5% acetic acid, 12.8% butyric acid, 14.8% caproic acid	(Cheah et al., 2019)
7, 10	food waste and thermal-hydrolysed sewage sludge	anaerobic sludge	35	pH 10	71.3% acetic acid, 24.8% butyric acid, 1.7% propionic acid	(Gong et al., 2021)
5.5, 6.5	saccharification residue from food waste ethanol fermentation	sewage sludge	37	pH 6.5	79.3% butyric acid, 9.4% propionic acid, 4.6% acetic acid; Higher percentage of butyric acid (81%) was obtained at pH5.5	(Jin et al., 2019)

5, 7, 11	potato peel waste	anaerobic digested sludge	37	pH 5	47.1% butyric acid (47.1%)	(Lu et al., 2020)
Initial 4, 5, 6, 7, 8, 9	vegetable waste	anaerobic activated sludge	37	pH 8 and 9	Acetic acid, propionic acid and butyric acid were the three major products accounting over 80%	(Cai et al., 2024)
4, 5, 6	citrus waste	anaerobic digested sludge	37	pH 6	32% acetic acid, 21% caproic acid, 15% butyric acid	(Eryildiz et al., 2020)
4, 5, 6	fruit and vegetable wastes	anaerobic activated sludge	37	pH 4 and 5	pH 4, 97.5% ethanol; pH 5, 37.0% butyric acid, 34.8% acetic acid, 20.0% propionic acid; pH 6, sum of butyric acid and acetic acid accounted for 89.9%	(Zheng et al., 2015)
4, 4.5, 5, 5.5, 6, 6.5	dairy wastewater	anaerobic sludge	37	pH 6.5	34% acetic acid, 14% butyric acid, 12% propionic acid	(Yu and Fang, 2002)
4, 4.5, 4.7, 5, 5.3, 5.7	93% milk–5% yoghurt–2% cheese, w/w	anaerobic sludge	37	pH 4.7	56.2% butyric acid, 21.9% acetic acid, 15.1% lactic acid	(Stavropoulos et al., 2016)

3.5, 4.25, 5.25, 5.5, 6	whey wastewaters	biomass digester	37	pH 5.25	approximately 50% acetic acid, 25% acetic acid, 20% propionic acid	(Bengtsson et al., 2008)
5, 10	cheese production wastewater	anaerobic granular seed sludge	35	pH 5	23% acetic acid, 22% propionic acid, 21% butyric acid, 15% valeric acid	(Atasoy and Cetecioglu, 2022)
4, 4.5, 5, 5.5, 6, 6.5, 7	gelatin-rich wastewater	anaerobic sludge	37	pH 7.0	35.0% acetic acid, 22.1% butyric acid, 11.3 iso-butyric acid	(Yu and Fang, 2003)
4.5, 5, 5.5, 6, 6.5, 7, 7.5	a mixture of olive mill wastewater, cheese whey and liquid cow manure	anaerobic sludge	37	pH 6.5	about 62.0% butyric acid, 21.9% propionic acid, 10.9% acetic acid	(Dareioti et al., 2014)
5, 5.2, 5.4, 5.5, 5.7, 5.9	cassava wastewater	sludge from UASB reactor	34	pH 5.9	100% acetic acid; highest proportion of butyric acid (61.5%) at pH 5.7	(Sanchez-Ledesma et al., 2024)
5.5, 11	leachate	active mixed microbial consortia	37	pH 11	The concentration of butyric acid increased at alkaline pH 11 rather than at acidic pH 5.5	(Begum et al., 2018)
4.5, 5, 5.5, 6	sugar beet silage	digestate	60	pH 4.5	The highest percentage of	(Kumanowska et al., 2017)

7,10	heat-alkaline pretreated waste activated sludge	dewatered sludge	35	pH 7	butyric acid was obtained at pH 5	(Ma et al., 2016)
3, 5, 7, 9, 11, 12	proteinaceous sewage sludge	sludge	35	pH 9	57.0% acetic acid, 22.3% butyric acid	(Liu et al., 2012a)
8, 10	waste activated sludge	anaerobic digestion sludge	37	pH 10	about 43.85% acetic acid, 21% propionic acid, 10.29% butyric acid	(Pan et al., 2024)
4.5, 5, 5.5, 6	sorghum and Cow Manure	-	37	pH 6	44.48% acetic acid, 26.46% propionic acid, 10.18% butyric acid	(Dareioti et al., 2022)
initial 5, 6, 7, 9	chicken manure	granular sludge from UASB reactor	37	pH 6 and 9	The highest percentage of butyric acid was at pH 5.0	(Yin et al., 2021)
5.5, 6.5, 7.5, 8.5	dairy cattle manure	-	20	pH 8.5	butyric acid accumulated only in small amounts at pH	(Castro-Ramos et al., 2022)
					37% butyric acid, 23% acetic acid, 17% propionic acid; highest proportion of butyric acid (46%) at pH 6.5	

2.3.1.2 Temperature

Temperature impacts the microbial ecosystems, and furtherly influences the stability and efficiency of the AD process (Nie et al., 2021). The hydrolysis and acidification of substrate is affected by temperature (Dooms et al., 2018), resulting in the difference in butyric acid production and conversion at varying temperatures.

The AD process is generally operated under four temperature ranges: psychrophilic (4 - 20 °C) (Dev et al., 2019; Tiwari et al., 2021; Wang et al., 2018), mesophilic (20 - 45 °C, and optimal temperature is at 35 - 37 °C) (Fernández-Rodríguez et al., 2016; Guo et al., 2013; Nie et al., 2021), thermophilic (50 - 60 °C, and 55 °C is regarded as optimum) (Fernández-Rodríguez et al., 2016; Wang et al., 2012) and hyper/extreme-thermophilic (60 - 80 °C) (Fernández-Rodríguez et al., 2016; Wang et al., 2012). Many researchers have studied VFAs production at various temperatures, noting that the optimal temperature varies depending on the composition of VFAs. Even when focusing solely on butyric acid production, the optimal temperature differs across studies.

Some previous results have indicated that thermophilic and extreme-thermophilic temperature ranges are more favorable for butyric acid production in comparison to mesophilic conditions (Garcia-Aguirre et al., 2017; He et al., 2012; Yang et al., 2003). However, due to the favorable conditions for VFA production at mesophilic temperatures, some studies have indicated that butyric acid accumulation could be higher under mesophilic conditions. For example, it was observed that butyric acid concentrations decreased as temperature increased from 35 to 55 °C (Lin et al., 2016; Pan et al., 2024). Interestingly, some studies observed that temperature did not significantly affect butyric acid production. For instance, no obvious change in butyric acid concentrations was observed across a temperature range from 20 to 55 °C in the acidogenesis of gelatin-rich wastewater (Yu and Fang, 2003). Similarly, Fernández-Domínguez et al. (Fernandez-Dominguez et al., 2020) reported that the proportion of butyric acid was stable (25 - 29%) regardless of the fermentation temperature from 20 to 70 °C. The different optimal temperature may be attributed to differences in substrates. Vázquez-Fernández et al. (Vázquez-Fernández et al., 2022) found that mesophilic temperatures were more effective for VFA production when using carbohydrate-rich solid substrates, while thermophilic temperatures were more advantageous for VFA production with protein-rich substrates. Temperature is a crucial

factor affecting VFA production and composition, but the anaerobic digestion process involves diverse and complex microbial communities; the impact of various factors such as pH, temperature, and substrate on butyric acid production can be synergistic, antagonistic, or vary in degree.

2.3.1.3 Substrate

The organic compositions of substrates generally include fats, fiber, proteins, lipids, sugar, starch, cellulose and hemicellulose (Adekunle and Okolie, 2015). The biodegradability of the substrate is related to its structure and concentration (Raposo et al., 2012). In addition, different substrates could lead to different microbial communities and dominant species in the AD process, resulting in various dominant VFAs products (Garcia-Aguirre et al., 2017). Therefore, the substrates composition and concentration are also critical factors influencing the butyric acid production.

It was reported that butyric acid production was correlated with chemical composition of organic waste, and the carbohydrate content was the main factor influencing butyric acid production (Alibardi and Cossu, 2016). The similar results have been reported that carbohydrate-rich substrates are more conducive to butyric acid production, such as winery wastewater (W_{ww}), the organic fraction of municipal solid waste (OFMSW) (Garcia-Aguirre et al., 2017), sugar beet (Lindner et al., 2016), food waste rich in carbohydrates (Rafieenia et al., 2017), carrot waste (Zhang et al., 2020) and starch (Elbeshbishy and Nakhla, 2012). Butyric acid, acetic acid and propionic acid were the predominant products when using glucose, peptone and glycerol as substrates, respectively (Yin et al., 2016). Butyric acid concentration increased from $11.4 \pm 3.2\%$ to $34.3 \pm 3.7\%$ when the substrate was changed from hay/straw to sugar beet substrate (Lindner et al., 2016). It is likely that microorganisms can easily utilize carbohydrates, which enhances the consumption of carbon-rich substrates and corresponds to the increased production of butyric acid (Ma et al., 2017). In addition, a balance of nutrients in fermentation substrates is important to promote microbial growth and enhance the activity of relevant enzymes (Feng et al., 2022). Feng et al. (2009) found that addition of carbohydrate substrate enhanced the consumption of protein in sludge and improved VFAs generation because of the activation of enzymes involved in protein hydrolysis.

In addition, the organic loading rate (OLR) or total solid (TS) content, affects the butyric acid production. Butyric acid production can occur in both wet and dry AD process, whereas high TS fermentation is favorable for butyric acid production (Capson-Tojo et al., 2017; Motte et al., 2013; Wang et al., 2015). However, the water content in high TS fermentation limits microorganisms to access solids, resulting in low substrate utilization. Therefore, the difficulties in high TS fermentation could limit the butyric acid yield. The research shows that the percentage of butyric acid in VFAs broth increased from 32% to 46% when the TS content increased from 27.5% to 35%, while butyric acid concentration decreased (Capson-Tojo et al., 2017). Therefore, the threshold value of TS for butyric acid needs to be further studied. On the other hand, VFAs distribution could be controlled by changing OLR due to the fact that changes in OLR can be used to control the microbial community structure and dynamics (Ferguson et al., 2016). Butyric acid concentration was found to be improved by increasing OLR (Begum et al., 2018; Li et al., 2022a). The butyric acid fermentation was facilitated by increasing OLR from 8 to 24 g volatile total solids (VTS)/L/d in AD of fruit waste (Li et al., 2022a).

The ratio of inoculum to substrate (ISR) is another crucial factor. In the AD of lignocellulosic hydrolysate, butyric acid concentrations were 3500, 2000 and 150 mg/L at ISR of 1:2, 1:1 and 2:1, respectively, suggesting that lower ISR was better for butyric acid production (Li et al., 2020d). While, in Lukitawesa et al' s study (2020), butyric acid was the predominant product at ISR of 1:1 in the AD of food waste, while no butyric acid was detected when the ISR was changed to 3:1. These results have been confirmed by various studies, indicating that ISR significantly affects butyric acid production (Eryildiz et al., 2020; Ning et al., 2024; Xu et al., 2012). However, the optimal ISR for butyric acid production varied across studies, likely due to the different properties of the inoculum and substrates in these studies.

These above studies reaffirm that the carbohydrates-rich substrates are most suitable for butyric acid production. However, the substrate concentration and the ISR influence hydrolysis and acidification kinetic rates, ammonia nitrogen release and pH value (Capson-Tojo et al., 2017; Wang et al., 2015; Xu et al., 2012). As a result, there are still many uncertainties regarding the optimal substrate concentration and ISR.

2.3.1.4 Metabolic engineering

Currently, microbial fermentation to produce butyric acid is attracting attention as an environmentally friendly approach. Low-cost substrates such as food waste, lignocellulosic biomass, starch biomass and spent coffee grounds were selected for butyric acid production. However, there are many obstacles to utilize these complex substrates for butyric acid production, such as carbon catabolite repression, the low purity of butyric acid, and by-products that inhibit microbial activity (Luo et al., 2018). Metabolic engineering is increasingly being employed to address the co-production of acetic acid alongside butyric acid and to optimize the use of cost-effective feedstock (Bao et al., 2020), which can be utilized to enhance the butyric acid yield and purity by knocking out or overexpressing key genes in the butyric acid synthesis pathway (Luo et al., 2018).

Clostridium are recognized as the genera that produce butyric acid, mainly including *Clostridium butyricum*, *Clostridium tyrobutyricum*, *Clostridium thermobutyricum*, *Clostridium acetobutylicum* and *Clostridium pasteurianum* (Jang et al., 2014; Kim et al., 2016; Malaviya et al., 2011). Therefore, as shown in Table 2.3, the *Clostridium* strains are mostly modified to improve the yield of butyric acid. *C. tyrobutyricum* is the most used strain for butyric acid production in different substrate, such as rice straw, sugar-glycerol mixture and lignocellulosic hydrolysate (Chi et al., 2018; Lee et al., 2015; Oh et al., 2019; Rebroš et al., 2016). Besides for the *Clostridium*, recombinant *Escherichia coli* can produce butyric acid at high productivity and purity (Lim et al., 2013; Saini et al., 2014; Wang et al., 2019). Conventional strategies of metabolic engineering for the enhancement of butyric acid production consist of two types: the first is by knocking out genes encoding key enzymes for the production of other metabolites (acetic acid, ethanol, butanol, lactic acid), and the second is to overexpress the gene encoding butyric acid production enzymes (Baur et al., 2022; Fu et al., 2022b; He et al., 2020; Jang et al., 2014; Liu et al., 2021; Wang et al., 2019). It should be noted that the lack of genetic engineering tools limits the prospects of metabolic engineering. Therefore, strains with good performance that require no modification are more popular. Recently, *Clostridium beijerinckii* and *Clostridium butyricum* have been reported to directly utilize sugars for high butyric acid yields (Fonseca et al., 2020; Fu et al., 2022a). However, the strict environmental requirements and costs associated with pure inoculum cannot be overlooked.

Table 2.3 Butyric acid fermentation of metabolically engineered strains

Strain	substrate	Engineering strategy	Butyric acid yield	References
<i>Escherichia coli</i>	glucose	Knockout of the genes encoding the competing enzymes at the pyruvate node and genes encoding acetyl-CoA to other products	28.4 g/L (0.37 g/g glucose)	(Wang et al., 2019)
<i>Clostridium tyrobutyricum</i>	lignocellulosic hydrolysate	Inactivation of <i>hprK</i> and <i>xylR</i> together to eliminate carbon catabolite repression	12.4 - 13.4 g/L (0.32 – 0.40 g/g substrate)	(Fu et al., 2022b)
<i>Clostridium tyrobutyricum</i>	rice straw hydrolysate	Knockout of <i>ack</i> gene and overexpression of <i>cat1</i> gene	26.25 g/L	(Liu et al., 2021)
<i>Clostridium acetobutylicum</i>	glucose	Knockout of genes <i>adhE</i> , <i>hydA</i> , <i>ctfB</i> , <i>pta</i> and <i>buK</i>	32.5 g/L (0.39 g/g glucose)	(Jang et al., 2014)
<i>Clostridium saccharoperbutyl acetonicum</i>	lignocellulose-derived sugars	Knockout of genes <i>pta</i> and <i>bld</i> and overexpression of the gene encoding butyryl-CoA	14.3 g/L (0.6 mM/ mM sugars)	(Baur et al., 2022)

2.3.2 Butyric acid degradation

Butyric acid accumulation in AD system is not only related to its production, but also depends on its degradation (Liu et al., 2012b). However, there are very few studies on butyric acid degradation and its toxic effects on methane production.

2.3.2.1 Indicator

In AD, the accumulation of butyric acid could result in excessive acidification of digestate, which is one of the most common factors leading to the reactor instability and failure. The excessive acidification often leads to a pH drop, severely affects the microbial activity, and reduces the biogas production (Alavi-Borazjani et al., 2020). Many studies have suggested that butyric acid concentrations would be an effective indicator to monitor the process stability (Li et al., 2017; Nakakubo et al., 2008). When AD systems experience acidification, butyric acid concentrations can increase dramatically, rising up to 20 times from 0.06 to 1.30 g/L (Moset et al., 2012). Therefore, it's important to monitor the butyric acid accumulation level to avoid reactor failure. Additionally, the accumulation of butyrate inevitably affects the methane yield (Zhang et al., 2023b). Moset et al. (2012) reported a stronger inverse correlation between the methane yield and butyric acid concentrations compared to other VFAs ($R = -0.71$, $P < 0.05$) and the accumulation of butyric acid severely affected the methane yield than other VFAs. The maximum methane yield happened at butyric acid concentration of 1800 mg/L (Wang et al., 2009). Accelerating the degradation of butyric acid could substantially increase the daily methane yield; one study demonstrated a 16.6% improvement (Wang et al., 2020a). Therefore, it is essential to investigate the effects of butyric acid levels on AD performance and identify specific concentrations that inhibit methane production and consequently lead to reactor instability.

2.3.2.2 Factors affecting butyric acid degradation

Butyric acid is more difficult to be degraded than other VFAs since it can't be utilized by methanogens and its oxidation pathway is not thermodynamically viable. Butyric acid is degraded to acetic acid via β -oxidation as shown in Fig 2.2. As Eq. (2-1) shows, the oxidation of butyric acid to acetic acid is endergonic and thermodynamically unfavorable. The butyric acid degradation reaction usually is accomplished by the butyric acid oxidizing bacteria and methanogens (Amani et al., 2011; Golkowska and Greger, 2013). During this process, acetic acid and hydrogen are consumed by acetoclastic and hydrogenotrophic methanogenic archaea respectively, as shown in Eq. (2-3) and (2-4). With acetic acid and hydrogen consumption, the oxidation of butyric acid can occur and the overall reaction equation can be formulated as shown in Eq.(2-5), which is favorable under standard conditions (Montero et al., 2010). The intermediate metabolites including acetic acid and hydrogen could inhibit butyric acid degradation (Siriwongrungronson et al., 2007). Researchers have found that even though the

actual ΔG of butyric acid oxidation remained negative, the degradation of butyric acid was inhibited with increasing acetic acid and H_2 concentrations (Labib et al., 1992; Wu et al., 2022). Montero et al. (2010) observed that butyric consumption was related to hydrogenotrophic methanogens in the start-up stage, and to acetoclastic methanogens in the stabilization stage. Butyric acid degradation was found to be inhibited in high salinity owing to the reduction of methanogenesis (Yin et al., 2022). All these results indicate that the degradation of butyric acid and methane production are symbiotic processes. Therefore, any factors that affect methane production, in turn, would impact the degradation of butyric acid.



Prevailing literature indicates that a high ammonia concentration, especially in its free molecular form (NH_3) (FAN), is a major cause of inhibition of VFAs degradation and methane production in the AD process (Jiang et al., 2019). As shown in Eq. (2-6), FAN concentration is related to temperature, pH and TAN concentration. Hence, pH is a crucial factor that affects butyric acid degradation. Previous studies have found that methane production was inhibited when ammonia concentration exceeded 3.0 g TAN/L (Yenigün and Demirel, 2013). Additionally, an increase in ammonia concentration from 2.2 to 4.5 g TAN/L resulted in the gradual shift from the predominance of acetoclastic methanogens to hydrogenotrophic methanogens (Wang et al., 2022b). The accumulation of butyric acid was high, up to 1.5 g/L in AD using ammonia-acclimated sludge as inoculum (Dennehy et al., 2016). Ammonia inhibition of methanogenesis may also hinder butyric acid degradation, but there is little research on how ammonia specifically impacts butyric acid degradation. It's essential to explore the effect of TAN or FAN on the degradation of butyrate to acetate. Bonk et al. (2018) investigated the impact of ammonia on the degradation of VFAs and reported minimal impacts on butyrate degradation within an ammonia concentration range of 52 to 277 mM (equivalent to 0.73 to 3.88 g TAN/L). However, in AD with high-nitrogen substrate (manure, food waste or slaughterhouse waste), ammonia levels could be far higher than 3.88 g/L (Capson-Tojo et al., 2020). Therefore, the impact of ammonia inhibition on butyric acid degradation still requires further investigation.

$$FAN = TAN / \left[1 + 10^{\left(0.09018 + \frac{2729.72}{T+273.15} - pH \right)} \right] \quad (2-6)$$

where, *FAN* and *TAN* represent free ammonia concentration and total ammonia concentration, respectively, mg/L; *T* is the temperature, °C.

Temperature is crucial in anaerobic digestion. As previously mentioned in 2.3.1, temperature is a key factor influencing butyric acid production. Similarly, it also affects the degradation of butyric acid. Li et al. (2020a) explored the kinetic and thermodynamic effects of temperature on butyric acid degradation and found that butyric acid exhibited the same highest maximum microbial specific growth rates of 0.8 d⁻¹ at 37 °C and 55 °C. Interestingly, the methanogenesis of butyric acid increased at 55 °C, with a longer lag time compared to 37 °C, suggesting methanogenesis could be adaptable at 55 °C due to the syntrophic relationship between methanogenesis and butyric acid degradation. Additionally, butyric acid levels have a certain inhibition on microorganism. It was reported that butyric acid gradually began to accumulate when butyric acid concentration was as high as 3275.5 mg/L (Amani et al., 2011). However, in Xu et al. (2023) 's study, high butyric acid loading up to 3.6 g/L/d didn't affect butyric acid degradation and hydrogenotrophic methanogenesis was the main pathway to consume H₂.

2.4 Summary

This review comprehensively analyzes the factors influencing butyric acid degradation and production in anaerobic digestion, as well as the underlying mechanisms involved. Butyric acid degradation is not only a crucial step in the anaerobic digestion process but also significantly impacts the accumulation of butyric acid. Despite its importance, there is a noticeable gap in research specifically focused on the degradation of butyric acid. Furthermore, the review identifies key factors such as temperature, pH, and ISR, which influence butyric acid production. However, due to the variability in experimental conditions across all studies, the findings from the literatures are inconsistent, which underscores the need for further research to establish conditions that can reliably optimize butyric acid production and degradation in anaerobic systems.

Chapter 3
Ammonia-induced constraints on butyrate
degradation in anaerobic digestion: Impact of
ammonia levels and pH conditions, and recovery
behaviour

3.1 Introduction

The degradation of VFAs (propionate and butyrate) primarily occurs through acetogenic reactions facilitated by acetogenic bacteria. However, thermodynamic constraints in most acetogenic reactions (Table 3.1) and susceptibility to inhibition by metabolite accumulation, especially acetate and hydrogen, necessitate the formation of syntrophic associations between acetogenic bacteria and methanogenic archaea for the effective degradation of VFAs (Amend and Shock, 2001; Muller et al., 2010). Nevertheless, VFAs accumulation frequently occurs in anaerobic digesters, particularly under conditions of high organic loading rates (Wang et al., 2023a) and in response to environmental stressors (e.g., ammonia) (Capson-Tojo et al., 2020). This accumulation often leads to over-acidification, detrimentally affecting the methane yield and potentially causing AD process failure. Therefore, greater attention to VFA degradation during AD operations is imperative in practical applications.

Table 3.1 Reactions of butyrate and propionate degradation

Substrate	Reaction (pH=7, 1atm)	ΔG^θ (KJ/mol) 25°C
Propionate	$\text{CH}_3\text{CH}_2\text{COO}^- + 2\text{H}_2\text{O} \rightarrow \text{CH}_3\text{COO}^- + 3\text{H}_2 + \text{CO}_2$	+ 76.5
	$\text{CH}_3\text{CH}_2\text{COO}^- + 2\text{HCO}_3^- \rightarrow 2\text{CH}_3\text{COO}^- + \text{H}^+ + 3\text{HCOO}^-$	+72.4
Butyrate	$\text{CH}_3\text{CH}_2\text{CH}_2\text{COO}^- + 2\text{H}_2\text{O} \rightarrow 2\text{CH}_3\text{COO}^- + 2\text{H}_2 + \text{H}^+$	+48.1
	$\text{CH}_3\text{CH}_2\text{CH}_2\text{COO}^- + 2\text{HCO}_3^- \rightarrow 2\text{CH}_3\text{COO}^- + \text{H}^+ + 2\text{HCOO}^-$	+45.5

Butyrate accumulation has been observed in the AD of specific substrates. Dennehy et al. (2016) reported significant butyrate accumulation during the AD of food waste and pig manure. Moreover, this accumulation persisted without degradation, leading to concerns about its potential impact on the overall efficiency and stability of the AD process. Similarly, Peng et al. (2018) observed a gradual build-up of butyrate during the long-term high-solid AD of food waste. Previous studies have consistently indicated that butyrate accumulation occurs recurrently in animal manure digestion (Ao et al., 2021; Beneragama et al., 2013; Lu et al., 2019) and food waste digestion (Capson-Tojo et al., 2017; Kim et al., 2006; Kong et al., 2016). A plausible hypothesis for this recurring butyrate accumulation is its potential link to ammonia stress, considering that animal manure is nitrogen-rich feedstock and high

organic loading of food waste leads to elevated ammonia nitrogen levels (Ao et al., 2021; Capson-Tojo et al., 2017).

The impact of ammonia-induced inhibition on AD, particularly on methanogenesis, has been extensively investigated (Capson-Tojo et al., 2020). According to Wang et al. (2022), it has been observed that a low TAN concentration ranging from 1.0 to 4.0 g N/L led to irreversible inhibition of acetoclastic methanogens, while 50% inhibition of hydrogenotrophic methanogens occurred at TAN concentrations of 4.7-6.8 g N/L. Numerous studies have demonstrated that microorganisms participating in each stage of AD are impacted by ammonia inhibition, and methanogenic archaea appear to be more sensitive to ammonia stress compared to the majority of bacteria (Bonk et al., 2018). However, the influence of ammonia stress on anaerobic biodegradation of butyrate and the response of syntrophic butyrate oxidizing bacteria (SBOB) remain poorly understood. Furthermore, the factors leading to butyrate accumulation under high ammonia stress, whether due to metabolite build-up resulting from ammonia inhibition of hydrogenotrophic methanogenesis or direct ammonia toxicity affecting SBOB, require further investigation.

Traditionally, free ammonia (NH_3) has been considered more inhibitory in AD than ammonium ion (NH_4^+), due to its high permeability through bacterial cell membranes (Muller et al., 2006; Rajagopal et al., 2013). In most studies, the inhibitory effects have usually been examined through the assessment of free NH_3 and TAN, with comparatively less attention paid to ammonium ions (NH_4^+). However, recent findings by Wang et al. (2022b) suggest a greater role of NH_4^+ in the ammonia-induced inhibition of hydrogenotrophic methanogens, particularly at pH levels below 8.0, as indicated by inhibition modelling analysis.

Consequently, there is a need for further investigation into the distinct impacts of NH_4^+ and free NH_3 on the anaerobic biodegradation of butyrate. In addition, pH is another crucial operating factor, which affects the microbial growth rate and influences the distribution of NH_4^+ and NH_3 (Jiang et al., 2019); the NH_3 concentration was increased by eight folds when pH was increased from 7.0 to 8.0. pH range in AD systems for nitrogen-rich substrates is from 7.0 to 8.5 without adjustment, while researchers have found that it is not favourable for methanogenesis when pH is over 8.0 (Cai et al., 2021; Qiu et al., 2023). Furthermore, the recoverability of biodegradation of butyrate in AD subsequent to severe ammonia inhibition remains inadequately explored, necessitating in-depth examination to advance our understanding of the recovery process and ammonia-induced inhibition in AD systems.

Consequently, the primary objectives of this study were: (1) to elucidate the impacts of ammonia (TAN) concentration and pH on butyrate degradation, (2) to assess the individual inhibitory effects of NH_4^+ and free ammonia (NH_3) on butyrate degradation, and (3) to examine the potential reversibility of butyrate degradation following severe ammonia inhibition. This investigation aimed to deepen the understanding of ammonia inhibition on butyrate degradation in AD process. Such insights are expected to contribute significantly to the development of targeted strategies for mitigating ammonia inhibition and reducing butyrate accumulation in AD systems, thereby enhancing the efficiency and stability of the AD process.

3.2 Materials and methods

3.2.1 Anaerobic inoculum

The anaerobic inoculum is dewatered anaerobic sludge, taken from a local municipal wastewater treatment plant in Galway, Ireland. It was anaerobically stored in a cold room with an average temperature of 11 °C. Before being used in the experiments, the sludge was fed with glucose (2 g COD/L) every week for approximately six months at 37 °C to obtain high biomass activity. The specific methanogenic activity of the inoculum, using acetate as carbon source, was determined as 0.143 g COD/ g VSS/ d, indicating relatively good activity (Hussain and Dubey, 2017). Prior to incubation, the activated anaerobic sludge underwent three washes with phosphate buffer solution (PBS) to eliminate ammonia and remaining organic matter. The washed sludge after centrifugation had 11.90% total solids (TS) and 6.44% volatile solids (VS).

3.2.2 Experimental operation

In this study, two types of batch experiments were carried out: ammonia inhibition experiments and recovery experiments following ammonia removal. Serum bottles were served as bioreactors in both batch experiments with a working volume of 200 ml. Additionally, the sole carbon source was butyrate with 2 g COD/L. The initial butyrate concentration detected in reactors was 2288.77 mg COD/L. The concentrations of the medium added were: K_2HPO_4 1062.5 mg/L, NaH_2PO_4 467.84 mg/L, $\text{CaCl}_2 \cdot 2\text{H}_2\text{O}$ 150 mg/L, $\text{MgSO}_4 \cdot 7\text{H}_2\text{O}$ 200 mg/L, NaHCO_3 1000mg/L and 1mL/L trace elements. The trace element concentrations are as following: $\text{FeCl}_3 \cdot 3\text{H}_2\text{O}$ 1000 mg/L, $\text{CoCl}_2 \cdot 6\text{H}_2\text{O}$ 1000 mg/L, HBO_3 50

mg/L, $\text{CuCl}_2 \cdot 2\text{H}_2\text{O}$ 15 mg/L, $\text{MnCl}_2 \cdot 4\text{H}_2\text{O}$ 250 mg/L, ZnCl_2 50 mg/L, $\text{NaSeO}_3 \cdot 5\text{H}_2\text{O}$ 100 mg/L, $(\text{NH}_4)_6\text{Mo}_7\text{O}_{24} \cdot 4\text{H}_2\text{O}$ 90 mg/L, $\text{NiCl}_2 \cdot 6\text{H}_2\text{O}$ 50 mg/L, EDTA 1000 mg/L and 36% HCl 1 mL/L, as reported previously by Wang et al. (2022b). The pH condition in the reactors was adjusted by the addition of 2 M HCl or 2M NaOH. All bottles underwent a 5-minute purge with pure N_2 gas, were sealed with butyl rubber stopper and aluminum covers, and were then incubated at 37 °C with manual shaking twice a day. The batch experiments were considered complete when the butyrate levels in the reactors stabilized. All the experiments were conducted in triplicates.

Ammonia inhibition experiments were conducted under various ammonia concentrations and pH values, as detailed in Table 3.2. An inoculum to substrate (I/S) ratio of 5:1 (based on VSS: COD), was employed to ensure a robust population of acetogens and methanogens (Astals et al., 2018). Each serum bottle was introduced 38.4 mL of sludge and 161.6 mL of substrate. To obtain specific TAN concentrations, ammonia chlorides was introduced to the reactors, as chloride exhibited lower inhibition compared to ammonium (Wang et al., 2022b). The TAN concentration in food waste and animal manure digestion varies a lot, sometimes with extremely high TAN concentrations, for instance, ammonia concentration in food waste AD of over 5 g TAN/L (Zhang et al., 2017). In animal manure, especially in chicken manure, the ammonia concentration can be as high as 33.9 to 50 g TAN/ g dry matter (Fuchs et al., 2018; Molaey et al., 2018). Poirier et al. (2016) reported that methanogenesis was severely inhibited when TAN concentration was from 8.0 to 13.0 g TAN/L. Therefore, in this experiment, the TAN concentrations studied were 0.18, 2.0, 4.0, 8.0, 12.0, 16.0, 20.0 g N/L at pH 7.5, labelled as R1 to R7, respectively. Additionally, experiments to assess the impacts of varying pH levels (7.0, 7.5 and 8.0) were conducted at a TAN concentration of 4.0 g/L, labelled as R8, R9, and R10, respectively.

The recovery experiment, designed as R11, was carried out with 0.18 g TAN /L at pH 7.5. Prior to commencement, sludge from the R7 reactor, where severe inhibition was observed, underwent centrifugation at 6000 rpm for 15 minutes (Hettich® ROTOFIX 32A, Andreas Hettich GmbH & Co. KG, Germany). Subsequently, the sludge was thoroughly washed three times using PBS and then transferred into serum bottles to proceed with the recovery experiment.

Table 3.2 Experimental conditions for inhibition and recovery experiments

Batch experiments	No.	Inoculum	pH levels	TAN (g N·L ⁻¹)
	R1		7.5	0.18
	R2		7.5	2.0
	R3		7.5	4.0
	R4		7.5	8.0
Inhibition experiments	R5	anaerobic	7.5	12.0
	R6	sludge	7.5	16.0
	R7		7.5	20.0
	R8		7.0	4.0
	R9		7.5	4.0
	R10		8.0	4.0
Recovery experiments	R11	Refreshed sludge from R7	7.5	0.18

3.2.3 Model analysis

3.2.3.1 Kinetic model

To evaluate the effects of ammonia concentration on butyrate degradation kinetics, the first-order kinetic model and the modified Gompertz kinetic model were introduced for the simulation of butyrate degradation. In the first-order kinetic model, the rate of butyrate degradation was assumed to only be proportional to butyrate concentration, with a constant proportionality factor, as expressed in Eq. (3-1). Considering the diverse effects that may arise from varying concentrations of ammonia on butyrate degradation and microorganisms' activities, the modified Gompertz kinetic model, described in Eq. (3-2), was employed for the simulation (Wang et al., 2020b).

$$C(t) = C_0 \cdot (1 - \exp(-k \cdot t)) \quad (3-1)$$

$$C(t) = C_{max} \cdot \exp\left\{-\exp\left[\frac{\mu_m \cdot e}{C_{max}} \cdot (\lambda - t) + 1\right]\right\} \quad (3-2)$$

where, $C(t)$: butyrate degradation concentration at a certain time (t) (mg COD/L); k : the first-order degradation rate (d^{-1}); t : time (d); and C_0 : initial butyrate concentration (mg COD/L);

C_{max} : maximum butyrate degradation concentration (mg COD/L); μ_m : maximum butyrate degradation rate (mg COD/L/d); λ : lag phase (d); e : Euler's Number (2.7183).

3.2.3.2 Inhibition model

To evaluate the inhibition degree from different ammonium species (NH_4^+ and NH_3), the inhibition model (Eq. (3)) was introduced. I_X ($I_{NH_4^+}$ or I_{NH_3}) represents the inhibition degree caused by NH_4^+ or NH_3 . $I_{NH_4^+}$ and I_{NH_3} were calculated based on a simple and modified Monod inhibition model can be expressed in Eq. (3-4) and Eq. (3-5), respectively (Wang et al., 2022). The simple inhibition model (Eq. 3-4) considered that ammonia inhibition is a non-competitive inhibition. In the modified Monod model (Eq. 3-5), a new parameter m was introduced, representing the strong increase of the inhibition with increasing free ammonia or ammonium concentration.

$$\mu = \mu_{max} \cdot I_{NH_4^+} \cdot I_{NH_3} \quad (3-3)$$

$$I_X = \frac{P_X}{P_X + C_X} \quad (3-4)$$

$$I_X = \frac{P_X^m}{P_X^m + C_X^m} \quad (3-5)$$

where μ is butyrate degradation rate (mg/L/d); μ_m is the maximum butyrate degradation rate (mg/L/d); C_X is the concentration of NH_4^+ or NH_3 (mg N/L); P_X ($P_{NH_4^+}$ or P_{NH_3}) is the concentration of NH_4^+ or NH_3 that halves the maximum butyrate degradation rate (mg N/L).

3.2.4 Analytical method

TS and VS were determined according to the standard methods (APHA, 2012). pH was analyzed using a digital pH meter (PHS-3C, Leici, Shanghai, China). The liquid samples were centrifuged at 10,000 rpm for 5min (Hettich® ROTOFIX 32A, Andreas Hettich GmbH & Co. KG, Germany) and were filtered using 0.45 μ m nylon syringe filters before determining ammonia and VFAs concentrations. TAN concentration was measured using a nutrient analyzer (Gallery plus, Thermo Clinical Lab systems, Finland). Free ammonia concentration was calculated using Eq. (2-6). VFAs (acetate, propionate, iso-butyrate, butyrate, iso-valerate and valerate) were determined using gas chromatography (GC 8860,

Agilent Technologies, USA) equipped with a DB-FFAP column (25 m × 320 μm × 0.5 μm, Agilent Technologies, USA) and a flame ionization detector (FID). The temperature of the column was set at 80 °C for 2 min, then increased to 200 °C at a rate of 10 °C /min and held at 200 °C for 1 min. The carrier gas was hydrogen at a flow rate of 1.2 mL/ min. The injector and detector were operated at 250 °C. The composition of biogas including H₂, CH₄ and CO₂ were analyzed by gas chromatography (GC 7890A, Agilent Technologies, USA) referring to previous studies (Wang et al., 2021a; Wang et al., 2020b). The pressure in the headspace of each serum bottle was measured with a pressure manometer (Testo 512, Testo, USA). The volume of CH₄ was calculated based on biogas pressure and CH₄ concentration, following the methodology developed by Santos et al. (2020). Subsequently, this volume was converted to the standard volume under standard condition (0 °C and 1 atm), as expressed in Eq. (3-6).

$$V_{CH_4} = V_H \cdot \frac{P+1013.25}{1013.25} \cdot \frac{273.15}{273.15+T} \cdot C_{CH_4} \quad (3-6)$$

where, V_{CH_4} is CH₄ volume at standard condition (NmL at 1atm and 273.15K), V_H is the headspace volume of serum bottle (mL), P is the headspace pressure at t day (hPa), C_{CH_4} is the CH₄ concentration in the headspace of the serum bottle. Note: Water vapor in the biogas was not explicitly corrected in this study. At 37°C, saturated water vapor contributes approximately 6.3 kPa to the total pressure (ca. 3–5% of the total volume under typical conditions). This may cause a slight overestimation of methane yield. However, since all treatments were measured under identical conditions, this does not affect the comparative conclusions.

The activity of electron transport system (ETS) was analyzed using the 2-(p-iodophenyl)-3-(p-nitrophenyl)-5-phenyltetrazolium chloride-electron transport system (INT-ETS) method (Lizama et al., 2019). Extracellular polymeric substances (EPS) extraction was performed following the heat-extraction method (Shen et al., 2022) and the methodologies for carbohydrate and protein measurements (Nielsen, 2017; Qi et al., 2023). The Gibbs free energy calculations for butyrate and acetate oxidation at 37 °C under different ammonia concentrations were conducted using the Nernst and van't Hoff equations.

3.2.5 Data statistical analysis

All experimental results were expressed as mean \pm standard deviation. Figures were generated, and non-linear curve fitting was conducted for both kinetic model and inhibition models using OriginPro 2021 software.

3.3 Results and discussion

3.3.1 Anaerobic digestion performance

3.3.1.1 Butyrate degradation and methane production

In this study, the impacts of ammonia concentration and pH on both butyrate degradation and methane production were explored. As shown in the Fig. 3.1(a), the degradation of butyrate exhibited sensitivity to varying levels of ammonia concentration. Although butyrate can be completely degraded at high TAN level (up to 8.0 g N/L), the time required for complete degradation significantly increased with higher TAN concentrations. Specifically, the requisite time for complete degradation time was observed to be 8 days at a TAN concentration of 0.18 - 2.0 g N/L, 10 days at 4.0 g N/L, and 23 days at 8.0 g N/L. When the initial ammonia concentration exceeded 12 g TAN/L, butyrate degradation was severely inhibited, leading to the prevention of complete degradation. The ultimate degradation rates of butyrate were determined to be 95.1%, 94.3% and 11.3% at TAN concentration of 12.0 g N/L, 16.0 g N/L and 20.0 g N/L TAN, respectively. In a related study, Bonk et al. (2018) investigated the impact of ammonia on the degradation of VFAs and reported minimal impact on butyrate degradation within an ammonia concentration range of 52 to 277 mM (equivalent to 0.73 to 3.88 g TAN/L). However, when the ammonia concentration was increased to 8.0 g TAN/L or higher, significant prolongation or even complete inhibition was observed. These findings are consistent with the observations in the present study.

The cumulative methane production resulting from butyrate degradation under varying TAN concentrations is illustrated in Fig. 3.1b. The maximum cumulative methane volume, approximately 120 NmL, was attained between days 14 and 18 at ammonia concentrations of 0.18 - 4.0 g TAN/L. As the ammonia concentration exceeded 4.0 g TAN/L, the rate of methane production gradually decreased along with increasing ammonia concentration. Notably, even at 8.0 g TAN/L, the maximum methane yield remained at 120 NmL. However, achieving this yield took a longer time (approximately 90 days) with obvious fluctuation in

AD system, as evidenced by the large error bars in Fig. 3.1. This instability in methane production may be attributed to the erratic activity of methanogens. Methanogens would be adapted to ammonia inhibition after a prolonged lag phase when ammonia concentration was high, up to 6.8 g TAN/L (Agyeman et al., 2021). At 8.0 g TAN/L, methanogens encountered significant challenges in overcoming ammonia inhibition, leading to unstable methane production. In addition, further increases in ammonia concentrations led to the severe inhibition of methane production. At 20.0 g TAN/L, methane was undetectable in the reactors, indicating complete inhibition of methane production, despite marginal butyrate degradation observed (Fig. 3.1a). In R5 with 12.0 g TAN/L, butyrate degradation was initially impeded, however, after 20 days, the degradation process proceeded consistently, achieving a degradation rate of approximately 95%. Despite this, only approximately 23 NmL of methane was produced upon completion of butyrate degradation. This observation may be attributed to the heightened sensitivity of acetate metabolism (or acetotrophic methanogenesis) to ammonia exposure, as indicated in Fig 3.2. Fig. 3.2 demonstrates the sequential oxidation of butyrate to acetate, followed by the conversion of acetate to methane in the absence of inhibitory factors. The concentration of acetate initially rose, followed by a gradual decrease, with complete degradation observed in R1-R4 with TAN below 4.0 g N/L. Conversely, in R5 and R6, despite the near-complete degradation of butyrate by the end of the reaction, an accumulation of acetate up to 1500 mg COD/L was observed. These results suggest that the degradation rate of butyrate was not hindered by the accumulation of acetate. Furthermore, these findings underscore the greater sensitivity of methanogenic archaea to ammonia stress compared to butyrate-degrading bacteria. Previous studies have indicated that methane production is inhibited when ammonia concentration exceeds 3.0 g TAN/L (Yenigün and Demirel, 2013). Additionally, an increase in ammonia concentration from 2.2 to 4.5 g TAN/L can result in the gradual shift from the predominance of acetoclastic methanogens to hydrogenotrophic methanogens (Gao et al., 2015; Wang et al., 2022b).

Fig. 3.1 c and d illustrate the effects of varying pH (7.0, 7.5 and 8.0) on both butyrate degradation and methane production at a TAN concentration of 4.0 g N/L. In R8-R10, while maintaining the same TAN concentration, free ammonia concentrations were increased from 50.6 to 454.5 mg/L as pH rose from 7.0 to 8.0. The results indicate that the time needed for the complete degradation of butyrate remained constant at 9 days, regardless of the pH variation within the range of 7.0 to 8.0. This suggests that under these conditions, pH

variation did not significantly influence butyrate degradation. However, the impact on methane production exhibited a progressively deepening trend with the increase of pH, although the maximum cumulative methane yield appeared to slightly decrease. The maximum cumulative methane yield was obtained on days 13, 15 and 20 at pH levels of 7.0, 7.5 and 8.0, respectively. Given that the TAN concentrations in R8 - R10 were constant, it can be inferred that methane production was affected by both free ammonia concentration and pH value. Compared to butyrate degradation, methane production may be more sensitive to variations in free ammonia concentration.

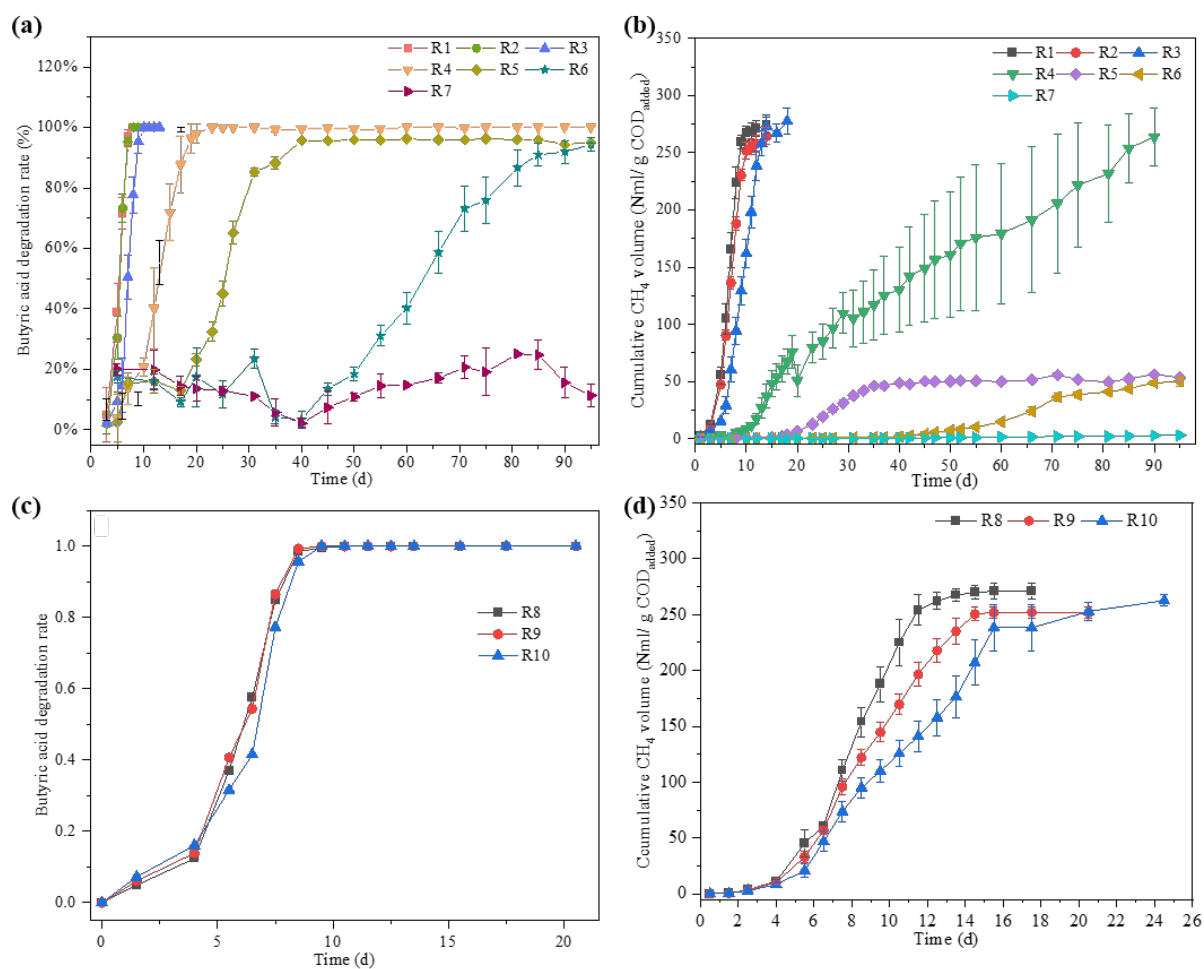


Figure 3.1 Effects of ammonia concentration and pH on anaerobic butyrate degradation and methane production: (a) butyrate degradation, (b) methane production at different TAN concentrations (0.18 – 20.0 g N/L); (c) butyrate degradation, (d) methane production at pH levels (7.0, 7.5 and 8.0)

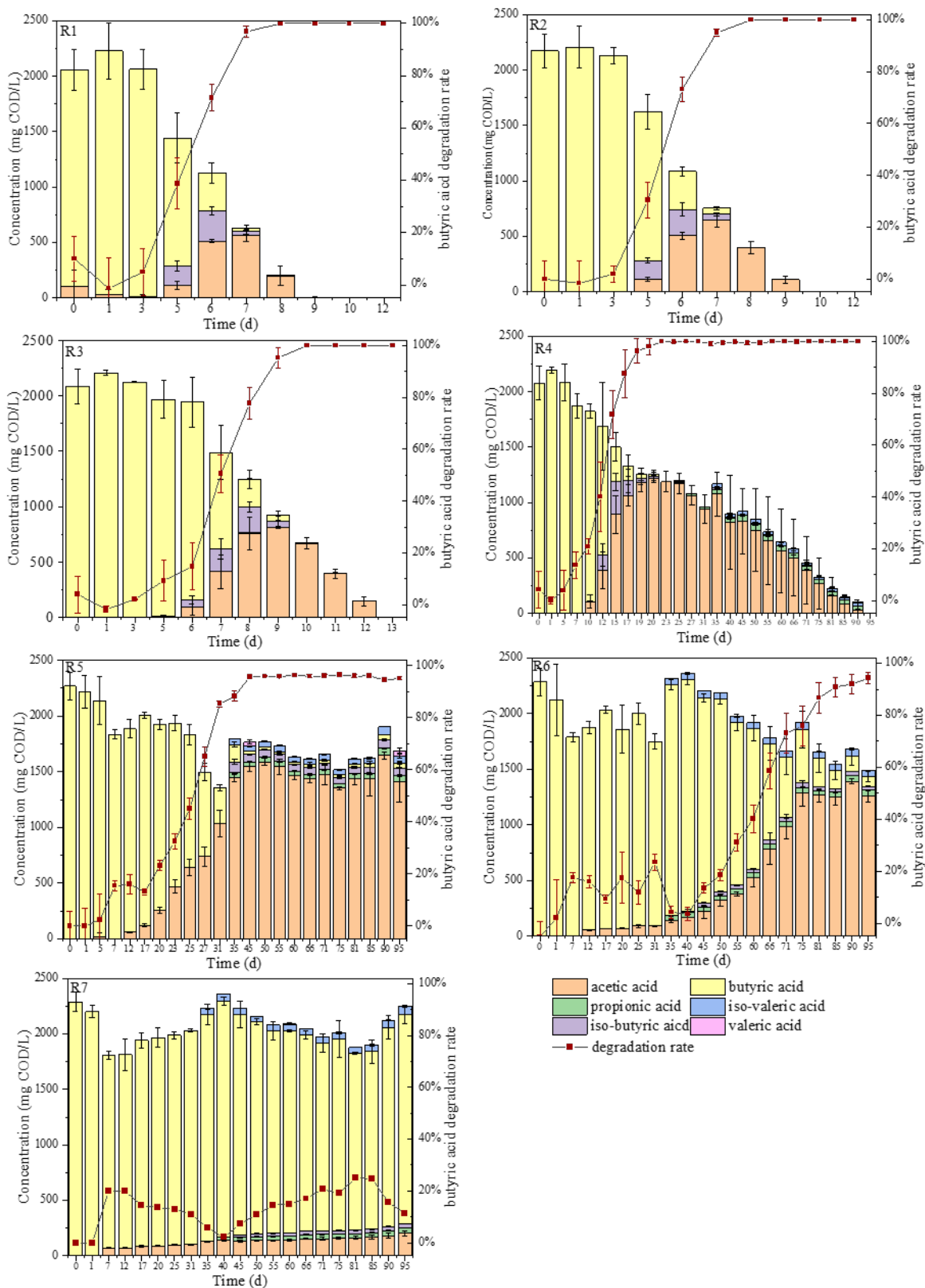


Figure 3.2 VFAs composition change in the entire process at different ammonia concentrations

3.1.1.2 Extracellular polymeric substances and INT- electron transport system

Ammonia-induced stress was found to hinder the degradation of butyrate and methane production in AD. This inhibition, at varying levels of ammonia, is potentially linked to the activity and performance of bacteria such as SBOB and methanogen (Liu et al. 2024). To delve deeper into how ammonia levels would affect the anaerobic degradation of butyrate, the properties of EPS and INT-ETS were examined under different ammonia conditions.

EPS refers to a complex polymer mixture of macromolecules present extracellularly in microbial aggregates, derived from microbial cell autolysis, cell secretion, and cell surface abscission (Comte et al., 2006). EPS serves as an external protective layer for cells, particularly under stress, and plays a crucial role in enzyme accumulation and intercellular communication (Ramesh et al., 2006). EPS structures can be classified into three layers: soluble EPS (SMP), loosely bound EPS (L-EPS), and tightly bound EPS (T-EPS) (Tang et al., 2020). Carbohydrate and protein are the primary constituents of EPS. Fig. 3.3a illustrates the concentrations of carbohydrates and proteins across the different EPS layers. The total EPS concentration in R1-R5 increased from 114.8 to 153.0 mg/L, as ammonia concentrations were increased from 0.18 to 12.0 g N/L, suggesting an increase in bacterial EPS secretion to form a protective barrier against ammonia toxicity. Additionally, the increase in ammonia concentration, which inherently increases alkalinity (Sterling Jr et al., 2001), can cause ionization of charged groups, leading to enhanced production of proteins and carbohydrates in EPS (Ping et al., 2018). Conversely, in R6 and R7, total EPS concentration decreased, likely due to excessive ammonia concentration levels destabilizing microbial aggregates (Mikkelsen and Nielsen, 2001). The protein content, accounting for 57%-75%, was significantly higher than that of carbohydrates. The rapid increase in the protein content suggests that bacteria trend towards producing enzymes adapted to ammonia concentration from 0.18 to 12.0 g TAN/L, such as the existence of a significant quantity of exoenzymes (Frølund et al., 1995). Additionally, as the ammonia concentration was increased, the protein content increase in SMP was more pronounced than in L-EPS and T-EPS. The increase in NH_4Cl concentration, leading to higher salinity, would result in the accumulation of SMP, especially proteins (Li et al., 2013).

INT-ETS is indicative of the dehydrogenase activity of the sludge, which is linked to the respiratory activity of microorganisms such as methane production and butyrate degradation

(Tian et al., 2017; Yin et al., 2018). Fig. 3.3b demonstrates the ETS activity at varying ammonia concentrations. Compared to R1, the ETS activity rose in all reactors, indicating that ammonia concentration increased microbial interspecies electron transfer activity. In R1 to R5, butyrate was completely degraded after different adaption time and in these reactors ETS activities were significantly increased from 7.49 to 10.39 $\mu\text{g}/(\text{mL}\cdot\text{min})$ ($p < 0.05$). The results showed that the microbial interspecies electron transfer process was stimulated to address ammonia inhibition after certain time adaption. Whereas ETS activity decreased in R6 and R7 and was still higher than R1, too high ammonia concentration may cause the decay in SBOB and the severe inhibition on the activities of key enzymes related to acetogenesis and methanogenesis, such as acetate kinase and coenzyme F₄₂₀ (Tian et al., 2017).

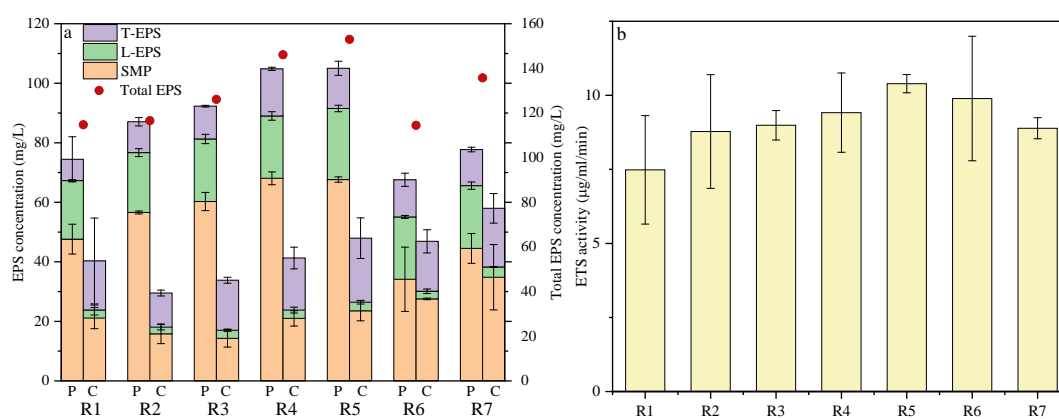


Figure 3.3 EPS concentration (a) and ETS activity (b) of substrate with different ammonia concentration. P: protein. C: carbohydrate.

3.3.2 Thermodynamics and kinetics of butyrate degradation

3.3.2.1 Thermodynamics evaluation of butyrate degradation

The degradation of butyrate to acetate is endergonic under standard conditions, as indicated by a positive Gibbs free energy change ($\Delta G^{\theta} > 0$) (Muller et al., 2010). This process is primarily driven by the reduction of partial hydrogen pressure and acetate concentration, ensuring a negative actual Gibbs energy change (ΔG) to facilitate the reaction (Labib et al., 1992; Siriwongrungron et al., 2007). Notably, the degradation of butyrate remains unaffected by the acetate accumulation within the ammonia concentration range of 0.18- 16.0 g N/L. Fig. 3.4 illustrates the actual ΔG of butyrate degradation ($\text{CH}_3\text{CH}_2\text{CH}_2\text{COOH} + 2\text{H}_2\text{O} \rightarrow \text{CH}_3\text{COOH} + 2\text{H}_2$) at various ammonia concentrations. Thermodynamic analysis reveals that

the actual ΔG value of butyrate degradation was in the range of $-50 \sim -300$ KJ/mol throughout the process under different ammonia concentrations. The negative ΔG indicates that butyrate anaerobic degradation was thermodynamically spontaneous, even at high ammonia concentrations. Consequently, the observed inhibition of butyrate degradation under specific ammonia conditions (exceeding 4.0 g TAN/L) was not attributed to the buildup of metabolites such as hydrogen and acetate, which usually takes place when methanogenesis is inhibited at high ammonia levels. Instead, it arose from the diminished activity of butyrate-degrading bacteria due to the presence of high ammonia concentrations (exceeding 4.0 g TAN/L). It is noteworthy that the actual ΔG value of butyrate degradation differed from the results ($-40 \sim -60$ KJ/mol) obtained by Li et al. (2020) at 35 °C. This disparity might be attributed to higher operating temperature and the lower acetate concentrations and hydrogen partial pressures in this experiment.

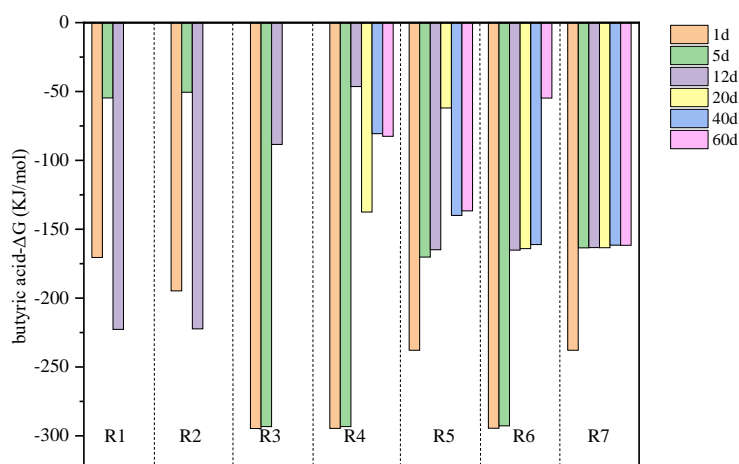


Figure 3.4 Gibbs energy of butyrate oxidation

3.3.2.2 Kinetics of butyrate degradation

The utilization of kinetic modelling provides insights into the dynamic aspects of the butyrate degradation process under varying ammonia concentrations. Based on the preceding findings (Section 3.3.1) that indicate pH variations within the range of pH 7.0-8.0 had negligible effects on butyrate degradation, the kinetics analysis focused solely on the impact of ammonia stress. Therefore, butyrate degradation process was simulated using the first-order kinetic model and modified Gompertz model were employed to systematically explore under varying TAN concentrations, as illustrated in Fig. 3.5.

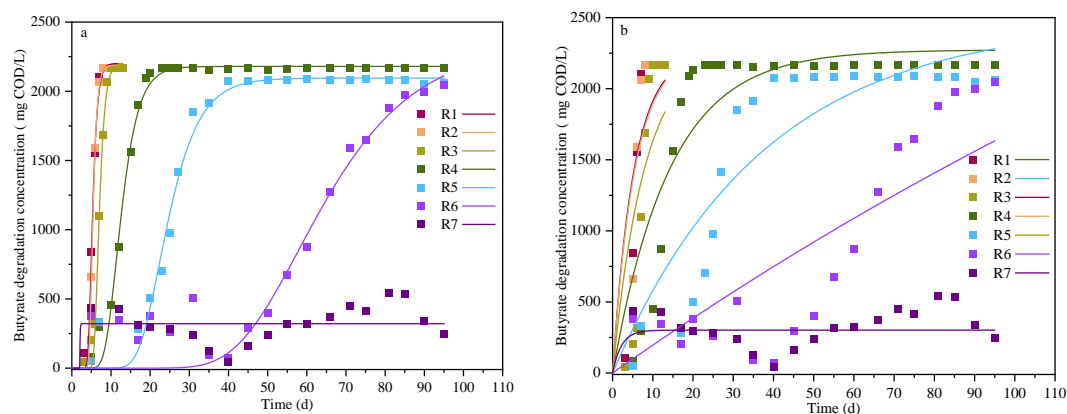


Figure 3.5 Butyrate degradation concentration under different ammonia concentration with different models. (a): Gompertz model; (b): modified first-order kinetic model.

The kinetic parameters of the first order and modified Gompertz models are detailed in Table 3.3. The results indicate that both models effectively describe butyrate degradation under all ammonia concentrations with the range of 0.18 - 16.0 g TAN/L, except for the extreme condition in R7 (20.0 g TAN/L), where almost no butyrate was degraded due to severe ammonia inhibition. Upon comparative analysis of the two models, it is evident that the modified Gompertz model exhibits superior fitting with the measured data, with all R^2 values being greater than 0.92 (shown in Table 3.3). C_{max} and μ_m are related to the predicted butyrate degradation potential and maximum butyrate degradation rate, respectively, while λ represents the lag phase time of butyrate degradation. The variation of C_{max} , μ_m and λ at different ammonia concentrations are illustrated in Fig. 3.6 (excluding R7, as the model did not work in R7 due to severe ammonia inhibition). Analysing the results depicted in Fig.3.6 and table 3.3, it is apparent that with increasing ammonia concentration, the predicted butyrate degradation potential undergoes a subtle transition from 2095.5 to 2432.4 mg COD/L. In contrast, the maximum butyrate degradation rate experiences a gradual decline from 965.8 to 52.9 mg COD/L/d. Simultaneously, the lag phase time of butyrate degradation exhibits a gentle increase from 4.2 d to 41.8 d. These observations suggest the sensitivity of SBOB to ammonia exposure, with increasing inhibition of their activity when ammonia concentration increased from 0.18 to 16.0 g TAN/L. However, SBOB demonstrates the ability to adapt to ammonia inhibition, eventually achieving a consistent butyrate degradation capacity after adaption. Notably, with rising TAN concentrations, SBOB necessitates an extend duration to acclimate to escalating ammonia stress. At a TAN concentration of 20.0 g N/L, SBOB experiences severely inhibited, resulting in almost no butyrate degradation. From

the value of C_{max} , it is evident that the maximum butyrate degradation concentration is approximately 2400 mg COD/L. This concentration exceeds the initial butyrate concentration of 2288.77 mg COD/L, indicating a greater potential for butyrate degradation.

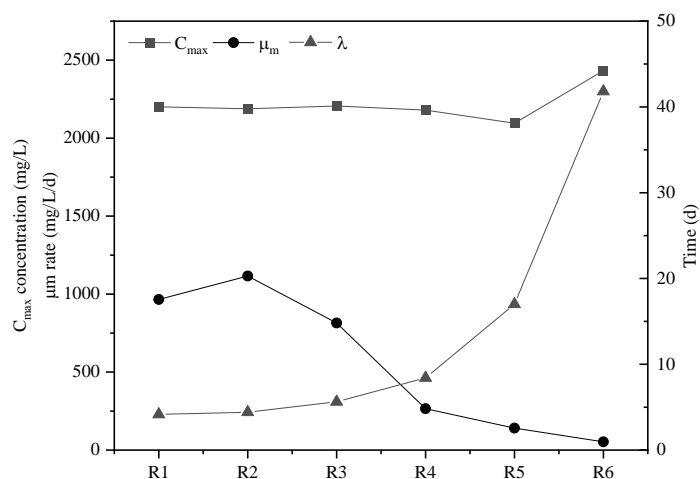


Figure 3.6 Variation in C_{max} , μ_m and λ at different ammonia concentrations

Table 3.3 Kinetic parameters of first order and modified Gompertz models

No.	First-order model			Modified Gompertz model			
	C_0	k	Adj. R^2	C_{max}	μ_m	λ	Adj. R^2
R1	2254.102	0.188	0.8289	2200.760	965.841	4.153	0.9879
R2	2257.382	0.182	0.8242	2187.819	1116.257	4.416	0.9992
R3	2283.601	0.125	0.7767	2206.176	814.875	5.638	0.9938
R4	2273.168	0.0703	0.8606	2179.503	265.597	8.420	0.9924
R5	2478.503	0.0266	0.8745	2095.487	140.932	17.000	0.9779
R6	6256.305	0.00318	0.8296	2432.375	52.911	41.802	0.9198
R7	301.511	0.458	0.3455	321.065	1967.590	2.002	0.3941

Note: k : d^{-1} ; C_0 : mg COD/L; C_{max} : mg COD/L; μ_m : mg COD/L/d; λ : d.

3.3.3 Inhibition model

In AD systems utilizing nitrogen-rich substrates such as manure and slaughterhouse wastewater, ammonia emerges as a prevalent inhibitor, including free ammonia (NH_3), and ammonium ion (NH_4^+). Extensive research has been conducted on the inhibitory effects of

ammonia inhibition, primarily on methane production and acetate degradation (Yellezuome et al., 2022). Nonetheless, the impact of ammonia on butyrate degradation has received limited attention, with rare exploration into the inhibition degree attributed to different ammonia species (Bonk et al., 2018). Therefore, both simple and modified Monod models were employed to evaluate ammonium and free ammonia inhibition on butyrate degradation. As detailed in Table 3.4, the Adj. R^2 for two models were 0.863 and 0.998, respectively. The superior fit of the modified Monod inhibition model to the experimental results led to its selection for further investigation. The results from the modified Monod model demonstrated that the concentrations of NH_4^+ or NH_3 , which induced a 50% inhibition of butyrate degradation, were 6606.0 ± 187.8 mg N/L and 673.3 ± 56.3 mg N/L, respectively. Additionally, at a TAN concentration of 6606.0 mg N/L and at pH 7, the calculated NH_3 concentration using Eq. (2-6) was at 257.4 mg N/L. Remarkably, this calculated NH_3 concentration was lower than the predicted NH_3 concentration (P_{NH_3}), indicating a heightened sensitivity of SBOB to NH_4^+ compared to NH_3 .

To evaluate the individual inhibitory effects of NH_4^+ and NH_3 on butyrate degradation, a new index, the ratio of $I_{\text{NH}_4^+}/I_{\text{NH}_3}$ was introduced. Fig. 3.7 illustrates the ratios of $I_{\text{NH}_4^+}/I_{\text{NH}_3}$ for butyrate degradation under varying ammonia concentrations. The ratio of $I_{\text{NH}_4^+}/I_{\text{NH}_3} = 1$ indicates that NH_4^+ and NH_3 have equivalent contribution to the inhibition, while $I_{\text{NH}_4^+}/I_{\text{NH}_3} > 1$ signifies a greater contribution from NH_3 , and $I_{\text{NH}_4^+}/I_{\text{NH}_3} < 1$ indicates more contribution from NH_4^+ to the inhibition. As shown in Fig. 3.7, the observed ratios of $I_{\text{NH}_4^+}/I_{\text{NH}_3}$ at all ammonia concentrations were less than 1, indicating a greater contribution from NH_4^+ to the inhibition. Specifically, the contribution of NH_4^+ to the inhibition intensified with increasing ammonia concentration, concurrent with a decreasing contribution from free ammonia. Despite at 20.0 g TAN/L (equivalent to 779.2 mg NH_3 -N/L), the contribution from NH_3 rose but the ratio remained below 1. It is noteworthy that NH_3 concentration is influenced by pH, and reducing pH can decrease NH_3 concentration while favouring the presence of NH_4^+ . The findings suggest that pH control is likely not an effective strategy for mitigating ammonia inhibition in butyrate degradation. This underscores the necessity for a comprehensive and integrated approach to ammonia mitigation measures in AD system.

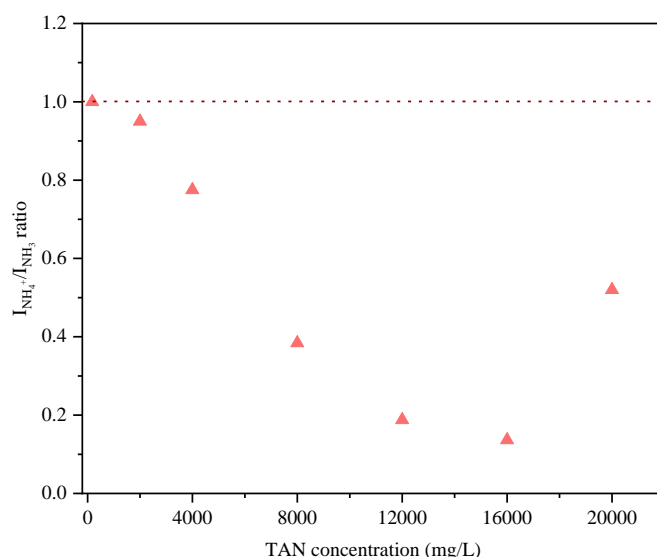


Figure 3.7 $I_{NH_4^+}/I_{NH_3}$ ratios for butyrate degradation under different ammonia concentrations

Table 3.4 Model parameters of simple and modified Monod model

Parameters	Simply Monod model	Modified Monod model
μ_m (mg/L/d)	191.71	166.94
$K_{NH_4^+}$	11211.46	6606.02
K_{NH_3}	436.68	673.28
n_1	-	2.47
n_2	-	13.79
Adj. R^2	0.8634	0.9983

3.3.4 Recovery after ammonia removal

A severe inhibition of butyrate degradation was observed at 20.0 g TAN/L. Subsequently, a recovery experiment was conducted to investigate the restoration of butyrate degradation and methane production after reducing the ammonia concentration from 20.0 to 0.18 g TAN/L. As shown in Fig. 3.8, both butyrate degradation and methane production were observed following the reduction in ammonia concentration. The recovery of the activity of methanogenic archaea and SBOB appeared to be a gradual process, necessitating an extended duration. In comparison to the control condition (R1) without ammonia inhibition, the time required for complete butyrate degradation was extended to approximately 20 d after removal of acute ammonia stress, with a lag phase time of around 9 d. Additionally, the cumulative

methane volume was decreased to 62.8 NmL from 125.5 NmL in R1, and the lag phase time for methane production was approximately 13 d. These results indicate that an extremely high ammonia concentration, such as 20.0 g TAN/L, led to irreversible inhibition to the activity of methanogens. Conversely, SBOB demonstrated full recovery of its activity from severe ammonia inhibition, provided that a prolonged adaption time was allowed.

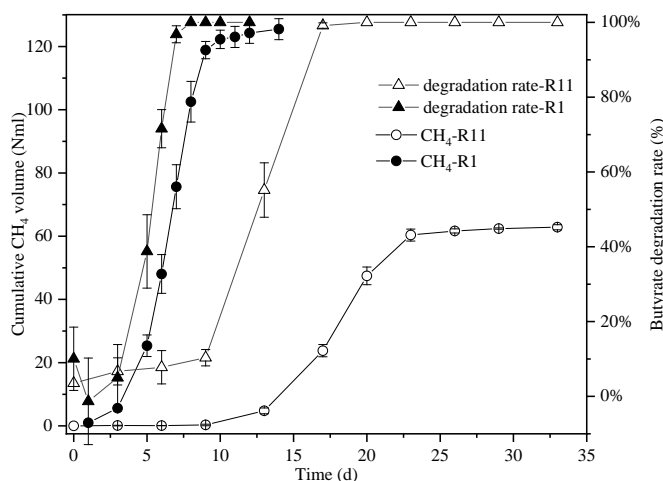


Figure 3.8 Recovery of methane production and butyrate degradation after severe ammonia inhibition

3.4 Conclusions

This chapter has demonstrated that the anaerobic degradation of butyrate experienced remarkable inhibition when TAN exceeded 8.0 g N/L at pH 7.5, while no discernible impacts were observed at pH 7.0 - 8.0 with 4.0 g TAN/L. Additionally, it was found that the lag phase for butyrate degradation was prolonged with increasing ammonia concentration. Notably, the complete recovery of butyrate-degrading bacteria was observed following severe ammonia inhibition, provided that an extended adaption period was allowed. Our findings indicate that NH_4^+ emerges as the predominant inhibitory factor within the TAN range of 2.0 - 20.0 g N/L, rather than NH_3 . The study also reveals that the inhibition of butyrate degradation caused by high ammonia concentration cannot be mitigated by simple lowering the pH level. Consequently, implementing an extended HRT strategy is recommended to mitigate the accumulation of butyrate in AD of nitrogen-rich substrates.

Chapter 4
Microbial transitions and degradation pathways
driven by butyrate concentration in mesophilic and
thermophilic anaerobic digestion under low
hydrogen partial pressure

4.1 Introduction

The substantial increase in fossil fuel consumption resulting from rapid industrial development has exacerbated climate change and caused energy shortages, thus necessitating a transition to renewable energy sources. Anaerobic digestion (AD) emerges as a sustainable and cost-effective waste treatment technology that not only treats organic waste but also recovers energy, such as biogas (Tisocco et al., 2024). Biogas, a clean alternative to fossil fuels produced from household, agriculture, and industrial waste, can considerably reduce greenhouse gas emissions (Zhang et al., 2021b). The AD process consists of four sequential and parallel processes: hydrolysis, acidogenesis, acetogenesis, and methanogenesis.

Acetogenesis and methanogenesis are commonly viewed as the rate-determining steps for most soluble organics, which are crucial for the efficiency of the AD system (Wang et al., 2021b). A major challenge in AD is the timely degradation of short-chain volatile fatty acids (VFAs) that are produced during the acetogenesis process. Ineffective degradation of these acids can hinder methane production and affect the stability of the AD process, which limits the practical application of AD technologies (Ferguson et al., 2016).

Despite extensive research on the degradation of propionate and acetate (Pan et al., 2021; Sitthi et al., 2022), the degradation of butyrate remains less explored. Butyrate, produced during acidogenesis, plays a crucial role in the subsequent stages of acetogenesis and methanogenesis. Its degradation primarily occurs through syntrophic interactions involving butyrate-oxidizing bacteria and methanogens due to thermodynamic constraints (Nikitina et al., 2022). Therefore, butyrate accumulation in AD systems is likely to happen when intermediates such as hydrogen and acetate build up due to the ineffectiveness of methanogenesis. Excessive butyrate can lower pH levels, create unfavourable conditions for microbial growth and potentially lead to reactor failure (Moset et al., 2012). Thus, monitoring butyrate levels could serve as an effective early indicator of stability of AD systems (Wu et al., 2022). When AD systems experience acidification, butyrate concentrations can increase dramatically, rising to 20-fold from 0.06 to 1.30 g/L (Moset et al., 2012). However, in a stable AD of food waste and pig manure, a high butyrate concentration of up to 2.2 g/L was observed (Dennehy et al., 2016). These varying thresholds underscore the critical importance of managing butyrate levels to ensure system efficiency. However, there is limited research on how elevated butyrate levels affect its own degradation within AD systems, especially on

its degradation pathways. The accumulation of butyrate inevitably affects the methane yield, as well as AD process efficiency and stability (Xu et al., 2023). A stronger inverse correlation between the methane yield and the butyrate concentration compared to other VFAs ($R = -0.71$, $P < 0.05$) was reported (Moset et al., 2012). Accelerating butyrate degradation has been shown to markedly enhance the daily methane production, with one study reporting a 16.6% increase in the methane yield (Wang et al., 2020a). Consequently, it is essential to examine the influence of butyrate levels on the AD performance and identify specific concentrations that inhibit methane production and lead to reactor instability.

Butyrate degradation and methane production are highly sensitive to operational conditions, particularly temperature, due to its notable influence on the metabolic activity and the growth of microorganisms during the AD process (Chen et al., 2024; Nie et al., 2021). It has been widely explored how temperature affects methanogenesis. For instance, the optimal temperature for methane production in AD was found to be 37 °C (Cao et al., 2020), and the predominate methanogens were *Methanoculleus* and *Methanothermobacter* at 37 °C and 55 °C, respectively (Chen and Chang, 2020). However, there have been limited studies focusing on the butyrate degradation process. Butyrate degradation and methanogenesis involve syntrophic interactions, and syntrophic butyrate-degrading microbes such as *Syntrophomonas* and *Methanotherrix* have been reported (Ziels et al., 2019). Li et al. (2020a) analysed the kinetic impact of temperature on butyrate degradation, which produces substrates for methanogenesis, and found that the rate of methane production by butyrate degradation was higher at 35 °C than at 55 °C. However, it is unclear how temperature regulates butyrate degradation, especially the functional microbial species at different temperatures. Therefore, it's important to investigate the microbial structure and the metabolic pathway of butyrate degradation at varying temperatures.

A deeper insight into the mechanisms of methane production and butyrate degradation will contribute to improvements in the diagnostic methods of AD and enable timely preventative measures. Therefore, the objectives of this study were to (1) examine the effects of butyrate levels and temperature on methane production and butyrate degradation, and (2) analyse microbial community characteristics and butyrate degradation pathways at varying butyrate concentrations under both mesophilic and thermophilic conditions. Through comprehensive analysis, this study aimed to achieve a deeper understanding of methane generation and

butyrate degradation at different butyrate concentrations and to provide valuable insights that could improve the performance of AD systems.

4.2 Materials and methods

4.2.1 Anaerobic inoculum

Dewatered anaerobic sludge, sourced from a mesophilic anaerobic digester at a local municipal wastewater treatment plant, was used as the anaerobic inoculum. The sludge was stored in a cold room and kept at an average temperature of 11 °C. Prior to experimentation, the sludge was conditioned by weekly feeding with glucose for several months at two different temperatures: 37 °C (Inoculum 1) and 55 °C (Inoculum 2), to enhance biomass activity. The specific methanogenic activity of Inoculum 1 and Inoculum 2, using acetate as the substrate, was determined to be 0.093 and 0.085 g COD/ g VSS/ d, respectively. The total solids (TS) and volatile solids (VS) for Inoculum 1 were 5.40% and 2.58%, respectively, while Inoculum 2 had TS and VS values of 4.98% and 2.12%, respectively. The VS/TS ratios of the two inocula were 47.8% and 42.6%, respectively. These relatively low ratios indicated that the seed sludge was highly stabilized, as much of its biodegradable organic matter had already been consumed. Such characteristics are typical of sludge subjected to extended anaerobic digestion or prolonged pre-treatment processes.

4.2.2 Experimental operation

The effects of butyrate concentration and temperature on the AD performance were assessed in batch experiments. Serum bottles with a working volume of 100 mL were used as the digesters and the headspace volume was 61 mL each. The experiments were conducted at two temperatures: 37 °C and 55 °C. Reactors operating at 55 °C were labelled RT1, RT2, RT3, and RT4, corresponding to butyrate concentrations of 2.0, 5.0, 10.0, and 20.0 g COD/L, respectively. Similarly, reactors at 37 °C were labelled RM1, RM2, RM3, and RM4, for the same butyrate concentrations.

In previous studies, the maximum butyrate accumulation was about 5.0 – 6.0 g/L (Wang et al., 2023b). In thermophilic anaerobic digestion, 170 mM butyrate (equivalent to 14.96 g/L) did not significantly inhibit methanogenesis after bioaugmentation. At high organic loading rates (18 g VS/L/d), the butyrate concentration accumulated to 35.09 g COD/L from fruit

waste, leading to the arrest of methanogenesis (Li et al., 2022a). Therefore, in this study, butyrate was used as the sole substrate to provide carbon source in the anaerobic digesters, with concentrations set at 2.0, 5.0, 10.0, and 20.0 g COD/L.

The substrate-to-inoculum ratio was controlled at 1:5 based on COD: VSS. The volumes of inoculum and substrate were 27.2 mL and 72.8 mL at 37°C, respectively, and 31.5 mL and 68.5 mL at 55°C, respectively. Butyric acid was directly added to the substrate according to the experimental setup. The composition of the substrate containing mineral medium, and trace elements, have been described previously (Shi et al., 2024a). Then, the initial pH of all reactors was adjusted to 7.0 using 2 M NaOH and KOH (1:1). Each reactor was purged with nitrogen gas for 5 minutes, and then sealed with butyl rubber stoppers and aluminium covers. Afterwards, reactors RT1 to RT4 were incubated at 55 °C, while reactors RM1 to RM4 were incubated at 37 °C, both at a shaking speed of 150 rpm. The batch experiments continued until the butyrate concentrations stabilized. All experiments were performed in triplicate.

4.2.3 Kinetic models

The conversion of butyrate to methane involves two primary steps: (1) the conversion of butyrate to acetate, and (2) the production of methane from acetate. The simplified reaction pathways for butyrate degradation are shown in Fig. 4.1. To evaluate the reaction rates under different conditions, a kinetic model was employed to simulate the experimental data.

Considering the complexity of butyrate biochemical degradation, the following assumptions were made for building the kinetic model: (1) the activity of microorganisms involved in butyrate degradation was stable; (2) butyrate degradation was simplified to the two steps: acetate production and methane production; (3) the conversion of H₂ and CO₂ to methane was not considered due to the fact that the reactor headspace pressure was manually balanced with a nitrogen bag every one or two days, resulting in a hydrogen concentration close to zero and a hydrogen partial pressure below 10 Pa over the majority of the experimental timeline. Under these conditions, syntrophic butyrate degradation was theoretically thermodynamically feasible (Junicke et al., 2016).

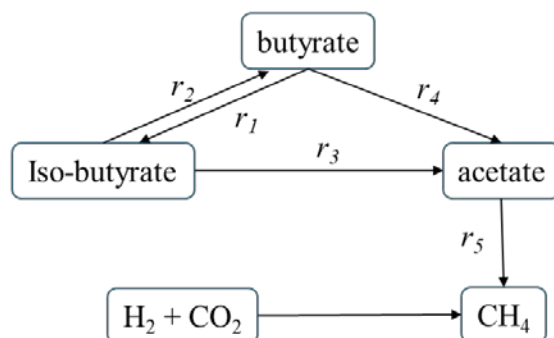


Figure 4.1 Simplified reaction scheme of butyrate degradation

A Monod-type kinetic equation was employed to describe butyrate oxidation (Eq. 4-1 and 4-4). Other reactions were modelled using a first order model (Shin & Song, 1995), considering the low concentrations of intermediates. The degradation reactions of butyrate, iso-butyrate, acetate, and CH₄ production are expressed as follows:

$$r_1 = k_1 * c_{butyrate} * [(c_0 - c_{butyrate}) + k_2] / (k_3 + c_{butyrate}) \quad (4-1)$$

$$r_2 = k_4 * c_{iso-butyrate} \quad (4-2)$$

$$r_3 = k_5 * c_{iso-butyrate} \quad (4-3)$$

$$r_4 = k_6 * c_{butyrate} * [(c_0 - c_{butyrate}) + k_7] / (k_8 + c_{butyrate}) \quad (4-4)$$

$$r_5 = k_9 * c_{acetate} \quad (4-5)$$

where: r_1, r_2, r_3, r_4 and r_5 : the degradation rate of butyrate to iso-butyrate, iso-butyrate to butyrate, iso-butyrate to acetate, butyrate to acetate and acetate to methane, respectively; k_1 and k_6 : maximum growth rate of butyrate degradation microorganisms (d^{-1}); k_2, k_7 : modifying factor (mg COD/L); k_3, k_8 : half-saturation constant (mg COD/L); k_4 : the degradation rate constant of iso-butyrate to butyrate (d^{-1}); k_5 : the degradation rate constant of iso-butyrate to acetate (d^{-1}); k_9 : the degradation rate constant of acetate to methane (d^{-1}); c_0 : initial butyrate concentration (mg COD/L); $c_{butyrate}, c_{iso-butyrate}, c_{acetate}$ and c_{CH_4} : butyrate, iso-butyrate, acetate and CH₄ concentration (mg COD/L).

The rate equations for the simultaneous degradation of butyrate, iso-butyrate, acetate, and CH₄ production are given by:

$$-\frac{dc_{butyrate}}{dt} = r_1 + r_4 - r_2 \quad (4-6)$$

$$-\frac{dc_{iso-butyrate}}{dt} = r_2 + r_3 - r_1 \quad (4-7)$$

$$-\frac{dc_{acetate}}{dt} = r_5 - r_3 - r_4 \quad (4-8)$$

$$\frac{dc_{CH_4}}{dt} = r_5 \quad (4-9)$$

where: t is the reaction time (d).

4.2.4 Analytical analysis

TS and VS were analysed following standard methods (APHA, 2023). The pH was recorded using a digital pH meter (PHS-3C, Leici, Shanghai, China). Samples of two milliliters were collected from all reactors at specific time intervals. Subsequently, these samples were filtered using 0.45 μm nylon syringe filters before VFAs analysis. VFAs and the composition of biogas were measured using gas chromatography (Shi et al., 2024a).

4.2.5 DNA extraction and metagenomic sequencing

DNA extraction and metagenome sequencing were performed on samples from the inoculum sludges activated at 55 °C (T0) and 37 °C (M0), as well as sludge samples withdrawn from reactors RT1 to RT4 and RM1 to RM4 at the end of the incubation (T1, T2, T3, T4, M1, M2, M3, and M4). Detailed sample collection information is provided in Table 4.1. Genomic DNA from microbial samples was extracted with the DNeasy PowerSoil Pro Kit (QIAGEN, UK) following the supplier's protocol. The DNA library was constructed using the Illumina PE-150 platform (Novegene, UK). Then the clean data were obtained using Readfq to reprocess the raw sequencing data (<https://github.com/cjfields/readfq>). Metagenome assembly of the clean data was performed using MEGAHIT software (v1.0.4). Open reading frame (ORF) was predicted using MetaGeneMark (v2.10), and the initial gene catalogue was generated with CD-HIT (v4.5.8) (Zeller et al., 2014). The gene read counts were calculated through Bowtie2 (v2.2.4), followed by the calculation of gene abundance based on the number of reads and gene lengths (Villar et al., 2015). DIAMOND software was used for taxonomic annotation and functional annotation by aligning genes with the NCBI database and the KEGG database, respectively (Kanehisa et al., 2017). The raw sequencing data have been submitted to the National Center for Biotechnology Information (NCBI) database (<https://www.ncbi.nlm.nih.gov/>), with accession number PRJNA1182101.

Table 4.1 Samples and reactors

Reactors	Samples Name	Group
Inoculum 1	T0	
R1	T1	
R2	T2	G1
R3	T3	
R4	T4	
Inoculum 2	M0	
R5	M1	
R6	M2	G2
R7	M3	
R8	M4	

4.2.6 Data analysis

Graphical representations were created using OriginPro 2021 software (<https://www.originlab.com/>). All experimental results are presented as mean \pm standard deviation. SPSS software was employed to calculate the correlation, and differences were considered statistically significant at $p < 0.05$. The linear curve fitting for kinetic models was performed using RStudio 4.1.2 (<http://www.rstudio.com/>).

4.3 Results and discussion

4.3.1 Methane production and butyrate degradation

The theoretical methane yield is 350.0 NmL/ gCOD_{added}. As shown in Fig. 4.2a, the cumulative CH₄ yields at 55 °C were 308.1 \pm 10.5, 273.1 \pm 6.1, 264.3 \pm 6.4, and 205.8 \pm 30.5 NmL/ gCOD_{added} with initial butyrate concentrations of 2.0, 5.0, 10.0, 20.0 g COD/L, respectively. At 37 °C, the cumulative CH₄ yields were 321.3 \pm 7.9, 294.9 \pm 4.0, 274.0 \pm 13.3 and 214.0 \pm 16.3 NmL/ gCOD_{added} with the same butyrate concentrations. These results indicate that the methane yield gradually decreased, suggesting that methane production was gradually inhibited with butyrate accumulation. Elevated butyrate concentrations not only reduced the methane yield, but also inhibited the methane production rate, especially at 37 °C. At this temperature, the period to attain the maximum methane yield increased from 14

days to 46 days as the butyrate concentration rose from 2.0 to 20.0 g COD/L. Fig. 4.2c illustrates the significant decrease in the methane production rate with increasing butyrate concentration (from 2.0 to 20.0 g COD/L). Table 4.2 shows a significant reduction ($p < 0.05$) in the methane yield with increasing butyrate concentration. Under the mesophilic condition (37 °C), both the methane yield and the production rate were higher than that under the thermophilic condition (55 °C) (Fig. 4.2c). This finding contrasts with previous studies, which concluded that higher temperatures (55 °C) can accelerate methane production without affecting the methane yield (Gu et al., 2020; Zhang et al., 2019). The lower methane yield and production rate observed under the thermophilic condition may be attributed to different methanogenesis pathways, which will be further discussed in the microbial community structure analysis (Section 4.3.3).

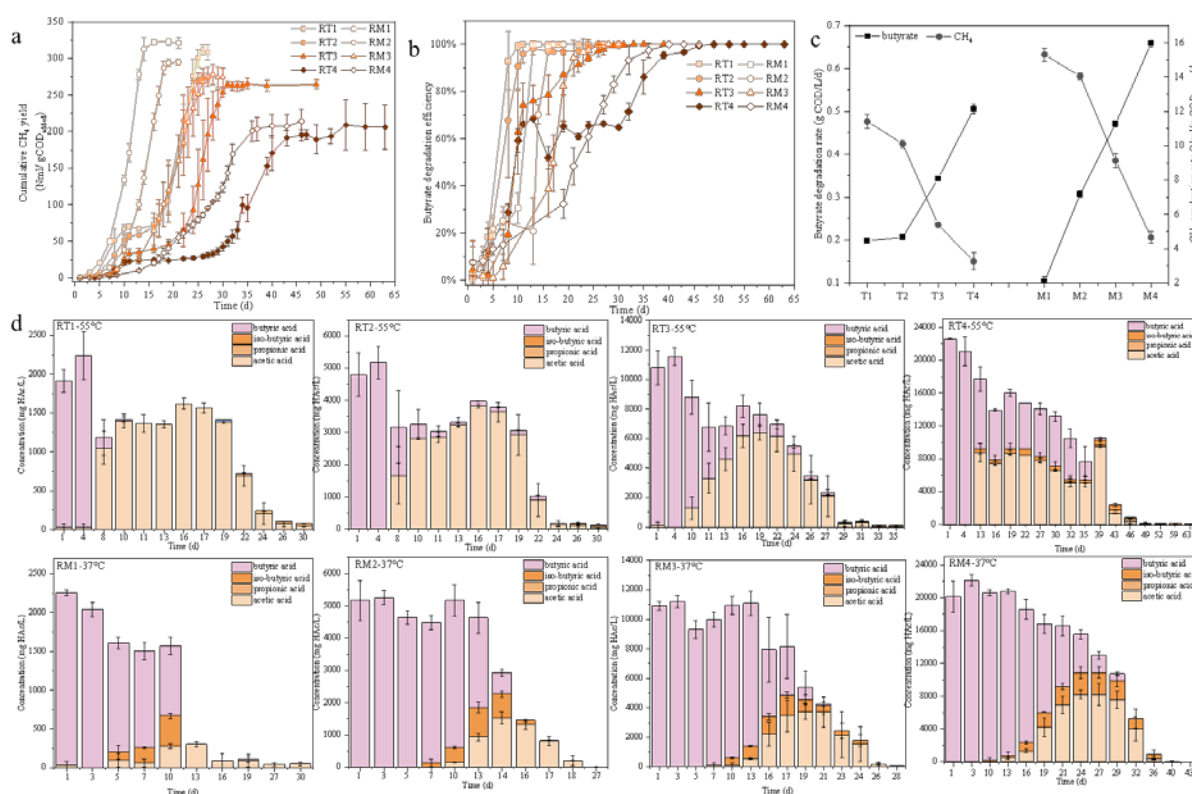


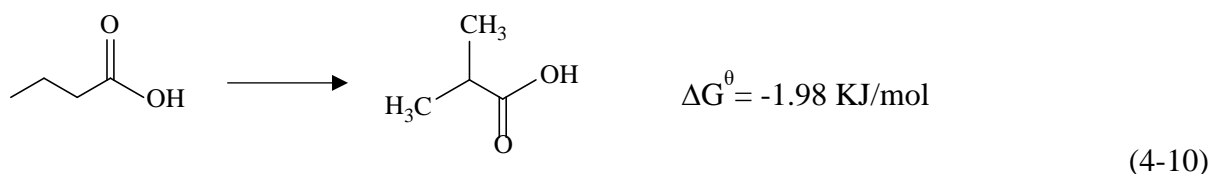
Figure 4.2 Cumulative methane yield (a), butyrate degradation efficiency (b), rate of butyrate degradation and methane production (c), and VFAs evolution (d) in the reactors

Table 4.2 Spearman's correlation between the methane yield and butyrate concentration at different temperatures

Type		Sperman correlation coefficient
Mesophilic condition	Methane yield	-0.996***
Thermophilic condition		-0.979**

Significance degree: ** P < 0.05, *** P < 0.005.

Fig. 4.2b shows the effect of the butyrate concentration and temperature on butyrate degradation. The results demonstrated that butyrate was completely degraded at initial concentrations ranging from 2.0 to 20.0 g COD/L at both 37 °C and 55 °C. However, the degradation efficiency varied with butyrate concentration and temperature. In the initial stage (1-10 days) of butyrate degradation, the degradation efficiency was higher at 55 °C, whereas it was higher at 37 °C at the latter stage, especially at a butyrate concentration of 20.0 g COD/L. The shift may be caused by different butyrate degradation pathways under thermophilic and mesophilic conditions, as shown in Fig. 4.2d. Under the thermophilic condition, iso-butyrate accumulation was observed only at a high butyrate concentration of 20.0 g COD/L, with iso-butyrate concentration reaching approximately 535 mg COD/L. Under mesophilic condition, iso-butyrate production at all butyrate concentrations was observed, with concentrations reaching 392.3, 980.1, 1524.8, and 2862.3 mg COD/L in RM1, RM2, RM3, and RM4, respectively. The conversion of butyrate to iso-butyrate is thermodynamically favourable, as shown in Eq. (4-10). Iso-butyrate exhibits lower toxicity to microorganisms compared to butyrate (De Leeuw et al., 2020), so the isomerization between butyrate and iso-butyrate is considered a detoxification mechanism to mitigate butyrate inhibition (Chen et al., 2016; Wu et al., 2000). This butyrate isomerization can be stimulated when butyrate or acetate accumulates (Angelidaki and Ahring, 1995; Wang et al., 1999).



Additionally, the butyrate degradation rate was influenced by temperature and butyrate concentration, as illustrated in Fig. 4.2c. At 55 °C, the period to reach complete butyrate

degradation increased from 11 to 49 days as butyrate concentration was elevated from 2.0 to 20.0 g COD/L. Similarly, at 37 °C, the degradation time extended from 13 to 40 days with increasing butyrate concentrations. Notably, the butyrate degradation rate increased with higher butyrate concentrations, regardless of temperature. Specifically, at a butyrate concentration of 2.0 g COD/L, the degradation rate was higher at 55 °C. However, as the butyrate concentrations were 5.0, 10.0, and 20.0 g COD/L, the degradation rate was higher at 37 °C. This variation could be ascribed to differences in the microbial communities present at varying temperature conditions.

4.3.2 Kinetics of butyrate degradation and methane production

To model the time course of butyrate degradation, a 4th order Runge-Kutta algorithm was employed to numerically solve the differential equations simultaneously. The optimization of kinetic parameters was conducted using genetic algorithms and the L-BFGS-B method to ensure the best alignment with experimental data, as shown in Table 4.3. The concordance between the simulated and experimental data for butyrate degradation is illustrated in Fig. 4.5, which validates the accurate modelling of the butyrate degradation and methane production.

Table 4.3 Kinetic parameters of the butyrate degradation model

Parameters	RT1	RT2	RT3	RT4	RM1	RM2	RM3	RM4
c_0	2000	5000	10000	20000	2000	5000	10000	20000
k_1	0.55	0.41	0.21	0.87	0.24	0.31	0.54	0.34
k_2	0.022	0.009	0.083	4.56	1.92	0.45	0.91	1.89
k_3	0.94	1.51	0.12	0.12	0.047	0.064	0.16	0.050
k_4	0.71	0.83	0.68	1.53	1.87	1.50	1.55	0.75
k_5	0.42	0.36	0.034	0.068	0.025	0.049	0.057	0.024
k_6	0.24	0.22	0.23	0.38	0.13	0.14	0.22	0.13
k_7	0.012	0.012	1.98	13.84	1.68	0.17	0.40	1.76
k_8	6.05	9.76	9.99	19.69	9.92	8.61	9.71	9.85
k_9	0.063	0.070	0.056	0.032	0.39	0.37	0.18	0.098

M_0 unit: mg COD/L; k_1 , k_4 , k_5 , k_6 , and k_9 units: d^{-1} ; k_2 , k_3 , k_7 and k_8 units: mg COD/L.

Analysis of the kinetic parameters reveals that the degradation behaviour of butyrate differed at 37 °C and 55 °C. At 55 °C, the maximum growth rates for the isomerization of butyrate to

iso-butyrate (k_1) initially decreased and then increased with butyrate concentration increasing (Table 4.3). In contrast, at 37 °C, the trend was completely opposite. In addition, the half-saturation constant (k_3) was higher at 55 °C than at 37 °C. These phenomena could be attributed to the fact that, at 37 °C, the individual microorganisms exhibited better adaptability, resulting in higher butyrate degradation rates (Fig. 4.2c). Moreover, the degradation behaviour of iso-butyrate varied significantly between the two temperatures. At 37 °C, the rate of iso-butyrate conversion to acetate (k_5) was markedly lower than its conversion to butyrate. However, it couldn't be overlooked, as it gradually increased with the increasing concentration of butyrate (Fig. 4.2d). Concurrently, k_4 gradually decreased as the butyrate concentration increased, which likely contributed to the progressive accumulation of iso-butyrate as the butyrate concentration increased from 2.0 to 20.0 g COD/L. The parameters k_6 , k_7 , and k_8 represented the conversion of butyrate to acetate. k_6 didn't vary significantly with the increase in the butyrate concentration, and it was higher at 55 °C compared to at 37 °C, which might explain the higher accumulation of acetate at 55 °C, as shown in Fig. 2d. At 55 °C, the methane production rate from acetate (k_9) exhibited slight alterations with increasing butyrate concentrations. Conversely, at 37 °C, k_9 decreased with butyrate concentrations increasing.

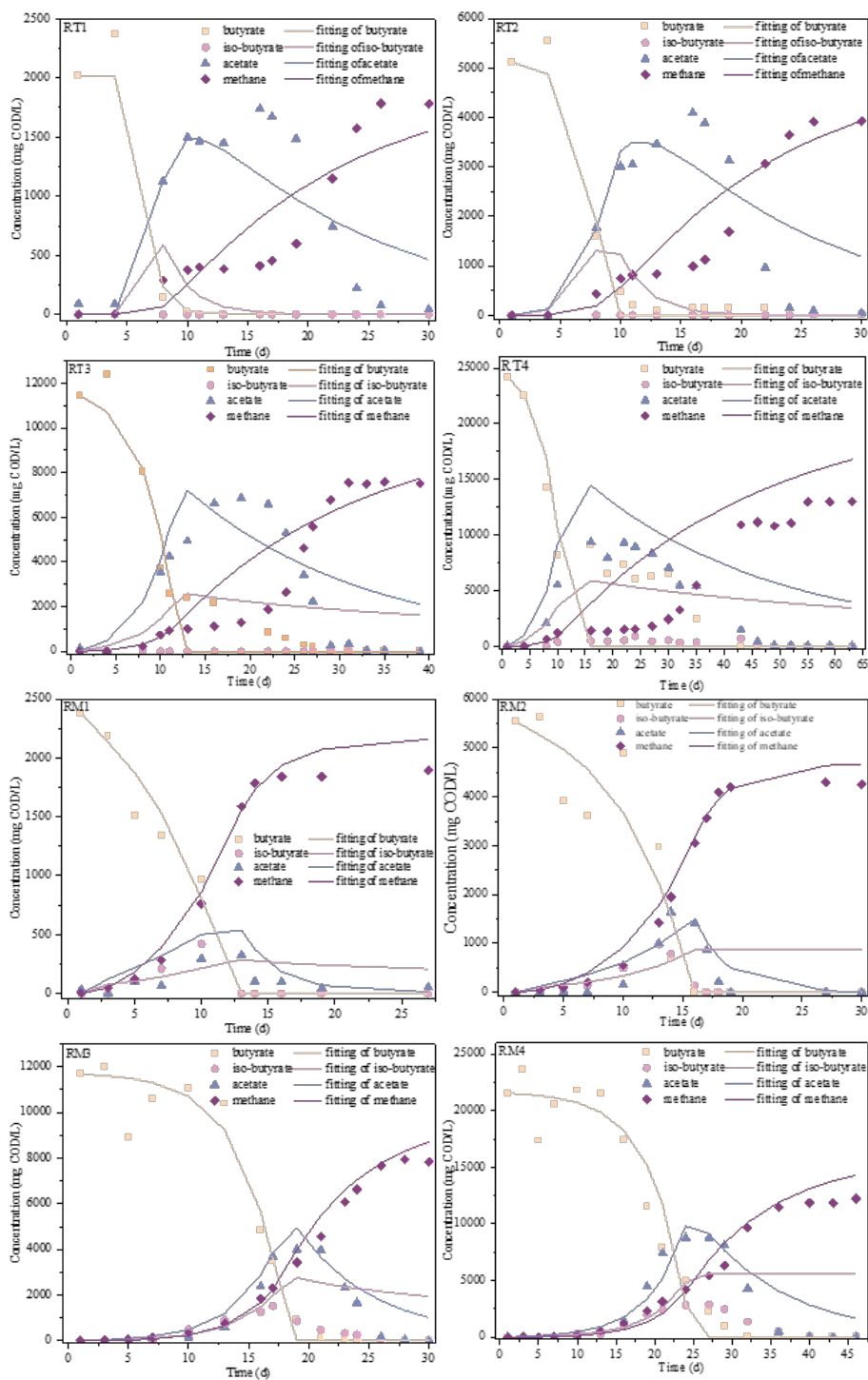


Figure 4.3 Fitting of the kinetic model of butyrate degradation in different reactors

4.3.3 Analysis of the microbial community structure

4.3.3.1 Microbial community diversity

To assess the alpha diversity of the microbial communities under different conditions, the Shannon and Simpson indices were analysed. These indices are comprehensive indicators of community heterogeneity. The Shannon index measures the richness of the microbial diversity, whereas the Simpson index assesses the evenness, especially focusing on dominance (Tang et al., 2022). The Shannon and Simpson index are shown in Figs. 4.4a and 4b. A higher Shannon index and lower Simpson index indicate a more diverse microbial community. At 37 °C, both indices decreased as the butyrate concentration increased, indicating that higher butyrate levels reduced the genus diversity. In contrast, at 55 °C, the indices were higher with butyrate addition compared to the initial inoculum, indicating the enhanced microbial diversity. Overall, the diversity indices for each temperature group (37 °C and 55 °C), shown in Figs. 4.5a and 5b, suggested that the microbial community structure at 55°C was more stable but simpler, with a limited capacity for dynamic adjustment and adaptability in response to environmental changes.

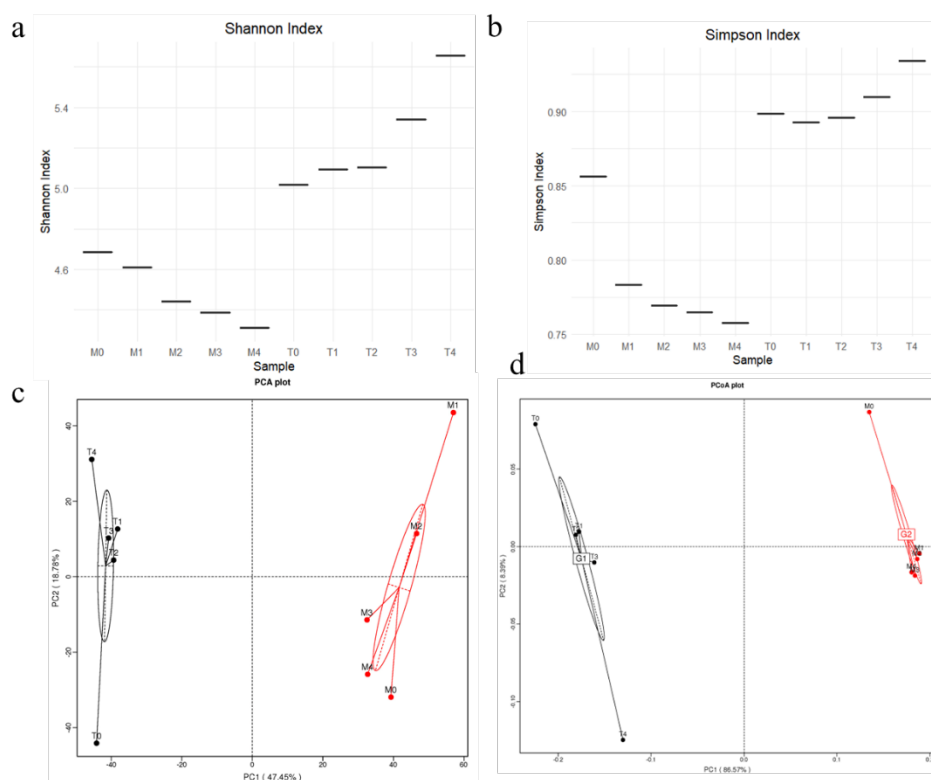


Figure 4.4 Comparisons of genus diversity under different conditions. (a): Shannon index at the genus level; (b) Simpson index at the genus level; (c) PCA (Principal Components Analysis) revealing the similarity of samples by analysing the top 12 most abundant genera in each sample; (d) PCoA (Principal Coordinates Analysis) revealing the separation of microbial communities based on Bray-Curtis distance

Principal Components Analysis (PCA) and Principal Coordinates Analysis (PCoA) were conducted to analyse the beta diversity of microbes. The results, depicted in Figs. 4.4c and 4d, showed significant differences in the microbial structure at 37 °C and 55 °C. At 55 °C, the genus composition remained similar across different butyrate concentrations, whereas at 37 °C, the confidence ellipse was larger, indicating greater variation with different butyrate concentrations. These analyses suggest that the microbial community at 37 °C was richer and possessed greater adaptability. This enhanced adaptability may contribute to the increased rate of butyrate degradation as the butyrate concentration increased, as discussed in Sections 4.3.1 and 4.3.2.

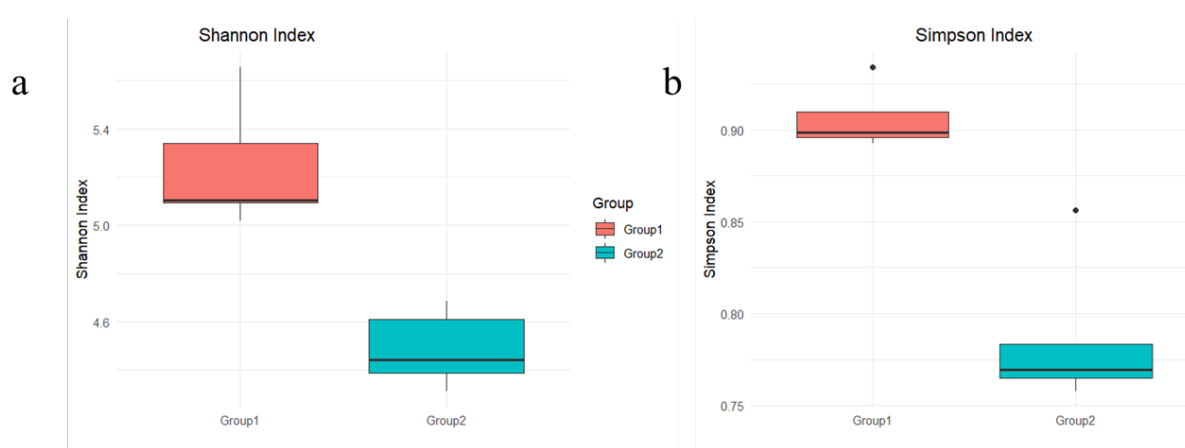


Figure 4.5 Comparisons of microbial diversity of different groups. (a) Shannon index; (b) Simpson index

4.3.3.2 Bacterial community structure

Microbial samples were collected at the end of butyrate degradation experiment in each reactor to study the effects of the butyrate concentration and temperature on the microbial community. Fig. 4.6a presents the relative abundance of the bacterial community at the genus level. The top 15 genera, each representing over 0.5% of the total abundance and cumulatively accounting for more than 50%, are discussed. In the seed sludge (M0) at 37 °C, the dominant genera included *Mesotoga* (12%), *Clostridium* (34%), *Alkalibacter* (21%), *Brevefilum* (20%), and *Nannocystis* (4%). The bacterial community of the inoculum at 55 °C (T0) differed from M0, with *Mesotoga*, *Defluviitoga*, and *Clostridium* being predominant. Particularly, *Clostridium* contributed to over 81% of the top 15 bacterial abundance as shown in Fig. 4.6a.

To clarify the relationships between these genera and system performance, including the butyrate degradation rate and methane production rate, Spearman's correlation analysis was carried out, as presented in Fig. 4.6c. Further analysis explored the correlation between the genera (relative abundance over 0.5%) and butyrate degradation and methane production rates. This revealed that the functional bacteria for butyrate degradation and methane production differed at 37 °C and 55 °C. At 55 °C, the relative abundances of genera such as *Syntrophomonas*, *Aminivibrio*, and *Amaricoccus* increased as the butyrate concentration increased, showing a significant positive correlation with butyrate degradation (Fig. 4.6c). *Syntrophomonas* has been identified as a syntrophic butyrate-oxidizing bacterium crucial for the β -oxidation pathway in anaerobic digestion (Kong et al., 2018a; Meng et al., 2022). *Aminivibrio* is related to butyrate degradation (Zeng et al., 2024), while *Amaricoccus*, predominantly utilizing acetate and propionate, is infrequently associated with butyrate degradation (Liu et al., 2016). *Nannocystis* showed a positive correlation with the methane production rate, known for utilizing glucose, butyrate, and acetate (Roy et al., 2022).

Conversely, at 37 °C, the bacteria showing strong positive correlations with the butyrate degradation rate, included *Syntrophaceticus* and *Candidatus Cloacimonas*, which are syntrophic acidogenic bacteria that partner with hydrogenotrophic methanogens for methane production (Li et al., 2022b; Li et al., 2020b). However, as shown in Fig. 4.6c, these genera negatively correlated with the methane production rate, likely because the methane production primarily relied on acetoclastic methanogenesis. Additionally, genera like *Syntrophorhabdus*, *Aminivibrio*, *Acetomicrobium*, and *Amaricoccus*, which typically convert glucose or VFAs into acetate, H₂ and CO₂ (Zhang et al., 2023a), showed negative correlations with the butyrate degradation rate and positive correlations with the methane production rate. This decrease in the relative abundance of these genera as butyrate concentrations increased at 37 °C (Fig. 4.6a) suggests a sensitivity to butyrate concentrations. This correlation analysis can help to identify the functional genera involved in butyrate degradation and offers insights in the incubation conditions of butyrate degradation bacteria.

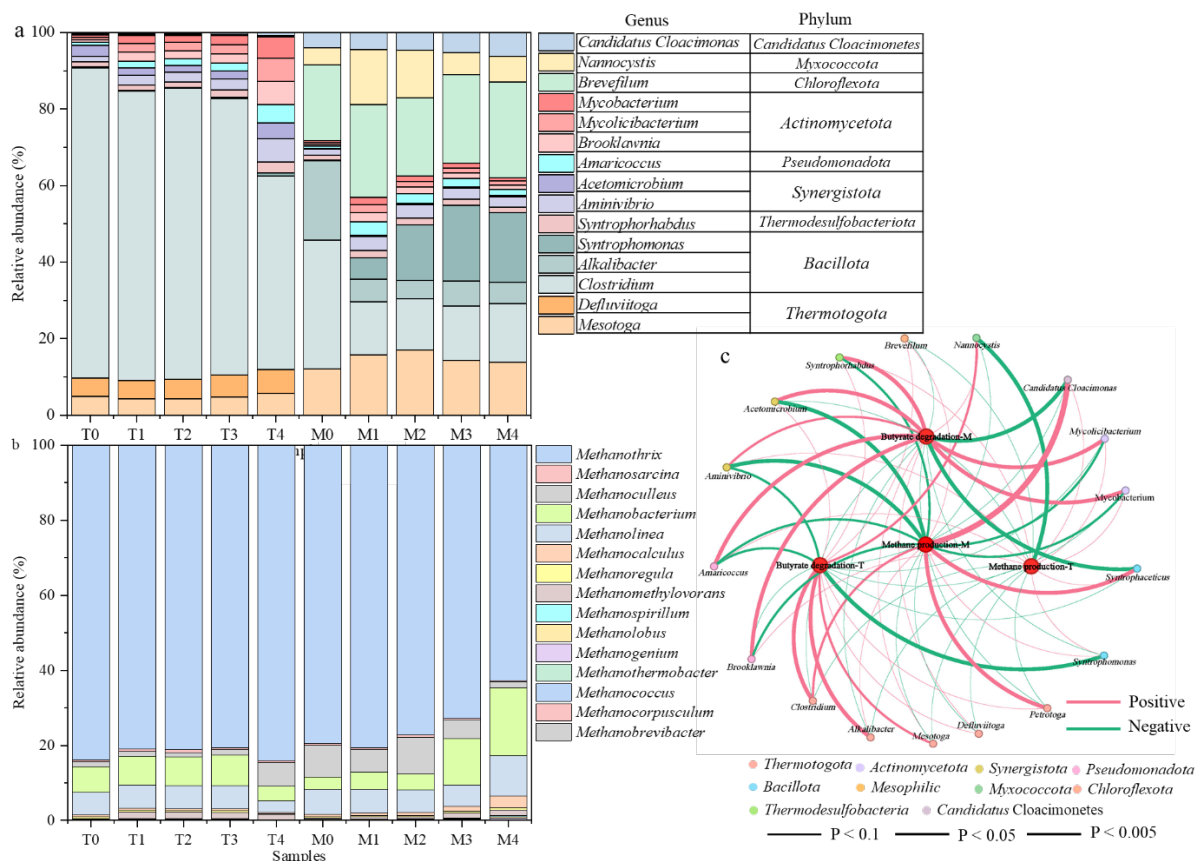


Figure 4.6 Composition of microbial communities in different reactors, showing bacterial (a) and archaeal (b) communities and Pearson's correlation analysis between bacterial genera and reactor performance (c)

4.3.3.3 Archaeal community structure

To gain a deeper insight of the methanogenesis process, the genus-level composition of archaeal communities across all reactors is shown in Fig. 4.6b. Methanogenesis occurs via three main pathways based on the substrates used: 1) hydrogenotrophic, 2) acetoclastic, and 3) methylotrophic methanogenesis (Ferry, 2011); the latter is rare in AD and is not discussed in this study. The key archaea involved in acetoclastic methanogenesis are *Methanotherix* (formerly *Methanosaeta*) and *Methanosarcina*, which also participate in mixed methanogenesis utilizing acetate, H₂/CO₂, methanol, and methylamine (Ziels et al., 2019). Predominant hydrogenotrophic methanogens include *Methanoculleus*, *Methanobacterium*, *Methanolinea*, *Methanocalculus*, and *Methanoregula* (Demirel and Scherer, 2008).

In the initial inoculum at 37 °C, *Methanotherix*, along with *Methanoculleus*, *Methanobacterium*, and *Methanolinea* dominated the archaeal community (Fig. 4.6b).

Methanotherix constituted about 79% of the archaea, indicating that methane production was primarily via acetoclastic methanogenesis. However, the relative abundance of *Methanotherix* gradually decreased with the increasing butyrate concentration, while the proportion of hydrogenotrophic methanogens, particularly *Methanobacterium*, increased. At 55 °C, *Methanotherix* remained the dominant acetoclastic methanogen, with a relative abundance reaching up to 84% (Fig. 4.6b). *Methanobacterium* and *Methanolinea* were the major hydrogenotrophic methanogens. Butyrate concentrations seemed to have little effect on the community communities' structure of methanogens at 55 °C. Kinetic analyses suggests that methane production rates are generally higher via hydrogenotrophic methanogenesis (Xu et al., 2015). Therefore, compared to the mesophilic condition, the lower relative abundance of hydrogenotrophic methanogens in the thermophilic condition may lead to the observed decrease in the methane production rate.

4.3.4 Metabolic pathways

4.3.4.1 Butyrate degradation metabolic pathways

To understand the metabolic pathways involved in butyrate degradation, functional genes using the KEGG database were analysed. As shown in Fig. 4.7a, the primary potential pathways include butyrate oxidation to acetate, acetate oxidation, and methanogenesis. Fig. 4.7b presents the relative abundance of functional genes encoding butyrate oxidation enzymes, which generally increased with higher butyrate concentrations.

As shown in Table 4.3 and Fig. 4.2, the production of iso-butyrate should not be underestimated, especially at elevated butyrate concentrations and a temperature of 37 °C. According to Angelidaki and Ahring (1995), iso-butyrate metabolism primarily occurs through two pathways: (1) isomerization to butyrate followed by β -oxidation to acetate and (2) degradation via propionyl-CoA. The isomerization is facilitated by isobutyryl-CoA mutase (EC 5.4.99.13) (Yi et al., 2020), with a relative abundance of approximately 0.001% across samples. Propionyl-CoA was not observed due to the absence of the gene encoding 3-hydroxyisobutyryl-CoA hydrolase (EC 3.1.2.4), as shown in Fig. 4.7. The actual metabolic pathway of iso-butyrate was predicted (Fig. 10a), where iso-butyrate is first oxidized to (S)-2-methylbutanoyl-CoA and then converted to acetyl-CoA through several reactions.

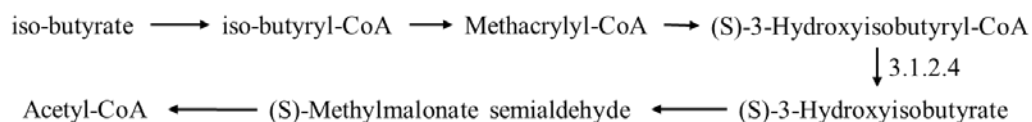


Figure 4.7 Schematic diagram of iso-butyrate metabolic pathway

At 55 °C, enzymes involved in iso-butyrate oxidation, such as isobutyryl-CoA dehydrogenase (EC 1.3.99.-), enoyl-CoA hydratase (EC 4.2.1.17) and 3-hydroxyacyl-CoA dehydrogenase (EC 1.1.1.35), were enriched and positively correlated with butyrate degradation ($p < 0.05$), indicating that iso-butyrate conversion was crucial to the overall butyrate degradation process (see Table 4.4). Additionally, enzymes such as 3-hydroxybutyryl-CoA dehydrogenase (EC 1.1.1.157), acetyl-CoA C-acetyltransferase (EC 2.3.1.9), and acetyl-CoA synthetase (EC 6.2.1.1) played critical roles in butyrate oxidation, involving metabolic pathways that were significantly strengthened ($p < 0.05$). However, the enzymes related to iso-butyrate oxidation showed no significant correlation with butyrate degradation at 37 °C. Moreover, some other enzymes such as butyryl-CoA synthetase (EC 6.2.1.2), acetate CoA-transferase (EC 2.8.3.8), butyryl-CoA dehydrogenase (EC 1.3.8.1), 3-hydroxybutyryl-CoA dehydrogenase (EC 1.1.1.57), acetyl-CoA C-acetyltransferase (EC 2.3.1.9), phosphate acetyltransferase (EC 2.3.1.8), acetate kinase (EC 2.7.2.1) and acetyl-CoA synthetase (EC 6.2.1.1), were negatively correlated with butyrate degradation (Table 4.4), which explains the accumulation of iso-butyrate at 37 °C. Overall, the genes involved in the butyrate oxidation pathway were enriched with increasing butyrate concentrations, with relative abundances ranging from 0.23% to 0.36% at 55 °C, and from 0.25% to 0.57% at 37 °C. The higher relative abundance corresponds to the high reaction rate at 37 °C, consistent with the data shown in Fig. 4.2.

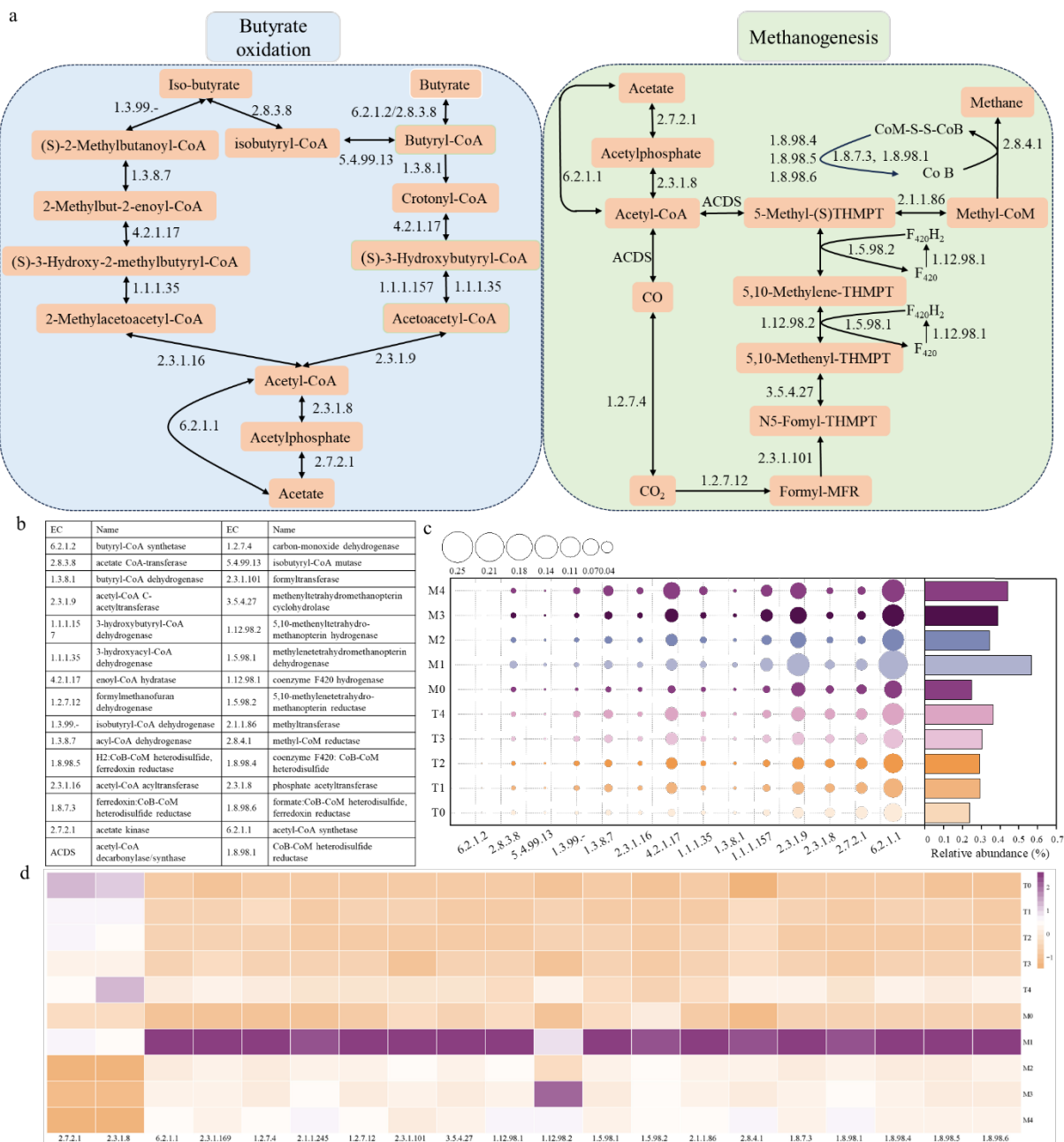


Figure 4.8 Analyses of metabolic pathways: (a) schematic diagram of butyrate metabolic pathway, including butyrate oxidation and methanogenesis; (b) names of enzymes involved in the metabolic pathways; (c) relative abundance of enzymes involved in butyrate oxidation; and (d) relative abundance of enzymes involved in methanogenesis present in different reactors

Table 4.4 Correlation between the metabolic pathway and butyrate degradation rate

Metabolic pathway (EC number)	Butyrate degradation rate	
	55°C	37°C
6.2.1.2		
2.8.3.8		
5.4.99.13		
1.3.99.-	*	**
1.3.8.7	*	*
2.3.1.16		**
4.2.1.17	*	***
1.1.1.35	*	**
1.3.8.1		
1.1.1.157	**	
2.3.1.9	**	
2.3.1.8		
2.7.2.1		
6.2.1.1	**	

4.3.4.2 Methane production metabolic pathways

As shown in Fig. 4.6b and Fig. 4.8a, methane production includes two main pathways: acetoclastic and hydrogenotrophic methanogenesis. The genes associated with these pathways were predominantly linked to *Methanotherix*, *Methanolinea*, *Methanoculleus*, and *Methanobacterium*. From Fig. 4.8d, it is evident that most functional genes associated with methanogenesis were more abundant under mesophilic conditions, particularly in M1, correlating with higher methane production rates at 37°C. The relative abundance of genes encoding the unique acetoclastic methanogenesis pathway, including acetate kinase (2.7.2.1) and phosphate acetyltransferase (2.3.1.8), was higher at 55 °C. In contrast, genes encoding enzymes related to hydrogenotrophic methanogenesis, including formylmethanofuran dehydrogenase (EC 1.2.7.12), acetyl-CoA C-acetyltransferase (EC 2.3.1.9), methenyltetrahydromethanopterin cyclohydrolase (EC 3.5.4.27), coenzyme F420 hydrogenase (EC 1.12.98.1) and methylenetetrahydromethanopterin dehydrogenase (EC1.5.98.1), were more abundant at 37 °C. This indicates the presence of distinct methanogenesis pathways at 37 °C and 55 °C.

Under mesophilic conditions, the relative abundance of most genes involved in acetoclastic methanogenesis decreased with increasing butyrate concentrations, while hydrogenotrophic methanogenesis increased. This was because hydrogenotrophic methanogenesis was more adaptable to the changes in the environment, compared to acetoclastic methanogenesis (Rafieenia et al., 2018). Conversely, at 55 °C, genes related to hydrogenotrophic methanogenesis showed little changes with increasing butyrate concentrations. This suggests that a shift towards hydrogenotrophic methanogenesis under the mesophilic condition occurred, whereas no obvious changes were observed under the thermophilic condition. Additionally, the overall relative abundance of genes related to methanogenesis decreased with increasing butyrate concentrations, which explains the decrease in the methane production rate under these conditions.

4.4 Conclusions

This chapter demonstrated that methane production and butyrate degradation were remarkably affected by temperature and butyrate concentrations. The methane yield was significantly inhibited, as butyrate increased from 2.0 to 20.0 g COD/L. 37 °C favoured methane production and butyrate degradation at butyrate concentration over 5 g COD/L. Metagenomics analysis identified that iso-butyrate conversion and key enzymes such as enoyl-CoA hydratase and 3-hydroxyacyl-CoA dehydrogenase, were crucial to butyrate degradation. The metagenomics analysis was based on a single incubation, and would not fully reflect the microbial dynamics in continuous operations. Nevertheless, the novel findings offered valuable insights for optimizing anaerobic digestion.

Chapter 5
Decoding butyrate fermentation: Parameter optimization and metagenomic insights with glucose as a model substrate

5.1 Introduction

The transition toward a sustainable bioeconomy is fundamental to achieving global climate neutrality by 2050. Central to this shift is the circular economy approach, which prioritizes resource efficiency, waste valorization, and the development of renewable sources (CEAP, 2020). A crucial aspect of circular economy strategies is the bioconversion of organic waste into valuable-added chemicals, reducing dependence on fossil resources while mitigating environmental impacts associated with waste disposal (Moretto et al., 2020). Among bio-based chemicals, volatile fatty acids (VFAs) have gained considerable attention due to their extensive industrial applications, serving as precursors of biofuels, biopolymers, and fine chemicals.

Butyrate, a highly valuable VFA, is widely used in the chemical, pharmaceutical, animal feed, and bioenergy sectors (Zhang et al., 2021a). According to the data reported by Duong and Nga (2024), its market value ranges from \$2000 to 2500 per ton, which is higher than that of propionic acid (\$1500 – 2000 per ton) and substantially greater than acetic acid (\$400 – 800 per ton). Biotechnological production of butyrate provides a viable alternative, as current industrial synthesis remains predominantly dependent on petroleum-based precursors such as propylene and butyraldehyde, which contribute to fossil fuel depletion and greenhouse gas emissions (Kelbert et al., 2024). Microbial fermentation using organic waste as a feedstock offers a sustainable alternative, consistent with waste-to-resource strategies (Perez-Esteban et al., 2025). However, in fermentation systems, butyrate is typically co-produced with other VFAs, including acetate, propionate, and caproate, complicating its recovery. Thus, optimizing fermentation parameters to maximize butyrate selectivity and yield is crucial to improve the economic and environmental viability of bio-based butyrate production.

Despite extensive research, no definitive consensus has been reached regarding the optimal conditions for butyrate production, primarily due to variability in reported pH values, temperature and inoculum-to-substrate (ISR) conditions. pH, one of the most influential factors, regulates microbial metabolic pathways and affects VFA selectivity. While some studies suggest that butyrate production is optimal at mildly acidic conditions (pH 4-7) (Eryildiz et al., 2020; Liu et al., 2025), others report butyrate accumulation under alkaline conditions (pH 8-11) (Atasoy et al., 2019; Begum et al., 2018). Similarly, temperature has a significant effect on butyrate production, influencing both microbial activity and metabolic pathways. While some studies report enhanced butyrate production at thermophilic temperatures (50-55 °C or higher)

(He et al., 2012; Perez-Esteban et al., 2025), others suggest that mesophilic conditions (35-37 °C) favor butyrate accumulation (Lin et al., 2016). Even some studies suggest that butyrate concentration remains relatively stable across a broad temperature range from 20 °C to 70 °C (Fernandez-Dominguez et al., 2020). Contradictory findings also exist regarding ISR effects on butyrate production. Some studies indicate an optimal ISR of 1:2 or 1:1 for butyrate accumulation in the anaerobic digestion of food waste (Li et al., 2022d), while others report no significant differences across a broad ISR range. These discrepancies underline the importance of a systematic evaluation of how pH, temperature, and ISR interact to influence butyrate production, particularly in terms of microbial activity and metabolic pathways.

Beyond process parameters, microbial community structure and functional metabolism play a critical role in butyrate fermentation. Butyrate is primarily produced by strictly anaerobic bacteria, including *Butyribacterium*, *Butyrivibrio*, *Clostridium* (especially *Clostridium tyrobutyricum* and *Clostridium butyricum*), *Coprococcus*, and *Eubacterium* (Harirchi et al., 2022; Lv et al., 2022). However, non-butyrogenic bacteria also influence butyrate production by generating butyrate precursors. For instance, lactate (from *Ruminococcaceae* and *Lactobacillaceae*), acetate (from *Ruminococcaceae* and *Actinomycetaceae*) and succinate (from *Actinomycetaceae*) contribute to butyrate synthesis (Detman et al., 2021; Esquivel-Elizondo et al., 2017). Additionally, *Ethanoligenens* has been reported to enhance butyrate production, via ethanol- and acetate- based chain elongation reaction (Montecchio et al., 2024). Despite these insights, little is known about how microbial populations shift under different fermentation conditions and how metabolic pathways are regulated to enhance butyrate production. There are two major metabolic pathways for butyrate biosynthesis from glucose: the succinate and the acetyl-CoA pathways (Vital et al., 2014). While, most butyrate-producing bacteria participate in the acetyl-CoA pathway, only a subset of species, particularly from *Firmicutes* and *Bacteroidetes* phyla, are involved in the succinyl-CoA pathway (Vital et al., 2017). The dominance of one pathway over another is often condition-dependent, yet limited studies have examined how environmental factors regulate these metabolic routes. Moreover, chain elongation reactions, which contribute to butyrate formation from ethanol and acetate, remain underexplored. Given these knowledge gaps, a deeper understanding of the relationship between fermentation parameters, microbial dynamics, and metabolic pathway regulation is essential for improving butyrate selectivity and process stability.

In this study, glucose was selected as a model substrate to systematically evaluate butyrate production mechanisms under controlled conditions. The objectives of this study were to (1) determine the optimal fermentation conditions (pH, temperature, and ISR) for selective butyrate production and (2) elucidate the microbial and metabolic mechanisms regulating butyrate biosynthesis. A comprehensive assessment of microbial community dynamics and metabolic pathways responses under different fermentation conditions is expected to provide fundamental insights into improving butyrate production efficiency. A better understanding of the optimal conditions and regulatory mechanisms of butyrate biosynthesis is essential for enhancing butyrate yield and facilitating its biorefinery from organic waste streams.

5.2 Material and Method

5.2.1 Anaerobic inoculum

The original anaerobic inoculum used in this study was anaerobic sludge, sourced from a mesophilic digester at a local municipal wastewater treatment plant in Galway, Ireland. The sludge was stored in polyethylene drums in a cold room where the temperature was maintained at around 11 °C. Prior to its use in the experiments, the sludge was acclimated and activated by weekly feeding with glucose (2 g COD/L) for several months at 37 °C to maintain a high activity. The total solids (TS) and volatile solids (VS) contents of the inoculum were 5.68% and 2.48%, respectively.

5.2.2 Experiment operation

All batch experiments were carried out in serum bottles with a working volume of 400 mL, inoculated with pre-activated anaerobic sludge. Glucose (3.0 g COD/L) was used as the carbon source and directly added to the reactors. The concentrations of medium and trace elements were supplemented in the reactors to support microbial growth according to previous study (Shi et al., 2024b). To inhibit methanogenesis and facilitate butyrate production, 50 mM 2-bromoethanesulfonate (BES) was added into all reactors (Eryildiz et al., 2020). To systematically investigate the effects of temperature, pH, and inoculum-to-substrate ratio (ISR) on anaerobic fermentation for butyrate production, two sets of batch experiments were conducted sequentially: (1) pH and temperature experiments, and (2) ISR experiments. The specific experimental conditions for both experiments are summarized in Table 5.1.

Table 5.1 Experimental condition for pH, temperature and ISR experiments

Batch experiments	Mesophilic conditions (T = 37 °C)		Thermophilic conditions (T = 55 °C)		Remark
	Groups	pH	Groups	pH	
pH and temperature experiments	RA-M1	Uncontrolled	RA-T1	Uncontrolled	ISR=2:1; except the uncontrolled groups, pH was adjusted every day
	RA-M2	4.5	RA-T2	4.5	
	RA-M3	5.0	RA-T3	5.0	
	RA-M4	5.5	RA-T4	5.5	
	RA-M5	6.0	RA-T5	6.0	
	RA-M6	6.5	RA-T6	6.5	
	RA-M7	7.0	RA-T7	7.0	
	RB-M1	Uncontrolled	RB-T1	Uncontrolled	
	RB-M2	8.5	RB-T2	8.5	
	RB-M3	9.0	RB-T3	9.0	
	RB-M4	9.5	RB-T4	9.5	
	RB-M5	10.0	RB-T5	10.0	
	RB-M6	10.5	RB-T6	10.5	
	RB-M7	11.0	RB-T7	11.0	
ISR experiments	ISR-1	3:1			Initial pH adjusted to 5.5; pH unregulated during the reaction
	ISR-2	2:1			
	ISR-3	1:1			
	ISR-4	1:2			
	ISR-5	1:3			

Previous studies have reported that the optimal pH ranges for butyrate production are 4.0 - 7.0 and 8.0 - 11.0 (Atasoy et al., 2019; Eryildiz et al., 2020; Liu et al., 2025). Based on these findings, two maintained pH ranges (4.5 - 7.0 and 8.5 - 11.0) were tested in the pH and temperature experiments using an ISR of 2:1(VSS: COD). As VFAs composition and yield are influenced by the pH control model strategy (uncontrolled vs. maintained pH) (Shi et al., 2022), daily adjustments were performed using 2M HCl or 2M NaOH to maintain the target pH throughout the process (Table. 5.1). A reactor without pH regulation was used as the control group, with an initial pH of approximately 7.3. For the ISR experiments, the optimal pH and temperature were 4.5 - 5.5 and 37 °C, respectively (see Section 5.3.1). Furthermore, as shown in Fig. 5.1, when the initial pH was adjusted to 5.5 using 2M HCl or 2M NaOH without further regulation, the final pH values remained within the optimal range of 4.5 - 5.5. Therefore, pH was not manually controlled in the ISR experiments to minimize chemicals addition and

operation interventions. Five ISRs (1:3, 1:2, 1:1, 2:1, and 3:1) were evaluated under these conditions (Table 1). The glucose concentration was consistently maintained at 3 g COD/L, while different ISR values were achieved by adjusting the inoculum volume. Specifically, the inoculum volumes of 96.1, 69.6, 38.1, 20.0 and 13.6 mL were used for ISRs of 3:1, 2:1, 1:1, 1:2 and 1:3, respectively.

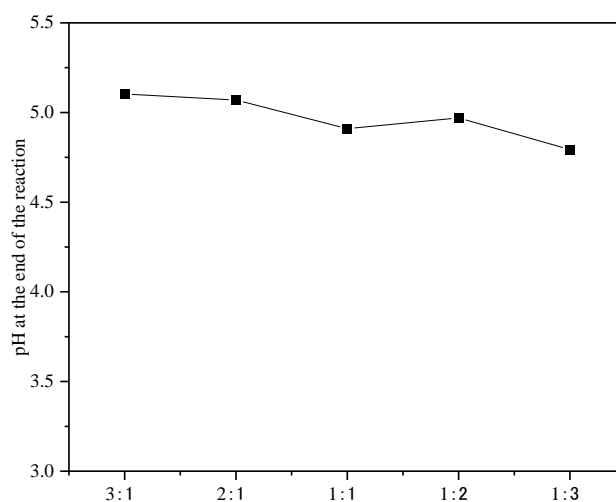


Figure 5.1 pH values at the end of the reaction in the ISR experiment

To establish anaerobic conditions, each reactor was purged with nitrogen gas for 5 minutes prior to sealing with butyl rubber stoppers and aluminium covers. The reactors were then incubated in shaking incubators at the specified temperatures (37°C and 55°C) at 150 rpm. Experiments are carried out until the concentrations of VFAs, ethanol and lactate concentrations stabilized. During the experiments, 2-mL samples were collected from all reactors every one or two days for physicochemical analysis. At the conclusion of the experiments, 50-mL samples were taken for further analysis, including NADH/NAD⁺ concentrations and INT-ETS activity, and metagenomic sequencing. All experiments were carried out in triplicates.

5.2.3 Analytical methods

5.2.3.1 Physicochemical analysis

TS and VS were measured following standard methods (APHA, 2012). The pH was analysed using a portable pH meter (HQ40d, Hach, Germany). VFAs, including acetate, propionate, iso-butyrate, n-butyrate, iso-valerate, n-valerate, as well as ethanol and lactate were measured using a gas chromatography (GC 8860, Agilent Technologies, USA) equipped with a DB-

FFAP column and a flame ionization detector (FID). For the clarity in the following context, butyrate concentrations represent the combined total of n-butyrate and iso-butyrate, while the valerate concentrations include both n-valerate and iso-valerate. The concentrations of NAD⁺/NADH at the conclusion of the experiments were analysed using a NAD⁺/NADH Assay Kit (Abcam, Netherland), following the protocol provided by the manufacture, as described in the supplementary. The activity of the electron transport system (ETS) was measured using the 2-(p-iodophenyl)-3-(p-nitrophenyl)-5-phenyltetrazolium chloride electron transport system (INT-ETS) method, as described in previous research (Shi et al., 2024b).

5.2.3.2 Production efficiency calculations

To evaluate the conversion efficiency of glucose under different conditions, the production efficiency (E) was calculated as the ratio of the total products to the initial total COD concentration, as shown in Eq. (5-1)

$$E = \frac{C_{products}}{COD_{reduction}} * 100\% \quad (5-1)$$

where $C_{products}$ represents either the concentration of butyrate or the concentration of total products including acetate, propionate, butyrate, valerate, lactate and ethanol (mg COD/L); $COD_{reduction}$ is the initial glucose concentration minus the glucose concentration at the end of the reaction (mg COD/L).

5.2.3.3 Metagenomic sequencing analysis

The primary objective of this analysis is to elucidate the microbial mechanisms underlying butyrate production under varying operational conditions. Based on the anaerobic fermentation performance, high temperature and alkaline conditions were considered unfavourable for butyrate production (see Section 5.3.1). Considering the optimal conditions for butyrate production and the variations observed across pH, temperature and ISR conditions, six representative samples (RA-M1, RA-M3, RA-M5, RA-T1, ISR-2 and ISR-5) were selected for sequencing analysis. These biomass samples were labelled as RM1, RM3, RM5, RT1, ISR2 and ISR5, respectively. Genomic DNA was extracted from these microbial samples using the DNeasy PowerSoil Pro Kit (QAIGEN, UK), following the manufacturer's protocol. Subsequently, the extracted DNA was sent to Novogene (Cambridge, UK) for sequencing and bioinformatic analysis as described by Shi et al. (Shi et al., 2024b).

5.2.3.4 Statistical analysis

All experimental results are presented as mean \pm standard deviation. Graphical representations were created using OriginPro 2021 software (<https://www.originlab.com/>) and linear curve fitting for kinetic models was performed using RStudio 4.1.2 (<http://www.rstudio.com/>). Correlations were calculated using SPSS software. Differences were considered statistically significant at $p < 0.05$. The heatmaps were generated using ChiPlot (<https://www.chiplot.online/>).

Normalized taxonomic classification data were used as input for the co-occurrence analysis, which was conducted in R utilizing the cooccur package, a distribution-free method that does not refer to a statistic (<http://www.rstudio.com/>). The output from the co-occurrence analysis, along with the normalized taxonomic classification data, were further processed in the software package Gephi (Bastian et al., 2009). According to module separation and modularity calculation, the key hubs were determined by the Zi-Pi method (Deng et al., 2012).

5.3 Results and discussion

5.3.1 Anaerobic fermentation performance

5.3.1.1 pH and temperature effects

As shown in Fig. 5.2 and Table 5.2, under mesophilic conditions (37 °C), when the pH ranged from 4.5 to 7.0, acetate, propionate and butyrate were the predominate products at 37 °C. The highest proportion of butyrate were observed at pH 4.5 (74%), 5.0 (70%), 5.5 (60%) and 6.0 (51%), with corresponding concentrations of 1260.5 mg COD/L, 1326.7 mg COD/L, 1314.8 mg COD/L, and 1113.9 mg COD/L, respectively. At pH 7.0, the predominant products were propionate and acetate. Under thermophilic conditions (55 °C), the predominant products shifted to ethanol, butyrate and acetate. The concentrations of butyrate at 55 °C were 213.8 (12%), 166.7 (9%), 503.8 (24%), 511.6 (23%), 518.5 (22%) and 620.9 mg COD/L (26%) at the pH of 4.5, 5.5, 5.5, 6.0 6.5 and 7.0, respectively (Table 5.2). These values were lower compared to those at 37 °C. Notably, ethanol production was favored at 55 °C, especially at pH 4.5 and 5.0, where ethanol accounted for over 50% of the total products. The optimal conditions for ethanol production were 37 °C (Shi et al., 2022) and pH values higher than 6.0 (Dionisi and Silva, 2016). Under alkaline conditions (pH 8.5 to 11.0),

butyrate production was substantially reduced, with concentrations consistently below 500 mg COD/L. The butyrate concentration was not detectable at pH 9.5 to 11.0, regardless of whether the conditions were mesophilic or thermophilic. Lactate began to accumulate at 55 °C when the pH was between 9.0 to 11.0.

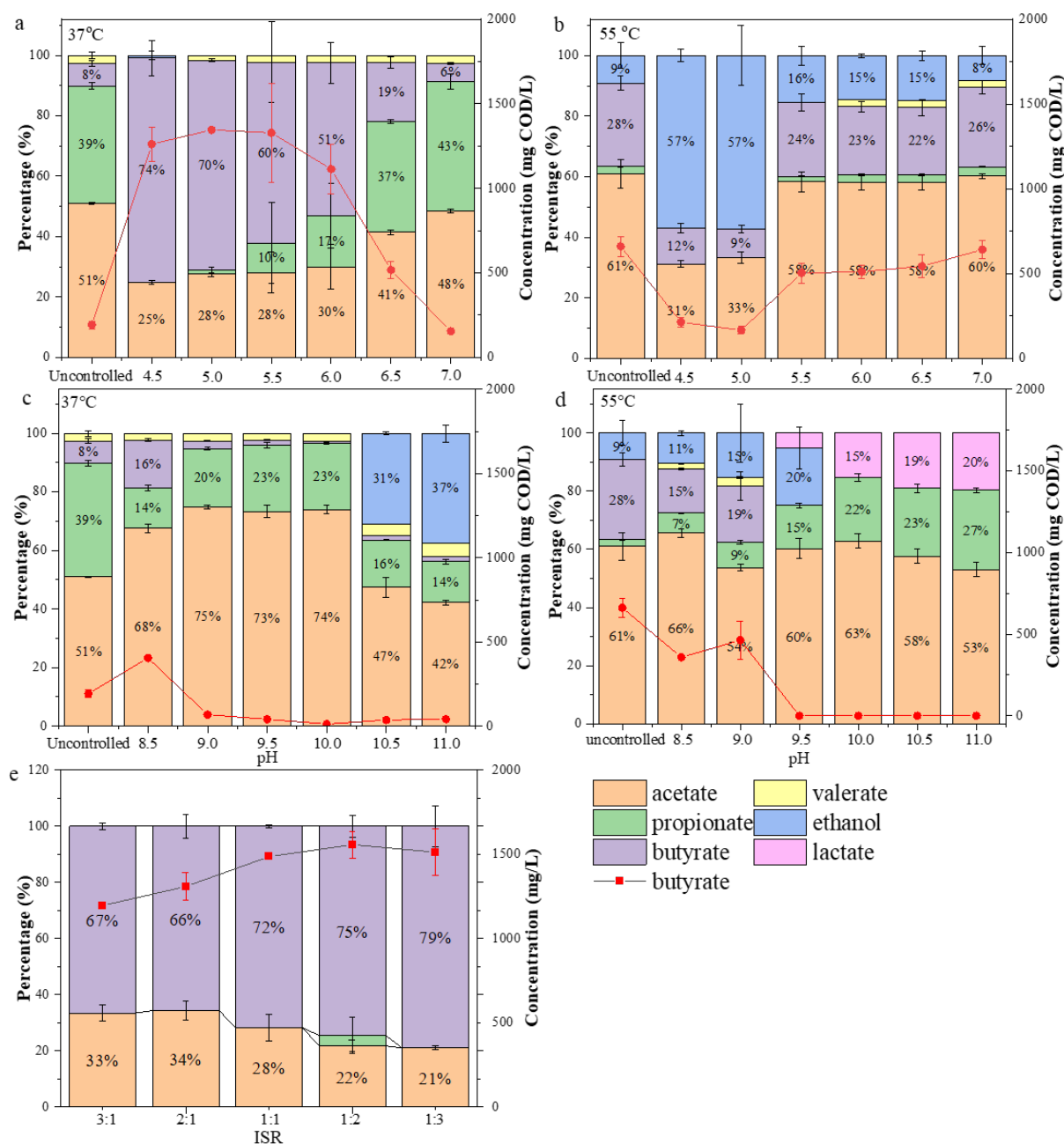


Figure 5.2 Percentage and concentration of butyrate in all reactors

As shown in Table 5.2, the production efficiency of butyrate from glucose was from 0 to 45.2% under different temperatures and pH values. These findings suggest that the optimal conditions for butyrate production are maintained at a stable pH range of 4.5 - 5.5 and a temperature of 37

°C. These results differ from those reported in previous studies (Atasoy et al., 2019; He et al., 2012; Shi et al., 2022). For instance, Atasoy et al (2019) reported the highest butyrate yield (60.0%) from glucose was under alkaline conditions (pH 8 and 10). However, this discrepancy could be attributed to the lack of pH control in their experiments, resulting in the effluent pH values around 5.0, which aligns with the optimal pH range observed in this study. In another study, He et al. (2012), examined the hydrolysis and acidification of food waste at an initial pH of approximately 7.0, and found that butyrate concentration was the highest at 55 °C compared to 37 °C and 70 °C, while ethanol production peaked at 37 °C. The final pH values in their experiment were approximately 3.75, 4.25 and 4.50 at 37 °C, 55 °C and 70 °C, respectively, highlighting the interplay between pH and temperature in influencing products distribution. Similarly, Shi et al. (2022) investigated the anaerobic fermentation of fruit and vegetables and observed a butyrate-type fermentation under controlled conditions of pH 6.0 and 35 °C. Overall, these variations emphasize the significant role of pH and temperature in shaping the metabolic pathways and product yields during anaerobic fermentation processes.

Additionally, pH and temperature mutually influenced the VFAs, ethanol and lactate production efficiency from glucose as shown in Table 5.2. The production efficiency declined as pH dropped from 6 to 4.5 regardless of the temperature, while compared to 37 °C, 55 °C improved the production efficiency at these pH levels due to the fact that 55 °C could promote glucose hydrolysis (Khan et al., 2016). At 37 °C, the production of VFAs, ethanol and lactate slightly increased when pH increased from 8.5 to 10.0, then decreased with pH 10.5 and 11. The alkaline condition (pH 8 and 9) could enhance the acidification efficiency (Cai et al., 2024). However, at 55 °C, the production efficiency abruptly decreased when pH increased to 9.5, which may be attributed to the formation of undetected soluble or insoluble intermediate products under high-temperature and highly alkaline conditions. As shown in Fig. 5.3, the mass balance was evaluated by calculating COD values of determined products. Under acidic conditions, the COD value of the final products consistently accounted for approximately 80% of the initial COD value of the added glucose regardless of temperature, demonstrating good mass balance. Under alkaline conditions, the COD value of the products remained around 80% of the initial COD at 37°C. However, at 55°C, when the pH increased to 9.5, the COD value of the final products decreased significantly, accounting for only about 40% of the initial COD. High alkaline pH (pH 9.9) and temperature (55 °C) can promote the hydrolysis process, but is not suitable for VFAs, ethanol and lactate production (Chen et al., 2017). The mass imbalance

could be attributed to intermediate products such as pyruvate and succinate. Therefore, when optimizing fermentation conditions for butyrate production, it is essential to consider both the percentage and butyrate production efficiency. In this study, the optimal pH and temperature for butyrate production were determined to be 5.5 and 37 °C, respectively.

Table 5.2 Concentration and conversion efficiency of products from glucose at the end of anaerobic fermentation

Reactor	Concentration (mg COD/L)							<i>E</i> (%)	
	HAc	HPr	HBu	HVa	Ethanol	LA	Glucose	E_{HBu}	E_{TVFA}
M1	1306.9	997.7	193.0	67.3	0.0	0.0	62.4	6.6	87.3
RA-M2	420.0	0.0	1260.5	0.0	14.8	0.0	76.2	43.1	58.0
RA-M3	537.9	22.5	1345.8	30.1	0.0	0.0	70.0	45.2	66.1
RA-M4	624.2	217.2	1328.1	49.2	0.0	0.0	58.1	44.6	70.3
RA-M5	658.5	370.4	1113.9	52.5	0.0	0.0	65.5	38.0	80.0
RA-M6	1101.0	973.7	517.2	62.8	0.0	0.0	61.44	17.6	90.3
RA-M7	1270.4	1128.5	154.6	68.6	0.0	0.0	37.9	5.2	88.5
RB-M2	1672.7	342.3	404.8	55.1	0.0	0.0	52.9	13.7	84.0
RB-M3	1865.1	497.0	68.3	63.5	0.0	0.0	42.4	2.3	84.3
RB-M4	1871.3	579.7	40.7	58.6	0.0	0.0	31.4	1.4	85.9
RB-M5	1866.4	572.7	12.2	72.4	0.0	0.0	46.6	0	85.5
RB-M6	1031.7	350.1	37.0	80.5	676.6	12.6	42.78	0	73.6
RB-M7	910.2	299.9	41.3	95.5	807.3	63.9	78.7	0	73.7
T1	1466.7	57.5	661.4	0.0	218.7	0.0	153.5	23.2	86.7
RA-T2	558.8	0.0	213.8	0.0	1021.7	0.0	162.6	7.5	65.5
RA-T3	595.1	0.0	166.7	0.0	1025.8	0.0	170.3	5.9	65.6
RA-T4	1204.8	37.5	503.8	0.0	320.7	0.0	164.5	17.7	74.9
RA-T5	1309.8	56.5	511.6	48.8	331.5	0.0	168.9	18.1	82.8
RA-T6	1425.1	69.4	543.9	57.6	363.1	0.0	160.8	18.3	86.6
RA-T7	1472.8	73.1	641.6	51.0	204.9	0.0	163.6	21.9	86.1
RB-T2	1559.7	163.2	357.9	46.6	218.7	0.0	171.3	23.8	84.0
RB-T3	1281.0	206.9	463.0	67.3	250.0	0.0	163.4	12.7	84.0
RB-T4	760.3	186.5	0.0	0.0	365.6	66.0	103.5	16.3	43.5

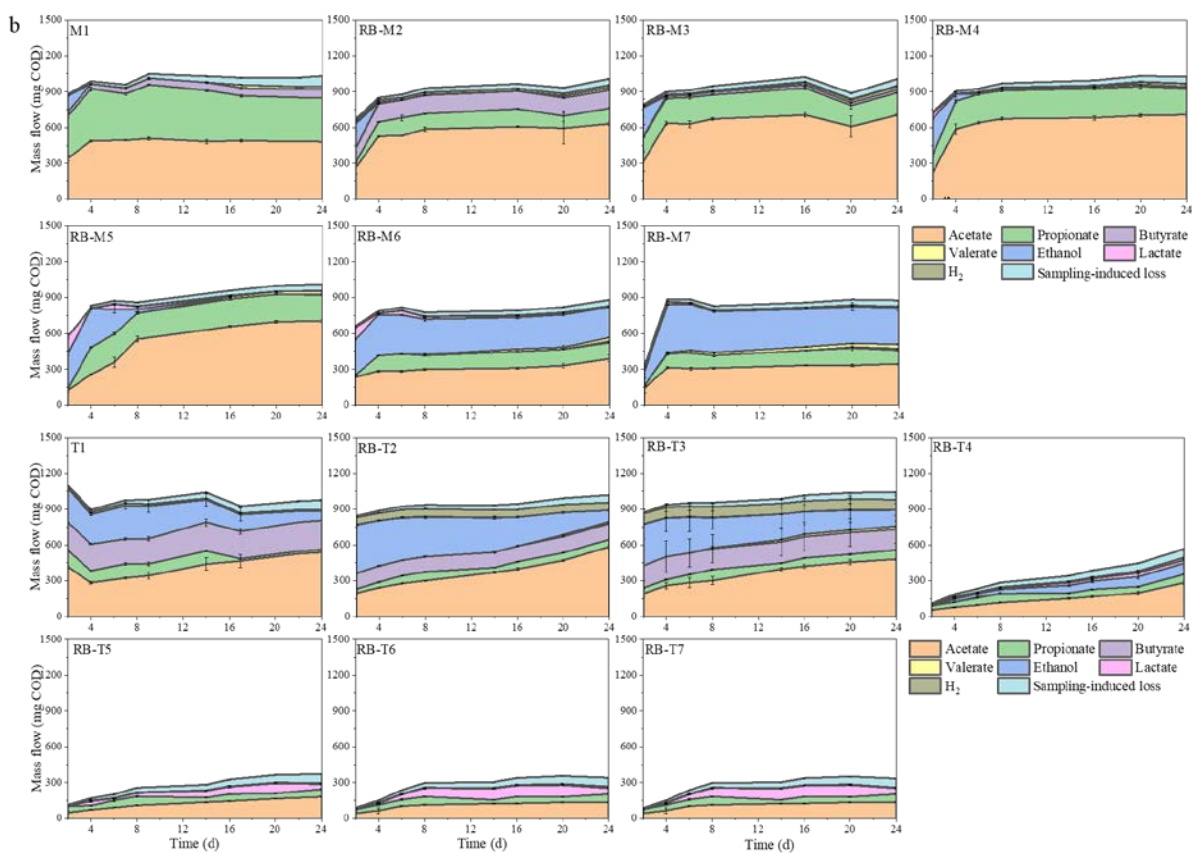
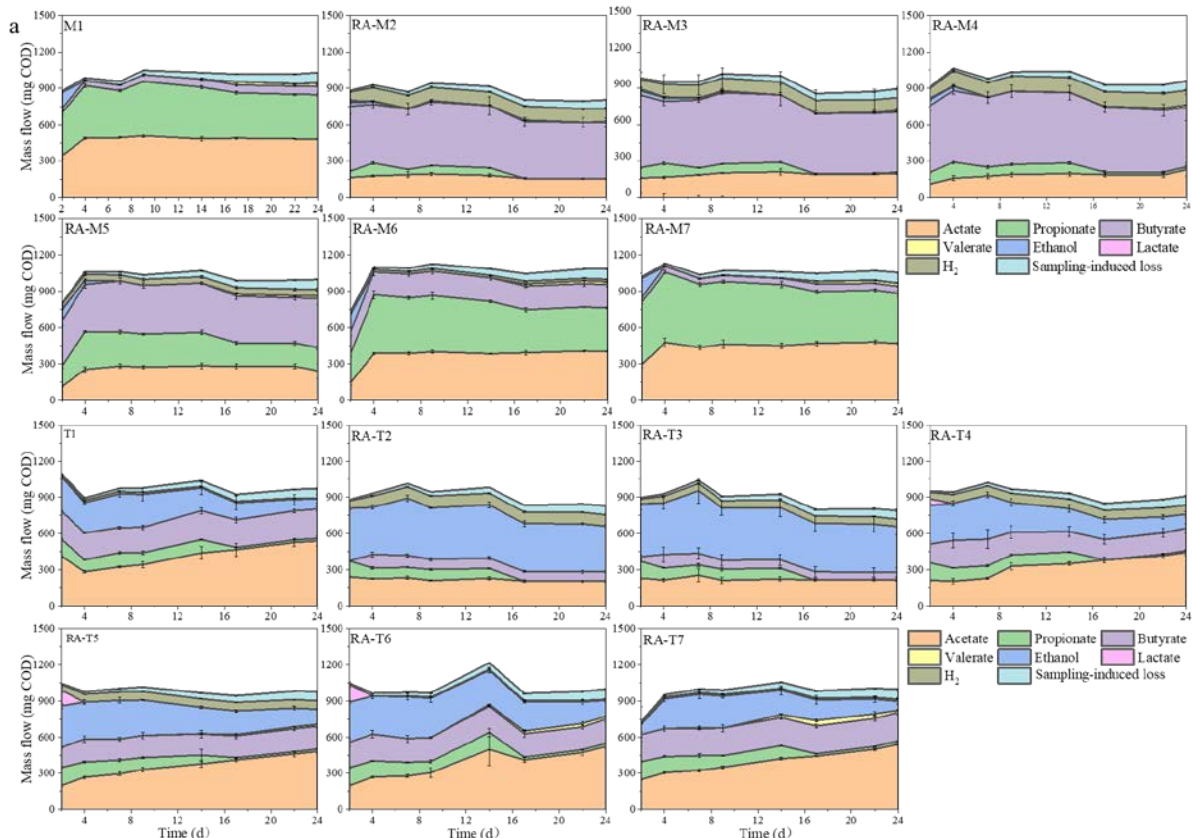
RB-T5	479.	166.3	0.0	0.0	247.8	117.0	93.6	0	26.3
RB-T6	433.5	174.8	0.0	0.0	0.0	143.1	130.3	0	26.2
RB-T7	356.2	183.0	0.0	0.0	0.0	131.6	154.1	0	23.6
ISR-1	601.7	0.0	1196.0	0.0	0.0	0.0	71.4	40.8	61.4
ISR-2	684.0	0.0	1308.7	0.0	0.0	0.0	110.3	45.3	69.0
ISR-3	586.0	0.0	1487.0	0.0	0.0	0.0	64.4	50.7	70.6
ISR-4	454.2	77.7	1557.9	0.0	0.0	0.0	16.5	52.2	70.0
ISR-5	401.7	0.0	1513.2	0.0	0.0	0.0	120.6	52.6	66.5

Note: HAc: acetate; HPr: propionate; HBu: butyrate; HVa: valerate; LA: lactate; E_{HBu} : the production efficiency of butyrate from glucose; E_{TVFA} : the production efficiency of total products including acetate, propionate, butyrate, valerate, ethanol and lactate.

5.3.1.2 Inoculum-to-substrate ratio effects

In the subsequent ISR experiment, as shown in Fig. 5.2e, the predominant products in anaerobic fermentation systems were acetate and butyrate. Only a small amount of propionate was detected when the ISR was set to 1:2, potentially resulting from the reductive disproportionation of butyrate and acetate (De Bok et al., 2001). The proportion and concentration of butyrate in VFAs increased as the ISR decreased from 3:1 to 1:3. Correspondingly, the production efficiency of butyrate from glucose increased from 40.8% to 52.6%. At an ISR of 1:3, the proportion and concentration of butyrate reached 79% and 1513.2 mg COD/L, with a production efficiency of 52.6% (Table 5.2). The production efficiency obtained in the experiment was much higher than previous studies (Atasoy et al., 2019; Lv et al., 2022), for example 35.25% in Atasoy et al.'s research and 32.55% in Lv et al.'s research.

Chapter 5



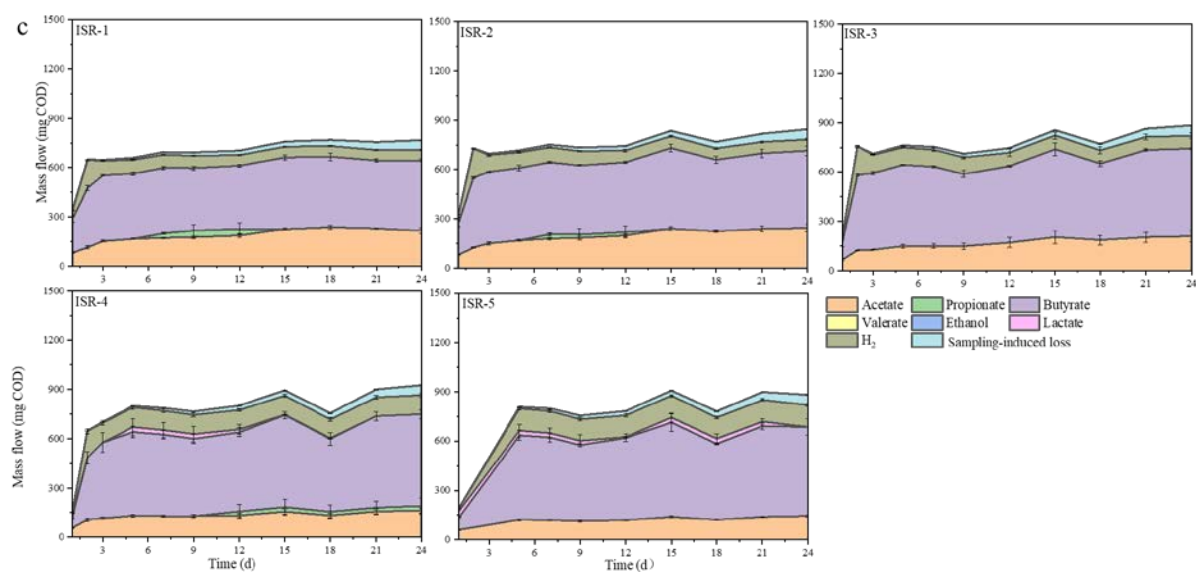


Figure 5.3 Mass balance of VFAs, ethanol, lactate and H₂ under the following conditions (a) pH range of 4.5 – 7.0 at 37 °C and 55 °C, (b) pH range of 8.5 – 11.0 at 37 °C and 55 °C, (c) various ISRs (1:3, 1:2, 1:1, 2:1, and 3:1) at 37 °C with uncontrolled pH

5.3.2 Microbial community

5.3.2.1 Microbial community diversity

Microbial community diversity was assessed using richness and diversity indices (Table 5.3). High coverage values (99.99%–100%) confirmed sufficient sequencing depth and reliable analysis. Ace and Chao1 indices, reflecting species richness, were slightly lower in reactor samples than in the inoculum, particularly in RT1 and ISR5, suggesting reduced richness under changing conditions. This observation is consistent with previous studies (Fykse et al., 2016), which reported that initial richness typically declines over time as the operational conditions change. Shannon and Simpson indices, which measure diversity and evenness, revealed that RM1, RM3, and RM5 had higher Shannon (4.990–5.33) and Simpson (0.878–0.906) values than the inoculum (4.934), indicating greater diversity and evenness. In contrast, RT1, ISR2, and ISR5 exhibited lower Shannon and Simpson values, with ISR5 showing the lowest diversity, likely due to the dominance of butyrate-producing species.

Table 5.3 Diversity and richness indices of the microbial community of samples under different conditions

Samples	Richness indices		Diversity indices		Coverage (%)
	Ace	Chao1	Shannon	Simpson	
Inoculum	3319.855	3336.719	4.934	0.877	99.999
RM1	3257.032	3257.114	4.990	0.878	100.000
RM3	3318.127	3330.113	5.312	0.906	99.999
RM5	3306.918	3317.620	5.333	0.888	100.000
RT1	2659.19	2659.852	4.525	0.817	100.000
ISR2	3309.516	3308.024	4.536	0.838	100.000
ISR5	2492.614	2491.282	2.133	0.410	99.999

5.3.2.2 Microbial community structure

In Fig. 5.4a presents a circular heatmap, illustrating the relative abundance of the top 10 phyla under different experimental conditions, including *Bacillota*, *Euryarchaeota*, *Chloroflexota*, *Bacteroidota*, *Actinomycetota*, *Thermotogota*, *Synergistota*, *Pseudomonadota*, *Candidatus Cloacimonadota* and *Atribacterota*. The *Bacillota* (formerly *Firmicutes*) phylum, primarily associated with hydrolysis and acidogenesis, was the most abundant phylum across all samples, particularly in RT1 (66%) and ISR5 (87%). The spore-forming ability of *Bacillota* likely supported their survival under thermophilic conditions (Fitamo et al., 2017). *Bacillota* was dominant in ISR5, where the highest butyrate production was observed, consistent with the previous microbial diversity analyse, indicating the existence of fewer but dominant species. *Euryarchaeota* was another abundant phylum in all reactors, with relative abundance ranging from 3% to 28%. This phylum mainly includes methanogenic archaea, crucial in methanogenesis, and is resilient and can persist under unfavourable conditions (Hailu et al., 2021). *Euryarchaeota* may persist in a dormant or less active state, even though methanogenesis was inhibited and methane was not detected throughout the process. *Chloroflexota*, *Bacteroidota*, and *Actinomycetota*, commonly found in anaerobic digestion, are crucial for glucose degradation and VFAs production (Parsy et al., 2024). The predominant phyla in all samples are involved in essential functions such as hydrolysis and acidification.

Fig. 5.4b presents the redundancy analysis (RDA) results, showing correlations between the top 10 phyla and the system parameters, such as VFAs, ethanol and environmental variables. RDA1 and RDA2 explained 74.68% and 18.75% of the variation in the phyla distribution, respectively, indicating that RDA1 played the dominant role in shaping the phyla distribution. System parameters such as pH, temperature, ISR, acetate, propionate, butyrate, and ethanol are represented by red arrows. The direction and angle of these arrows reveal the correlations between environmental variables, functional genes, and variations in specific VFAs. The RAD plot showed temperature and ISR had a greater impact on microbial community structure than pH. Furthermore, there was a competitive relationship between butyrate production and the production of acetate, propionate, and ethanol. The RDA plot also showed that butyrate concentration was closely related to *Bacillota* and *Candidatus Cloacimonadota*, indicating that these phyla were critical for butyrate production. As shown in Fig. 5.4a, the relative abundance of these two phyla was high in RM3 and ISR5, corresponding to increased butyrate production in these two conditions. In addition, ethanol production was strongly associated with temperature.

Fig. 5.4c listed the top 30 genera in the samples. Acidogenic genera in the phylum *Bacillota*, such as *Clostridium*, *Romboutsia*, *Ethanoligenens*, *Caproiciproducens* and *Caproicibacter* increased in all samples, compared to the inoculum, especially *Clostridium*. The abundance of *Clostridium* genus significantly increased in RM3, ISR2 and ISR5, likely contributing to butyrate production. To explore the relationship between the functional bacteria and environmental variables, a co-occurrence network was constructed (Fig. 5.4d). The network comprised 11 nodes and 14 edges, with node filtered based on a correlation coefficient greater than 0.7 and a p value of less than 0.05. The network confirmed that butyrate production competed with propionate and acetate production. For example, the *Tepidanaerobacter* genus was negatively correlated with butyrate production, but positively correlated with propionate production. Conversely, the genera of *Caproicibacter* and *Caproicibacterium* were positively correlated with butyrate production and negatively correlated with acetate production. Five genera were significantly correlated with butyrate production: *Caproicibacter*, *Caproicibacterium*, *Sporolactobacillus*, and *Ethanoligenens* showed positive correlations, while *Tepidanaerobacter* displayed a negative correlation. *Ethanoligenens* is known for its role in ethanol-type fermentation (Li et al., 2020c). *Sporolactobacillus* is recognized for its lactate production capability (Duan et al., 2021). The relative abundance of *Ethanoligenens*

and *Sporolactobacillus* were higher in RM3, ISR2 and ISR5. The genera *Caproicibacter* and *Caproicibacterium* are associated with chain elongation (Tang et al., 2023) and ethanol and lactate have been reported as the most ideal electron donors for inducing the chain elongation process (Wu et al., 2019). Hence, the higher butyrate production in these samples may result from chain elongation, utilizing ethanol or lactate as electron donors and acetate as the electron acceptor.

Moreover, the competition and cooperation among microorganisms were evident. The network (Fig. 5.4e) illustrates the relationships among the top 30 genera, with those lacking significant correlations excluded. A synergistic relationship was observed between *Caproicibacter* and *Caproicibacterium*, both of which were positively correlated with butyrate production. Additionally, *Terrisporobacter* was associated with butyrate production, negatively correlated with *Tepidanaerobacter*. Although *Clostridium* is known for producing butyrate and other VFAs (Atasoy et al., 2019), its relationship with butyrate production was not evident in the network analysis, likely because only certain species within *Clostridium* genus contributed to butyrate production. Core species were identified using the network topology to gain a deeper understanding of their contributions.

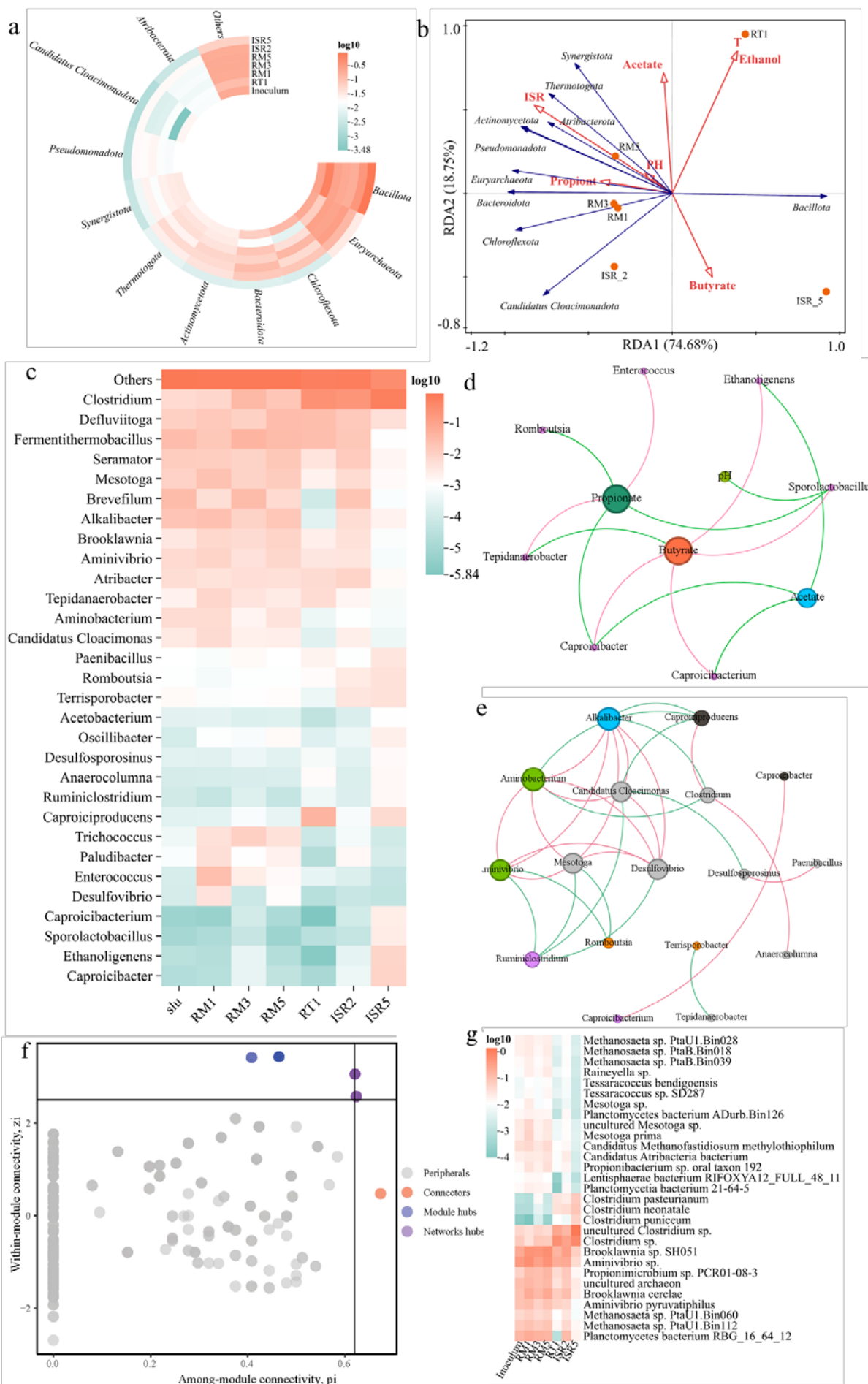


Figure 5.4 Microbial community structure, (a) top 10 phyla; (b) relationships between phyla and environmental variables; (c) top 30 genus; (d) co-occurrence network analysis of critical genus and reactor performance; (e) co-occurrence network analysis of top 30 genus with the red edges representing the positive associations and the green edges representing the negative associations; (f) identification of keystone species on their topological roles in networks with module hubs being identified as $Z_i \geq 2.5$, $P_i \leq 0.62$, connectors being identified as $Z_i < 2.5$, $P_i \geq 0.62$ and network hubs being identified as $Z_i \geq 2.5$, $P_i \geq 0.62$; (g) Relative abundance of 29 keystones presented in module hubs, connectors and network hubs.

In anaerobic fermentation systems, microbial diversity is extensive. The topological role of a node is an effective way to identify key microorganisms (Meng et al., 2023). In this study, the topological role of microorganisms across all samples was determined using Zi-Pi plot, as shown in Fig. 5.4f. The topological characteristics of the species was shown in Table 5.4. According to Zi and Pi values, nodes are divided four categories, including peripheral, connectors, network hubs and module hubs. Nodes classified as connectors, network hubs, and module hubs are recognized as keystone species, essential for maintaining the structural integrity and functional connectivity of the ecological network. A total of 29 keystone species were identified in the samples. Among them, *Aminivibrio pyruvatiphilus* and *Clostridium neonatale* were categorized as connectors, indicating that these two species were responsible for linking different modules. These two species belong to genera *Aminivibrio* and *Clostridium* genus, respectively, both of which play roles in glucose degradation and VFAs production (Xing et al., 2022). As illustrated in Figs. 5.4c and e, the abundance trends of these two genera in the samples were opposite, with no direct correlation observed between them. This suggests that these two species are likely responsible for producing different VFAs, while collectively serving as connectors between other functional processes. Additionally, 19 species were identified as the module hubs, with most belonging to the *Clostridium* genus. This finding suggests that *Clostridium* remain core microorganisms responsible for butyrate production, particularly *Clostridium sp.*, uncultured *Clostridium sp.*, and *Clostridium pasteurianum*. Studying the butyrate-producing function of *Clostridium*, with a focus on specific species, was more accurate. As shown in Fig. 5.4g, these two species (*Clostridium sp.* and uncultured *Clostridium sp.*) exhibited higher relative abundance compared to the inoculum, particularly in IR5, further confirming their critical role in butyrate production.

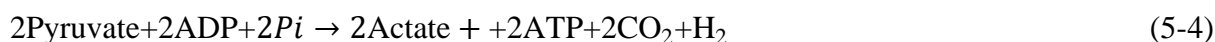
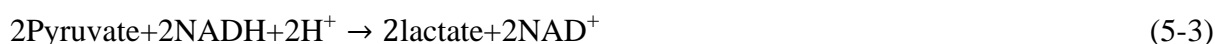
Table 5.4 Keystone species in Zi-Pi analysis

Species	zi	pi	type
<i>s__Aminivibrio pyruvatiphilus</i>	0.335	0.628	Connectors
<i>s__Clostridium neonatale</i>	0.335	0.628	Connectors
<i>s__Aminivibrio sp.</i>	2.971	0.459	Module hubs
<i>s__Planctomycetes bacterium RBG_16_64_12</i>	2.976	0.360	Module hubs
<i>s__uncultured archaeon</i>	2.971	0.459	Module hubs
<i>s__Methanosaeta sp. PtaU1.Bin112</i>	2.971	0.459	Module hubs
<i>s__Methanosaeta sp. PtaU1.Bin060</i>	2.971	0.459	Module hubs
<i>s__Mesotoga prima</i>	2.971	0.459	Module hubs
<i>s__uncultured Mesotoga sp.</i>	2.971	0.459	Module hubs
<i>s__Candidatus Methanofastidiosum methylothiophilum</i>	2.971	0.459	Module hubs
<i>s__Clostridium sp.</i>	2.678	0.466	Module hubs
<i>s__uncultured Clostridium sp.</i>	2.971	0.459	Module hubs
<i>s__Methanosaeta sp. PtaB.Bin018</i>	2.971	0.459	Module hubs
<i>s__Methanosaeta sp. PtaU1.Bin028</i>	2.971	0.459	Module hubs
<i>s__Mesotoga sp.</i>	2.678	0.466	Module hubs
<i>s__Planctomycetia bacterium 21-64-5</i>	2.976	0.360	Module hubs
<i>s__Methanosaeta sp. PtaB.Bin039</i>	2.971	0.459	Module hubs
<i>s__Planctomycetes bacterium ADurb.Bin126</i>	2.976	0.360	Module hubs
<i>s__Lentisphaerae bacterium RIFOXYA12_FULL_48_11</i>	2.976	0.360	Module hubs
<i>s__Clostridium pasteurianum</i>	2.678	0.466	Module hubs
<i>s__Clostridium puniceum</i>	2.678	0.466	Module hubs
<i>s__Brooklawnia sp. SH051</i>	2.920	0.621	Networks hubs
<i>s__Brooklawnia cerclae</i>	2.920	0.621	Networks hubs
<i>s__Propionimicrobium sp. PCR01-08-3</i>	2.920	0.621	Networks hubs
<i>s__Propionibacterium sp. oral taxon 192</i>	2.920	0.621	Networks hubs
<i>s__Candidatus Atribacteria bacterium s__Raineyella sp.</i>	2.920	0.621	Networks hubs
<i>s__Tessaracoccus sp. SD287</i>	2.920	0.621	Networks hubs
<i>s__Tessaracoccus bendigoensis</i>	2.920	0.621	Networks hubs

5.3.3 Metabolic pathway

5.3.3.1 electron transfer and NADH concentration

Eq. (5-2) – (5-7) indicate the metabolic pathways of microorganisms using glucose as the substrate to produce pyruvate, and the subsequent production of lactate, acetate, butyrate, propionate and ethanol by pyruvate. The equations clearly show that the difference of VFAs distribution was related to NADH/NAD⁺ and electron transfer (Chen et al., 2022).



NADH/NAD⁺ serves as a crucial cofactor in cytoplasmic redox reaction and is present in limited quantities within cells (Chen et al., 2022). In the conversion of glucose to pyruvate (key intermediate products of glucose degradation), NAD⁺ is reduced to NADH and must be regenerated to sustain the process. This regeneration occurs through the reoxidation of NADH via the reduction of organic intermediates, such as butyrate, propionate, and ethanol. The ratio of NADH/ NAD⁺ is shown in Fig. 5.5a, which varied with the proportion of butyrate. Acidic pH can result in an increase the NADH/NAD⁺ ratio as the excess protons can be utilized (Yang et al., 2024). This shift made NADH-consuming reactions more favourable, directing a greater electron flow toward more reduced compounds such as propionate, butyrate, and ethanol. This made butyrate production favourable with pH 4.5 to 6.0 (Fig. 5.2a). With the production of butyrate, NADH was gradually consumed, leading to the lower ratio of NADH/NAD⁺, especially in ISR2 and ISR5. Fig. 5.5c shows that the relative abundance of NADH dehydrogenases, which was consistent with the changes in NADH/NAD⁺ ratio and butyrate production, except in RT1. This may be due to the fact that ethanol production in RT1 also consumed NADH, but ethanol production did not generate ATP, and thus cannot provide energy to the microorganisms, resulting in a low abundance of NADH dehydrogenase genes (Cheng et al., 2020). The highest relative abundance of NADH dehydrogenases was found in ISR5, where butyrate production was also the highest. As described in Section 5.3.2.2, the ISR experiment demonstrated that butyrate production was promoted by the chain elongation process. This finding aligned with the rapid decrease in the

NADH/NAD⁺ ratio observed in the ISR2 and ISR5 reactors (Fig. 5.5a), as chain elongation (via reverse β -oxidation) requires a higher demand for reducing equivalents (NADH) (Spirito et al., 2014). These results suggested that butyrate production can be regulated through controlling NADH levels.

Figs. 5.5a and b shows the ETS activity, and the abundance of functional genes involved in electron transfer. The electron transport system (ETS) is commonly used to measure microbial metabolic activity, particularly the activity of the electron transport chain (Li et al., 2024). As described in Eq. (5-2) – (5-7), the consumption of NADH is accompanied by the generation of electrons, which could enhance the electron transfer and facilitate ATP synthesis. In RM3, RM5, and ISR2, ETS activity increased, corresponding to the increasing abundance of genes encoding electron transfer. The high abundance of electron transport genes suggests a strong potential for electron transport activity, which could promote butyrate production (Cheng et al., 2020). In ISR5, despite a high gene relative abundance, ETS activity was low. One potential reason could be that lower ISR may also contribute to the observed reduction in ETS activity. Alternatively, increased butyrate production relied on the electron transport chain to oxidize NADH to NAD⁺, potentially leading to limited NADH availability and thereby resulting in a lower ETS activity (Wang et al., 2022a).

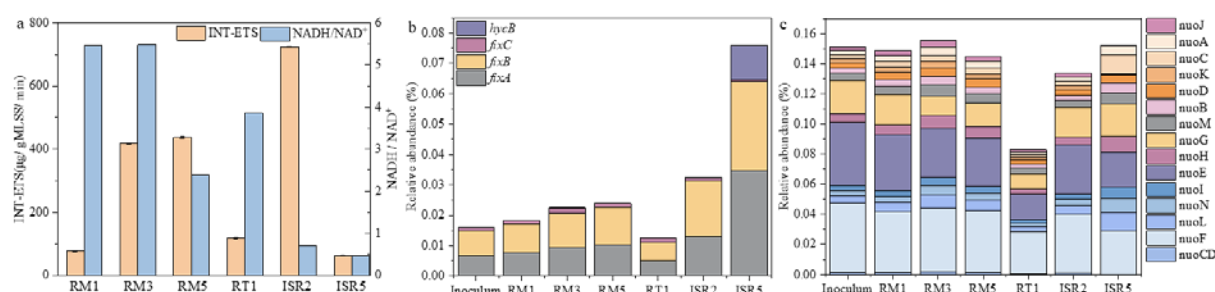


Figure 5.5 Electron transfer and NADH concentrations under different conditions: (a) ETS activity and the ratio of NADH/ NAD⁺; (b) abundance of functional genes involved in electron transfer (*hycB*: FeS-containing electron transfer protein; *fixC*: electron transfer flavoprotein-quinone oxidoreductase; *fixB*: electron transfer flavoprotein alpha subunit; *fixA*: electron transfer flavoprotein beta subunit); (c) relative abundance of NADH dehydrogenases

5.3.3.2 Hydrolysis process

Based on KEGG annotation, the metabolic pathways of glucose were constructed. As shown in Fig. 5.6a, the pathway for glucose glycolysis is mapped. Glycolysis, as a critical metabolic

step in anaerobic fermentation, directly provides substrates (such as pyruvate) for the acidogenesis stage, significantly influencing the production of VFAs (Guo et al., 2021). The expression and activity of enzymes are directly related to the rate of biochemical reactions, which participate in various biochemical processes that indicate cellular metabolism (Wang et al., 2024). The relative abundance of functional genes encoding the enzymes involved in the glycolysis process is shown in Fig. 5.6b. The names of enzymes in these metabolic pathways were shown in Table 5.5.

As shown in Fig. 5.6b, the total relative abundance of genes encoding enzymes involved in the hydrolysis process decreased under different conditions compared to the inoculum. The relative abundance showed little variation among RM1, RM3, and RM5, suggesting that the hydrolysis process was not affected by different pH levels. However, under different ISR conditions, the relative abundance significantly decreased, particularly in ISR5. Despite this, no significant differences of VFAs production efficiency were observed across the different ISR conditions (Fig. 5.2), suggesting that acidogenesis was enhanced in lower ISR reactors and butyrate production might be further promoted by improving glycolysis efficiency.

5.3.3.3 Acidogenesis process

In the experiments, the main products included butyrate, acetate, propionate, and ethanol. Consequently, the pathways for the production of these compounds are illustrated in Fig. 5.6c. Each metabolic pathway consists of a series of enzyme-catalysed reactions, and the gene abundances encoding these enzymes are shown in Fig. 5.6d.

Based on the speculation in the previous section (Section 5.3.2.2), the production of butyrate may involve a chain elongation process. Therefore, the metabolic pathways for butyrate production can be classified into three types: 1) succinyl-CoA pathway; 2) acetyl-CoA pathway; and 3) reverse β oxidation pathway. As shown in Fig. 5.6c, in the succinyl-CoA pathway, pyruvate is first converted into succinyl-CoA, which is subsequently converted into butyryl-CoA, and finally into butyrate (Esquivel-Elizondo et al., 2017). In the acetyl-CoA pathway, pyruvate is first converted into acetyl-CoA, which is then converted into acetoacetyl-CoA, followed by a series of reactions that ultimately produce butyrate. The reverse β -oxidation pathway is a carbon chain elongation process that partially overlaps with the acetyl-CoA pathway, as shown in Fig. 5.6c (red lines). In reverse β -oxidation, ethanol or lactate serves as the electron donor. It is first oxidized to acetyl-CoA, which is then coupled

with another acetyl-CoA, catalyzed by acetoacetyl-CoA thiolase, to form acetoacetyl-CoA. A series of enzymatic reactions then follow, involving NAD- and NADH-dependent 3-hydroxybutyryl-CoA dehydrogenase, 3-hydroxybutyryl-CoA dehydratase, and NAD-dependent butyryl-CoA dehydrogenase, ultimately producing the key intermediate butyryl-CoA. Finally, butyryl-CoA transfers its CoA to acetate (the electron acceptor), resulting in the formation of butyrate and the release of acetyl-CoA, catalysed by acetate CoA transferase (Wu et al., 2019).

Table 5.5 The names of enzymes in metabolic pathways

EC	Name
2.7.1.2	glucokinase
5.3.1.9	glucose-6-phosphate isomerase
2.7.1.11	6-phosphofructokinase
4.1.2.13	fructose-bisphosphate aldolase
5.3.1.1	triosephosphate isomerase
1.2.1.12	glyceraldehyde-3-phosphate dehydrogenase
1.2.1.59	glyceraldehyde-3-phosphate dehydrogenase
2.7.2.3	phosphoglycerate kinase
5.4.2.11	2,3-bisphosphoglycerate-dependent phosphoglycerate mutase
5.4.2.12	2,3-bisphosphoglycerate-independent phosphoglycerate mutase
4.2.1.11	enolase 1/2/3
2.7.1.40	pyruvate kinase
2.7.9.1	pyruvate, orthophosphate dikinase
2.7.9.2	pyruvate, water dikinase
1.2.5.1	pyruvate dehydrogenase (quinone)
1.2.7.11	2-oxoglutarate/2-oxoacid ferredoxin oxidoreductase subunit alpha
2.8.3.18	succinyl-CoA:acetate CoA-transferase
6.2.1.13	acetate---CoA ligase
1.2.3.3	pyruvate oxidase
2.7.2.1	acetate kinase
1.2.1.10	acetaldehyde dehydrogenase
1.2.1.3	aldehyde dehydrogenase
1.1.1.1	alcohol dehydrogenase
6.4.1.1	pyruvate carboxylase
1.1.1.37	malate dehydrogenase
4.2.1.2	fumarate hydratase
1.3.5.1	succinate dehydrogenase flavoprotein subunit

6.2.1.5	succinyl-CoA synthetase alpha subunit
5.4.99.2	methylmalonyl-CoA mutase
5.1.99.1	methylmalonyl-CoA
4.1.1.-	methylmalonyl-CoA decarboxylase
2.3.1.8	phosphate acetyltransferase
6.2.1.1	acetyl-CoA synthetase
1.1.1.27	lactate dehydrogenase
4.1.1.101	malolactic enzyme
2.8.3.1	propionate CoA-transferase
4.2.1.54	actoyl-CoA dehydratase
1.3.1.-	acrylyl-CoA reductase
1.2.1.76	succinate-semialdehyde dehydrogenase
1.2.1.79	succinate-semialdehyde dehydrogenase
1.1.1.-	glyoxylate/succinic semialdehyde reductase
2.8.3.-	4-hydroxybutyrate CoA-transferase
4.2.1.120	4-hydroxybutyryl-CoA dehydratase
1.3.1.44	trans-2-enoyl-CoA reductase
2.3.1.19	phosphate butyryltransferase
2.7.2.7	butyrate kinase
2.3.1.9	acetyl-CoA C-acetyltransferase
1.1.1.35	3-hydroxyacyl-CoA dehydrogenase
4.2.1.17	enoyl-CoA hydratase
1.3.1.86	crotonyl-CoA reductase
1.1.1.157	3-hydroxybutyryl-CoA dehydrogenase
4.2.1.55	3-hydroxybutyryl-CoA dehydratase
1.3.8.1	butyryl-CoA dehydrogenase
2.8.3.8	acetate CoA/acetoacetate CoA-transferase alpha subunit

As shown in Fig. 5.6d, the relative abundance of genes in the succinyl-CoA pathway and the acetyl-CoA pathway was higher in RM3, RM5, ISR2 and ISR5 compared to the inoculum. These results indicated that the activities of enzymes involved in butyrate production were enhanced, leading to high butyrate concentration in these reactors. Additionally, the relative abundance of genes involved in the succinyl-CoA pathway was higher than that in acetyl-CoA pathway, suggesting that butyrate production in this system mainly rely on the succinyl-CoA pathway. Notably, the relative abundance of genes involved in the reverse β oxidation was significantly increased in ISR5 from 0.06% to 0.11%. Additionally, the relative abundance of genes encoding ethanol production metabolic pathway and lactate conversion,

such as lactate dehydrogenase (EC 1.1.1.27) and alcohol dehydrogenase (EC 1.1.1.1), increased in ISR5. These results provide another evidence for carbon chain elongation, which enhanced butyrate production. In the RM3 and RM5, the relative abundance of genes associated with the succinyl-CoA and acetyl-CoA pathways primarily increased, whereas the relative abundance of genes encoding the reverse β -oxidation pathway showed a significant increase in the ISR2 and ISR5. These results showed that pH altered the activity of butyrate-producing bacteria to regulate butyrate production. Under the combined control of pH, temperature, and ISR (ISR2 and ISR5 samples), the butyrate production pathway gradually shifted to reverse β -oxidation pathway, which promoted butyrate production via carbon elongation reaction. This change can increase the concentration of butyrate and reduce the concentration of acetate, further improving the purity of butyrate.

As shown in Table 5.6, the key enzymes regulated butyrate production including acetate kinase (EC 2.7.2.1), acetate-CoA ligase (EC 6.2.1.13), lactoyl-CoA dehydratase (EC 4.2.1.54), succinic semialdehyde reductase (EC 1.1.1.-) and 3-hydroxybutyryl-CoA dehydratase (EC 4.2.1.55). Acetate kinase and lactoyl-CoA dehydratase showed a negative correlation with butyrate production, aligning with previous results that butyrate production competed with the production of acetate and propionate. In contrast, acetate-CoA ligase (EC 6.2.1.13), succinic semialdehyde reductase (EC 1.1.1.-) and 3-hydroxybutyryl-CoA dehydratase (EC 4.2.1.55) exhibited a positive correlation with butyrate production. The results indicated that in the succinyl-CoA pathway of butyrate production, regulating the succinic semialdehyde reductase activity may enhance butyrate production. Moreover, in reverse β -oxidation, the conversion of acetate to acetyl-CoA was vital for butyrate production.

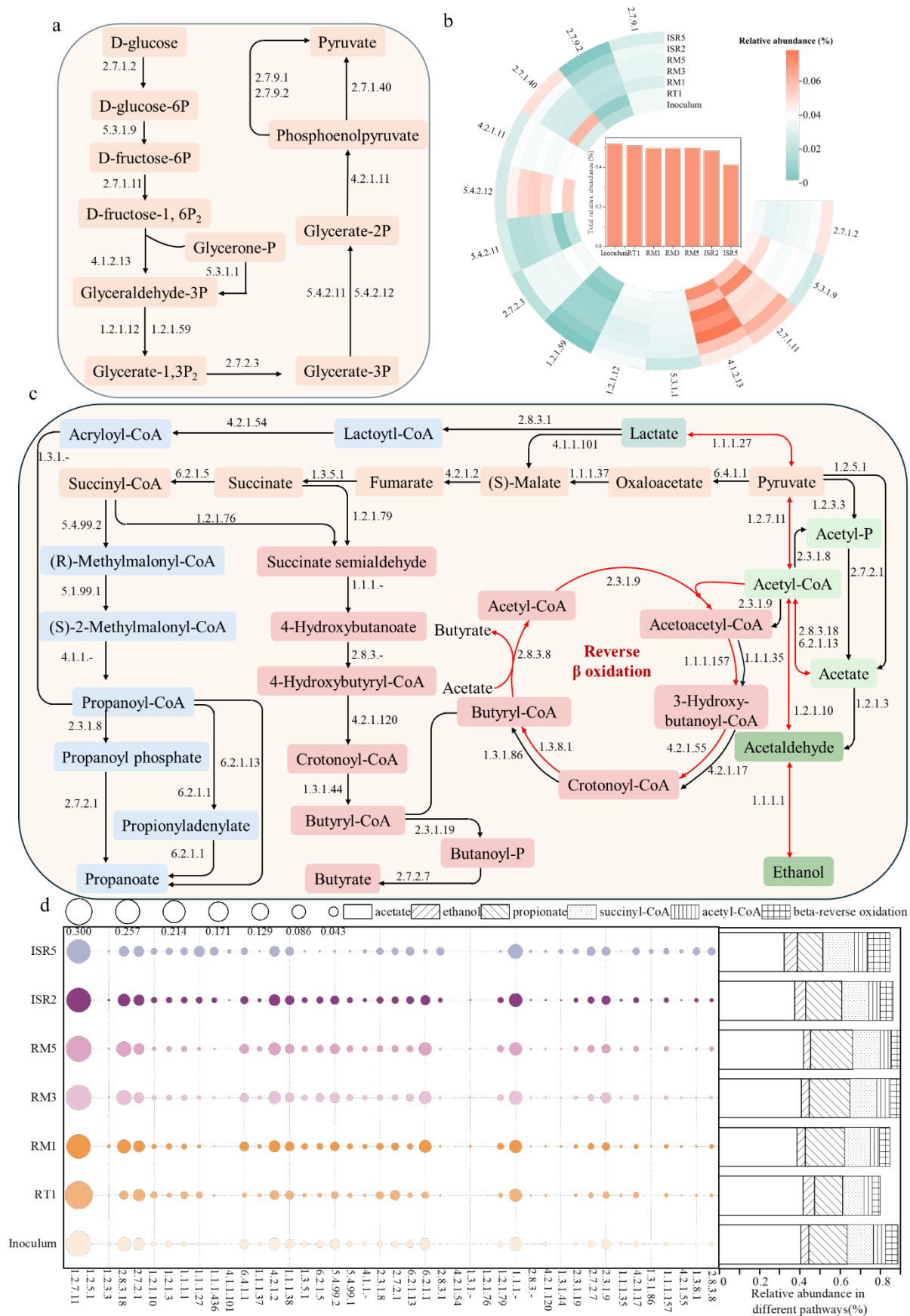


Figure 5.6 Analyses of metabolic pathways: (a) schematic diagram of the hydrolysis metabolic pathway; (b) schematic diagram of the acidogenesis metabolic pathway, including propionate, butyrate, acetate and ethanol production; (c) relative abundance of enzymes involved in the glycolysis process; and (d) relative abundance of enzymes involved in the acidogenesis process

Table 5.6 Pearson's correlation analysis between VFAs concentrations and the relative abundance of genes encoding key enzymes involved in metabolic pathways

EC number	Name of enzyme	Butyrate	Acetate	Propionate
2.7.2.1	acetate kinase	*	***	
6.2.1.13	acetate---CoA ligase	**	**	
4.2.1.54	lactoyl-CoA dehydratase	*		***
1.1.1.-	succinic semialdehyde reductase	**	**	
4.2.1.55	3-hydroxybutyryl-CoA dehydratase	*		*
2.3.1.19	phosphate butyryltransferase		*	
2.7.2.7	butyrate kinase		**	
2.3.1.9	acetyl-CoA C-acetyltransferase		*	

Note: (1) Significance levels: * $P < 0.1$; ** $P < 0.05$; *** $P < 0.005$.

(2) Color coding: Orange boxes represent positive correlations; blue boxes indicate negative correlations.

Since the production of acetate and propionate competes with butyrate production, exploring the metabolic pathways of propionate and acetate can help enhance butyrate yield. As shown in Figs. 5.6c and d, the metabolic pathways for propionate production can be categorized into two types: 1) the succinate pathway and 2) the acrylate pathway. The relative abundance of genes encoding the succinate pathway was higher than that in the acrylate pathway, indicating that the succinate pathway was the primary route for propionate production. However, lactoyl-CoA dehydratase (EC 4.2.1.54) showed a positive correlation with propionate production, which suggesting that the presence of lactate made the acrylate pathway crucial for propionate production. As for the metabolic pathway of acetate, acetate kinase (EC 2.7.2.1) exhibited a positive correlation with acetate production. Therefore, the reduction of activity of lactoyl-CoA dehydratase and acetate kinase may promote butyrate production.

5.4 Conclusion

This chapter investigated the effects of three fermentation parameters, including pH, temperature, and ISR, on butyrate selection production. Results demonstrated that different conditions lead to varying primary products. The optimal parameters for butyrate production were found to be pH 5.5, a temperature of 37°C, and an ISR of 1:3. Microbial community analysis showed that there was a competitive relationship between the production of butyrate and the production of acetate, propionate, and ethanol and the functional genera for butyrate production were *Clostridium*, *Ethanoligenens*, *Sporolactobacillus*, *Caproicibacter* and *Caproicibacterium*. Metabolic pathway analysis found the involvement of carbon chain elongation processes, which may have improved the production and purity of butyrate under the optimal condition. These findings provide valuable insights into optimizing butyrate production through controlling the operation parameters, highlighting the interconnected nature of microbial activity and metabolic flexibility in response to changes in external factors.

Chapter 6

Conclusions and Recommendations

6.1 Overview

This PhD research investigated the critical factors influencing both the degradation and production of butyric acid in anaerobic conditions. It uncovered the inhibitory impact of ammonia on butyrate degradation and examined the influence of temperature and butyric acid concentration on butyrate degradation. The study also identified optimal conditions for butyric acid production, alongside an in-depth exploration of the functional microbial communities and metabolic pathways across various environments.

6.2 Main conclusions

6.2.1 Inhibition of ammonia on butyrate degradation

- 1) The anaerobic degradation of butyrate experienced remarkable inhibition when TAN exceeded 8.0 g N/L at pH 7.5, while no discernible impacts were observed at pH 7.0 - 8.0 with 4.0 g TAN/L.
- 2) The lag phase for butyrate degradation was prolonged with increasing ammonia concentration from 0.18 to 20 g TAN/L.
- 3) Complete recovery of butyrate-degrading bacteria was observed following severe ammonia inhibition, provided that a sufficient adaptation period was available.
- 4) NH_4^+ emerged as the predominant inhibitory factor within the TAN range of 2.0 - 20.0 g N/L, rather than NH_3 .

6.2.2 Effect of temperature and butyrate concentration on butyrate degradation

- 1) High butyrate concentration significantly inhibited the methane yield. Specifically, the methane yield decreased from 321.3 to 214.2 N mL/ g $\text{COD}_{\text{added}}$ at 37 °C, and from 308.1 to 205.5 N mL/ g $\text{COD}_{\text{added}}$ at 55 °C, as butyrate concentrations increased from 2.0 to 20.0 g COD/L.
- 2) When the butyrate concentration exceeded 5 g COD/L, the methane production and butyrate degradation were more favourable at 37 °C than at 55 °C.

3) The kinetic modelling revealed that temperature and butyrate concentrations not only influenced the rate of butyrate degradation but also the distribution of intermediates.

4) The metagenomic sequencing analysis highlighted that the conversion of iso-butyrate played a crucial role in facilitating butyrate degradation.

6.2.3 Optimal conditions for butyrate selective production

1) The optimal conditions for butyrate production were found to be pH 5.5, a temperature of 37°C, and an ISR of 1:3.

2) The microbial community analysis showed that there was a competitive relationship between the production of butyrate and the production of acetate, propionate, and ethanol. The functional genera involved in butyrate production were probably *Clostridium*, *Ethanoligenens*, *Sporolactobacillus*, *Caproicibacter* and *Caproicibacterium*.

3) The metabolic pathway analysis found that carbon chain elongation processes improved the production and purity of butyrate under the optimal condition.

6.2.4 Summary

This PhD research offers valuable insights into the key factors affecting butyric acid production and degradation in anaerobic digestion systems, recognizing the dynamic nature of butyrate accumulation. It revealed that the inhibition of butyrate degradation caused by high ammonia concentrations, and the results have shown that the ammonia inhibition cannot be mitigated by simply lowering the pH level because NH_4^+ is the predominant inhibitory factor. Even at a high butyrate concentration of 20 g COD/L, butyrate degradation was not significantly affected, indicating that the accumulation of high butyrate concentrations does not lead to the collapse of the anaerobic reactor under pH control. Moreover, the increased butyrate concentration resulted in the inhibition of methane production, which is particularly advantageous in systems targeting higher butyrate yields, as it reduces methane production (a byproduct) and improves butyrate recovery from the anaerobic system. The optimal conditions for butyrate production were with pH 5.5, an ISR of 1:3 and at 37 °C. The results showed that carbon chain elongation enhanced butyrate yield and purity by using acetate as the substrate and ethanol or lactate as the electron donor. Providing additional electron donors (ethanol or lactate) could further improve the butyrate yield.

Overall, high ammonia concentration, moderate temperature, a pH of 5.5, and an inoculum-to-substrate ratio of 1:3 are the most favourable conditions for butyrate accumulation in anaerobic digestion. These results provide a comprehensive understanding of how to design reactors and control operational conditions to optimize butyrate production in anaerobic digestion.

6.3 Recommendations for future research

While this thesis has advanced the understanding of butyric acid production and degradation in anaerobic digestion systems, several areas warrant further investigation:

1) Coupling butyric acid production with biogas generation

Butyric acid accumulation in anaerobic digestion systems has been shown to influence methane production. While high butyrate concentrations can inhibit methanogenesis, controlled production of butyric acid alongside biogas generation offers potential advantages for integrated bioenergy systems. Future research should explore strategies to balance these two outputs, ensuring that butyric acid production does not excessively inhibit methanogenesis while still achieving high butyrate yields.

Several approaches could be considered for optimizing this balance. First, reactor operation strategies, such as phase separation or two-stage anaerobic digestion, could be further developed to facilitate selective butyrate accumulation in the first stage while maintaining methanogenesis in the second stage. Additionally, metabolic engineering and microbial consortia optimization could play crucial roles in tailoring microbial communities to selectively enhance butyrate production while controlling its conversion to methane. Understanding the kinetics of butyric acid-producing pathways and their interactions with methanogenic archaea would provide further insights into fine-tuning this balance. Moreover, co-substrate utilization (e.g., adding ethanol or acetate) could be investigated to enhance butyrate production while maintaining an efficient biogas yield.

2) Mechanisms of carbon chain elongation

The metabolic pathways governing carbon chain elongation remain an area of active research. Butyric acid production is closely linked to the availability of intermediate

metabolites such as ethanol, acetate, and lactate, which serve as precursors in chain elongation processes. Understanding how these intermediates contribute to butyric acid synthesis under different environmental conditions is essential for optimizing production efficiency.

Future studies should investigate the regulatory mechanisms governing chain elongation, particularly the role of specific microbial populations and their enzymatic activities. Metagenomic and metatranscriptomic analyses could provide deeper insights into the functional genes involved in these pathways. Additionally, factors such as pH, redox potential, and electron donors/acceptors should be systematically studied to identify conditions that favor efficient butyrate synthesis and further elongation to higher-value products like caproic acid.

Caproic acid, a valuable medium-chain fatty acid, can be derived from butyrate through chain elongation processes facilitated by specific microbial consortia. However, optimizing the metabolic conditions for this conversion remains a challenge. Investigating the electron transfer mechanisms and interactions between key microbial groups will be crucial for enhancing caproate production. Furthermore, bio-electrochemical approaches, such as microbial electrosynthesis, could be explored to drive the elongation of butyrate to caproate, thereby improving the overall economic viability of the process.

3) Enhancing butyrate purity for commercial applications:

In this study, the proportion of butyric acid in the fermentation products reached 79%, indicating promising selectivity. However, achieving higher purity remains a key challenge due to the presence of other volatile fatty acids (VFAs) in the fermentation broth. Enhancing butyrate purity is critical for reducing downstream purification costs and increasing the commercial value of the product.

Future research should focus on developing bio-electrochemical systems to enhance butyrate production while minimizing undesired byproducts. These systems can be designed to selectively favor butyrate-producing pathways by controlling electron flow and redox conditions. Moreover, innovative reactor designs, such as membrane bioreactors or integrated fermentation-separation systems, should be explored to improve process efficiency.

In addition to optimizing production strategies, advanced separation and purification techniques must be investigated. Membrane filtration, electrodialysis, and chromatographic methods offer potential solutions for selectively separating butyrate from complex VFA mixtures. For instance, membrane-based separation processes can enhance butyrate recovery while maintaining low energy requirements. Additionally, solvent extraction and pervaporation technologies could be explored for their ability to selectively concentrate butyric acid from fermentation broths. These techniques, combined with metabolic engineering approaches, could significantly improve the overall yield and purity of butyric acid.

Achieving high-purity butyric acid will not only reduce purification costs but also expand its potential applications in various industries, including bioplastics, and animal feed additives. Future studies should explore the feasibility of using high-purity butyric acid as a precursor for polyhydroxyalkanoates (PHA) synthesis, given its role in sustainable biopolymer production.

Bibliography

- Adekunle, K.F., Okolie, J.A. 2015. A Review of Biochemical Process of Anaerobic Digestion. *Advances in Bioscience and Biotechnology*, **06**(03), 205-212.
- Agyeman, F.O., Han, Y., Tao, W. 2021. Elucidating the kinetics of ammonia inhibition to anaerobic digestion through extended batch experiments and stimulation-inhibition modeling. *Bioresource Technology*, **340**, 125744.
- Al Battashi, H., Al-Kindi, S., Gupta, V.K., Sivakumar, N. 2020. Polyhydroxyalkanoate (PHA) Production Using Volatile Fatty Acids Derived from the Anaerobic Digestion of Waste Paper. *Journal of Polymers and the Environment*, **29**(1), 250-259.
- Alavi-Borazjani, S.A., Capela, I., Tarelho, L.A.C. 2020. Over-acidification control strategies for enhanced biogas production from anaerobic digestion: A review. *Biomass and Bioenergy*, **143**.
- Alibardi, L., Cossu, R. 2016. Effects of carbohydrate, protein and lipid content of organic waste on hydrogen production and fermentation products. *Waste Manag*, **47**(Pt A), 69-77.
- Amani, T., Nosrati, M., Mousavi, S. M., & Kermanshahi, R. K. . 2011. Study of syntrophic anaerobic digestion of volatile fatty acids using enriched cultures at mesophilic conditions. *International Journal of Environmental Science & Technology*, **8**(1), 83-96.
- Amend, J.P., Shock, E.L. 2001. Energetics of overall metabolic reactions of thermophilic and hyperthermophilic Archaea and Bacteria. *FEMS microbiology reviews*, **25**(2), 175-243.
- Angelidaki, I., Ahring, B.K. 1995. Isomerization of n-and i-butyrate in anaerobic methanogenic systems. *Antonie van Leeuwenhoek*, **68**, 285-291.
- Ao, T., Chen, L., Chen, Y., Liu, X., Wan, L., Li, D. 2021. The screening of early warning indicators and microbial community of chicken manure thermophilic digestion at high organic loading rate. *Energy*, **224**, 120201.
- APHA. 2023. *Standard Methods for the Examination of Water and Waste Water. 24th ed.* American Public Health Association, Washington, DC, USA.
- Astals, S., Peces, M., Batstone, D.J., Jensen, P.D., Tait, S. 2018. Characterising and modelling free ammonia and ammonium inhibition in anaerobic systems. *Water Res*, **143**, 127-135.

- Atasoy, M., Cetecioglu, Z. 2022. The effects of pH on the production of volatile fatty acids and microbial dynamics in long-term reactor operation. *J Environ Manage*, **319**, 115700.
- Atasoy, M., Eyice, O., Schnurer, A., Cetecioglu, Z. 2019. Volatile fatty acids production via mixed culture fermentation: Revealing the link between pH, inoculum type and bacterial composition. *Bioresour Technol*, **292**, 121889.
- Atasoy, M., Owusu-Agyeman, I., Plaza, E., Cetecioglu, Z. 2018. Bio-based volatile fatty acid production and recovery from waste streams: Current status and future challenges. *Bioresour Technol*, **268**, 773-786.
- Bao, T., Feng, J., Jiang, W., Fu, H., Wang, J., Yang, S.T. 2020. Recent advances in n-butanol and butyrate production using engineered *Clostridium tyrobutyricum*. *World J Microbiol Biotechnol*, **36**(9), 138.
- Barcenilla, A., Pryde, S.E., Martin, J.C., Duncan, S.H., Stewart, C.S., Henderson, C., Flint, H.J. 2000. Phylogenetic Relationships of Butyrate-Producing Bacteria from the Human Gut. *Applied and environmental microbiology*, **66**(4), 1654-1661.
- Bastian, M., Heymann, S., Jacomy, M. 2009. Gephi: an open source software for exploring and manipulating networks. *In Proceedings of the international AAAI conference on web and social media*, **3**(1), 361-362.
- Baur, S.T., Markussen, S., Di Bartolomeo, F., Poehlein, A., Baker, A., Jenkinson, E.R., Dürre, P. 2022. Increased Butyrate Production in *Clostridium saccharoperbutylacetonicum* from Lignocellulose-Derived Sugars. *Applied and Environmental Microbiology*, **88**(7), e02419-21.
- Begum, S., Anupoju, G.R., Sridhar, S., Bhargava, S.K., Jegatheesan, V., Eshtiaghi, N. 2018. Evaluation of single and two stage anaerobic digestion of landfill leachate: Effect of pH and initial organic loading rate on volatile fatty acid (VFA) and biogas production. *Bioresour Technol*, **251**, 364-373.
- Beneragama, N., Iwasaki, M., Lateef, S.A., Yamashiro, T., Ihara, I., Umetsu, K. 2013. Survival of multidrug-resistant bacteria in thermophilic and mesophilic anaerobic co-digestion of dairy manure and waste milk. *Anim Sci J*, **84**(5), 426-433.
- Bengtsson, S., Hallquist, J., Werker, A., Welander, T. 2008. Acidogenic fermentation of industrial wastewaters: Effects of chemostat retention time and pH on volatile fatty acids production. *Biochemical Engineering Journal*, **40**(3), 492-499.

- Bonk, F., Popp, D., Weinrich, S., Strauber, H., Kleinstaubler, S., Harms, H., Centler, F. 2018. Ammonia Inhibition of Anaerobic Volatile Fatty Acid Degrading Microbial Communities. *Front Microbiol*, **9**, 2921.
- Cai, F., Lin, M., Wang, L., Song, C., Jin, Y., Liu, G., Chen, C. 2024. Enhancing acidification efficiency of vegetable wastes through heat shock pretreatment and initial pH regulation. *Environ Sci Pollut Res Int*, **31**(1), 1079-1093.
- Cai, Y., Gallegos, D., Zheng, Z., Stinner, W., Wang, X., Proter, J., Schafer, F. 2021. Exploring the combined effect of total ammonia nitrogen, pH and temperature on anaerobic digestion of chicken manure using response surface methodology and two kinetic models. *Bioresour Technol*, **337**, 125328.
- Cao, L., Keener, H., Huang, Z., Liu, Y., Ruan, R., Xu, F. 2020. Effects of temperature and inoculation ratio on methane production and nutrient solubility of swine manure anaerobic digestion. *Bioresour Technol*, **299**, 122552.
- Capson-Tojo, G., Moscoviz, R., Astals, S., Robles, Á., Steyer, J.P. 2020. Unraveling the literature chaos around free ammonia inhibition in anaerobic digestion. *Renewable and Sustainable Energy Reviews*, **117**, 109487.
- Capson-Tojo, G., Trably, E., Rouez, M., Crest, M., Steyer, J.P., Delgenes, J.P., Escudie, R. 2017. Dry anaerobic digestion of food waste and cardboard at different substrate loads, solid contents and co-digestion proportions. *Bioresour Technol*, **233**, 166-175.
- Carlsson, M., Lagerkvist, A., Morgan-Sagastume, F. 2012. The effects of substrate pre-treatment on anaerobic digestion systems: a review. *Waste Manag*, **32**(9), 1634-1650.
- Castro-Ramos, J.J., Solis-Oba, A., Solis-Oba, M., Calderon-Vazquez, C.L., Higuera-Rubio, J.M., Castro-Rivera, R. 2022. Effect of the initial pH on the anaerobic digestion process of dairy cattle manure. *AMB Express*, **12**(1), 162.
- CEAP. 2020. Circular economy action plan, Vol. 2024. https://environment.ec.europa.eu/strategy/circular-economy-action-plan_en/ (access 9 December, 2024).
- Chaganti, S.R., Kim, D.-H., Lalman, J.A. 2011. Flux balance analysis of mixed anaerobic microbial communities: Effects of linoleic acid (LA) and pH on biohydrogen production. *International Journal of Hydrogen Energy*, **36**(21), 14141-14152.
- Cheah, Y.K., Vidal-Antich, C., Dosta, J., Mata-Alvarez, J. 2019. Volatile fatty acid production from mesophilic acidogenic fermentation of organic fraction of municipal

- solid waste and food waste under acidic and alkaline pH. *Environ Sci Pollut Res Int*, **26**(35), 35509-35522.
- Chen, B., Rupani, P.F., Azman, S., Dewil, R., Appels, L. 2022. A redox-based strategy to enhance propionic and butyric acid production during anaerobic fermentation. *Bioresour Technol*, **361**, 127672.
- Chen, H., Chang, S. 2020. Dissecting methanogenesis for temperature-phased anaerobic digestion: Impact of temperature on community structure, correlation, and fate of methanogens. *Bioresour Technol*, **306**, 123104.
- Chen, W.S., Huang, S., Strik, D.P., Buisman, C.J.N. 2016. Isobutyrate biosynthesis via methanol chain elongation: converting organic wastes to platform chemicals. *Journal of Chemical Technology & Biotechnology*, **92**(6), 1370-1379.
- Chen, X., Yuan, H., Zou, D., Liu, Y., Zhu, B., Chufo, A., Jaffar, M., Li, X. 2015. Improving biomethane yield by controlling fermentation type of acidogenic phase in two-phase anaerobic co-digestion of food waste and rice straw. *Chemical Engineering Journal*, **273**, 254-260.
- Chen, Y., Jiang, X., Xiao, K., Shen, N., Zeng, R.J., Zhou, Y. 2017. Enhanced volatile fatty acids (VFAs) production in a thermophilic fermenter with stepwise pH increase - Investigation on dissolved organic matter transformation and microbial community shift. *Water Res*, **112**, 261-268.
- Chen, Y., Liu, Y., Lv, J., Wu, D., Jiang, L., Lv, W. 2024. Short-time aerobic digestion treatment of waste activated sludge to enhance EPS production and sludge dewatering performance by changing microbial communities: The impact of temperature. *Water Cycle*, **5**, 146-155.
- Cheng, J., Li, H., Ding, L., Zhou, J., Song, W., Li, Y.-Y., Lin, R. 2020. Improving hydrogen and methane co-generation in cascading dark fermentation and anaerobic digestion: The effect of magnetite nanoparticles on microbial electron transfer and syntrophism. *Chemical Engineering Journal*, **397**, 125394.
- Chi, X., Li, J., Wang, X., Zhang, Y., Leu, S.Y., Wang, Y. 2018. Bioaugmentation with *Clostridium tyrobutyricum* to improve butyric acid production through direct rice straw bioconversion. *Bioresour Technol*, **263**, 562-568.
- Chiappero, M., Norouzi, O., Hu, M., Demichelis, F., Berruti, F., Di Maria, F., Mašek, O., Fiore, S. 2020. Review of biochar role as additive in anaerobic digestion processes. *Renewable and Sustainable Energy Reviews*, **131**, 110037.

- Comte, S., Guibaud, G., Baudu, M. 2006. Relations between extraction protocols for activated sludge extracellular polymeric substances (EPS) and EPS complexation properties. *Enzyme and Microbial Technology*, **38**(1-2), 237-245.
- Dahiya, S., Kumar, A.N., Shanthi Sravan, J., Chatterjee, S., Sarkar, O., Mohan, S.V. 2018. Food waste biorefinery: Sustainable strategy for circular bioeconomy. *Bioresour Technol*, **248**(Pt A), 2-12.
- Dareioti, M.A., Tsigkou, K., Vavouraki, A.I., Kornaros, M. 2022. Hydrogen and Methane Production from Anaerobic Co-Digestion of Sorghum and Cow Manure: Effect of pH and Hydraulic Retention Time. *Fermentation*, **8**(7), 304.
- Dareioti, M.A., Vavouraki, A.I., Kornaros, M. 2014. Effect of pH on the anaerobic acidogenesis of agroindustrial wastewaters for maximization of bio-hydrogen production: a lab-scale evaluation using batch tests. *Bioresour Technol*, **162**, 218-27.
- De Bok, F.A., Stams, A.J., Dijkema, C., Boone, D.R. 2001. Pathway of propionate oxidation by a syntrophic culture of *Smithella propionica* and *Methanospirillum hungatei*. *Appl Environ Microbiol*, **67**(4), 1800-1804.
- De Leeuw, K.D., de Smit, S.M., Sabine, v.O., Moerland, M.J., Buisman, C.J.N., Strik, D.P.B.T.B. 2020. Methanol-Based Chain Elongation with Acetate to n-Butyrate and Isobutyrate at Varying Selectivities Dependent on pH. *ACS Sustainable Chemistry & Engineering*, **8**(22), 8184-8194.
- De Vrieze, J., Hennebel, T., Boon, N., Verstraete, W. 2012. Methanosarcina: the rediscovered methanogen for heavy duty biomethanation. *Bioresour Technol*, **112**, 1-9.
- Demirel, B., Scherer, P. 2008. The roles of acetotrophic and hydrogenotrophic methanogens during anaerobic conversion of biomass to methane: a review. *Reviews in Environmental Science and Bio/Technology*, **7**(2), 173-190.
- Deng, Y.F., Jiang, Y.H., Yang, Y., He, Z., Luo, F., Zhou, J. 2012. Molecular ecological network analyses. *BMC bioinformatics*, **13**, 1-20.
- Dennehy, C., Lawlor, P.G., Croize, T., Jiang, Y., Morrison, L., Gardiner, G.E., Zhan, X. 2016. Synergism and effect of high initial volatile fatty acid concentrations during food waste and pig manure anaerobic co-digestion. *Waste Manag*, **56**, 173-80.
- Detman, A., Laubitz, D., Chojnacka, A., Kiela, P.R., Salamon, A., Barberan, A., Chen, Y., Yang, F., Blaszczyk, M.K., Sikora, A. 2021. Dynamics of dark fermentation microbial communities in the light of lactate and butyrate production. *Microbiome*, **9**(1), 158.

- Dev, S., Saha, S., Kurade, M.B., Salama, E.-S., El-Dalatony, M.M., Ha, G.-S., Chang, S.W., Jeon, B.-H. 2019. Perspective on anaerobic digestion for biomethanation in cold environments. *Renewable and Sustainable Energy Reviews*, **103**, 85-95.
- Dionisi, D., Silva, I.M.O. 2016. Production of ethanol, organic acids and hydrogen: an opportunity for mixed culture biotechnology? *Reviews in Environmental Science and Bio/Technology*, **15**(2), 213-242.
- Dooms, M., Benbelkacem, H., Buffière, P. 2018. High solid temperature phased anaerobic digestion from agricultural wastes: Putting several reactors in sequence. *Biochemical Engineering Journal*, **130**, 21-28.
- Duan, J.-L., Feng, Y., Feng, L.-J., Ma, J.-Y., Sun, X.-D., Wang, Q., Li, X.-Y., Xiao, F., Xu, P.-C., Tian, R.-K., Sun, W.-L., Yuan, X.-Z. 2021. Unraveling Anaerobic Digestion Foaming via Association between Bacterial Metabolism and Variations in Microbiota. *ACS ES&T Engineering*, **1**(6), 978-988.
- Duong, T.H., Nga, T.T.V. 2024. Production of Volatile Fatty Acids from Organic-Rich Waste Streams: Current Issues, Challenges, and Opportunities. *Current Pollution Reports*, **10**(4), 594-605.
- Dwidar, M., Kim, S., Jeon, B. S., Um, Y., Mitchell, R. J., & Sang, B. I. 2013. Co-culturing a novel Bacillus strain with Clostridium tyrobutyricum ATCC 25755 to produce butyric acid from sucrose. *Biotechnology for biofuels*, **6**, 1-10.
- EFSA. 2025. Nutrition applications: regulations and guidance, Vol. 23, European Food Safety Authority. EFSA Journal, pp. e12345.
- Elbeshbishy, E., Nakhla, G. 2012. Batch anaerobic co-digestion of proteins and carbohydrates. *Bioresour Technol*, **116**, 170-178.
- Eryildiz, B., Lukitawesa, Taherzadeh, M.J. 2020. Effect of pH, substrate loading, oxygen, and methanogens inhibitors on volatile fatty acid (VFA) production from citrus waste by anaerobic digestion. *Bioresour Technol*, **302**, 122800.
- Esquivel-Elizondo, S.I., Z. E., Garcia-Peña, E.I., Krajmalnik-Brown, R. 2017. Insights into butyrate production in a controlled fermentation system via gene predictions. *mSystems*, **2**(4), e00051-17.
- Fakkaew, K., Polprasert, C. 2021. Air stripping pre-treatment process to enhance biogas production in anaerobic digestion of chicken manure wastewater. *Bioresource Technology Reports*, **14**, 100647.

- Feng, K., Li, H., Deng, Z., Wang, Q., Zhang, Y., Zheng, C. 2020. Effect of pre-fermentation types on the potential of methane production and energy recovery from food waste. *Renewable Energy*, **146**, 1588-1595.
- Feng, K., Li, H., Zheng, C. 2018. Shifting product spectrum by pH adjustment during long-term continuous anaerobic fermentation of food waste. *Bioresour Technol*, **270**, 180-188.
- Feng, L.Y., Chen, Y.G., Zheng, X. 2009. Enhancement of waste activated sludge protein conversion and volatile fatty acids accumulation during waste activated sludge anaerobic fermentation by carbohydrate substrate addition: the effect of pH. *Environ. Sci. Technol.*, **43**, 4373-4380.
- Feng, S., Ngo, H.H., Guo, W., Chang, S.W., Nguyen, D.D., Liu, Y., Zhang, S., Phong Vo, H.N., Bui, X.T., Ngoc Hoang, B. 2022. Volatile fatty acids production from waste streams by anaerobic digestion: A critical review of the roles and application of enzymes. *Bioresour Technol*, **359**, 127420.
- Ferguson, R.M.W., Coulon, F., Villa, R. 2016. Organic loading rate: A promising microbial management tool in anaerobic digestion. *Water Res*, **100**, 348-356.
- Fernandez-Dominguez, D., Astals, S., Peces, M., Frison, N., Bolzonella, D., Mata-Alvarez, J., Dosta, J. 2020. Volatile fatty acids production from biowaste at mechanical-biological treatment plants: Focusing on fermentation temperature. *Bioresour Technol*, **314**, 123729.
- Fernández-Rodríguez, J., Pérez, M., Romero, L.I. 2016. Semicontinuous Temperature-Phased Anaerobic Digestion (TPAD) of Organic Fraction of Municipal Solid Waste (OFMSW). Comparison with single-stage processes. *Chemical Engineering Journal*, **285**, 409-416.
- Ferry, J.G. 2011. Fundamentals of methanogenic pathways that are key to the biomethanation of complex biomass. *Curr Opin Biotechnol*, **22**(3), 351-357.
- Fitamo, T., Treu, L., Boldrin, A., Sartori, C., Angelidaki, I., Scheutz, C. 2017. Microbial population dynamics in urban organic waste anaerobic co-digestion with mixed sludge during a change in feedstock composition and different hydraulic retention times. *Water Res*, **118**, 261-271.
- Fonseca, B.C., Bortolucci, J., da Silva, T.M., dos Passos, V.F., de Gouvêa, P.F., Dinamarco, T.M., Reginatto, V. 2020. Butyric acid as sole product from xylose fermentation by a

- non-solventogenic *Clostridium beijerinckii* strain under controlled pH and nutritional conditions. *Bioresource Technology Reports*, **10**, 100426.
- Frølund, B., Griebe, T., Nielsen, P.H. 1995. Enzymatic activity in the activated-sludge floc matrix. *Applied microbiology and biotechnology*, **43**, 755-761.
- Fu, B., Zhang, J., Fan, J., Wang, J., Liu, H. 2012. Control of C/N ratio for butyric acid production from textile wastewater sludge by anaerobic digestion. *Water Sci Technol*, **65**(5), 883-889.
- Fu, H., Yue, Z., Feng, J., Bao, T., Yang, S.-T., Cai, Y., Wang, J. 2022a. Consolidated bioprocessing for butyric acid production from raw cassava starch by a newly isolated *Clostridium butyricum* SCUT620. *Industrial Crops and Products*, **187**, 115446.
- Fu, H., Zhang, H., Guo, X., Yang, L., Wang, J. 2022b. Elimination of carbon catabolite repression in *Clostridium tyrobutyricum* for enhanced butyric acid production from lignocellulosic hydrolysates. *Bioresource Technology*, **357**, 127320.
- Fuchs, W., Wang, X., Gabauer, W., Ortner, M., Li, Z. 2018. Tackling ammonia inhibition for efficient biogas production from chicken manure: Status and technical trends in Europe and China. *Renewable and Sustainable Energy Reviews*, **97**, 186-199.
- Fuess, L.T., Ferraz, A.D.N.J., Machado, C.B., Zaiat, M. 2018. Temporal dynamics and metabolic correlation between lactate-producing and hydrogen-producing bacteria in sugarcane vinasse dark fermentation: The key role of lactate. *Bioresour Technol*, **247**, 426-433.
- Fykse, E.M., Aarskaug, T., Madslie, E.H., Dybwad, M. 2016. Microbial community structure in a full-scale anaerobic treatment plant during start-up and first year of operation revealed by high-throughput 16S rRNA gene amplicon sequencing. *Bioresour Technol*, **222**, 380-387.
- Gao, S., Zhao, M., Chen, Y., Yu, M., Ruan, W. 2015. Tolerance response to in situ ammonia stress in a pilot-scale anaerobic digestion reactor for alleviating ammonia inhibition. *Bioresour Technol*, **198**, 372-379.
- Garcia-Aguirre, J., Aymerich, E., Gonzalez-Mtnez de Goni, J., Esteban-Gutierrez, M. 2017. Selective VFA production potential from organic waste streams: Assessing temperature and pH influence. *Bioresour Technol*, **244**(Pt 1), 1081-1088.
- Goldberg, I., Rokem, J.S. 2009. *Organic and fatty acid production*. *Encyclopedia of microbiology (3rd ed)*. Academic Press, Oxford

- Golkowska, K., Greger, M. 2013. Anaerobic digestion of maize and cellulose under thermophilic and mesophilic conditions – A comparative study. *Biomass and Bioenergy*, **56**, 545-554.
- Gong, X., Wu, M., Jiang, Y., Wang, H. 2021. Effects of different temperatures and pH values on volatile fatty acids production during codigestion of food waste and thermal-hydrolysed sewage sludge and subsequent volatile fatty acids for polyhydroxyalkanoates production. *Bioresour Technol*, **333**, 125149.
- Gu, J., Liu, R., Cheng, Y., Stanisavljevic, N., Li, L., Djatkov, D., Peng, X., Wang, X. 2020. Anaerobic co-digestion of food waste and sewage sludge under mesophilic and thermophilic conditions: Focusing on synergistic effects on methane production. *Bioresour Technol*, **301**, 122765.
- Guo, H., Oosterkamp, M.J., Tonin, F., Hendriks, A., Nair, R., van Lier, J.B., de Kreuk, M. 2021. Reconsidering hydrolysis kinetics for anaerobic digestion of waste activated sludge applying cascade reactors with ultra-short residence times. *Water Research*, **202**, 117398.
- Guo, J., Dong, R., Clemens, J., Wang, W. 2013. Thermal modelling of the completely stirred anaerobic reactor treating pig manure at low range of mesophilic conditions. *J Environ Manage*, **127**, 18-22.
- Hailu, A.M., Palani, S.G., Asfaw, S.L., Tegaye, T.A. 2021. Insight into microbial community diversity and composition of two-stage anaerobic digestion: Focusing methanogenic stage. *Bioresource Technology Reports*, **15**, 100764.
- Harirchi, S., Wainaina, S., Sar, T., Nojoudi, S.A., Parchami, M., Parchami, M., Varjani, S., Khanal, S.K., Wong, J., Awasthi, M.K., Taherzadeh, M.J. 2022. Microbiological insights into anaerobic digestion for biogas, hydrogen or volatile fatty acids (VFAs): a review. *Bioengineered*, **13**(3), 6521-6557.
- He, F., Qin, S., Yang, Z., Bai, X., Suo, Y., Wang, J. 2020. Butyric acid production from spent coffee grounds by engineered *Clostridium tyrobutyricum* overexpressing galactose catabolism genes. *Bioresour Technol*, **304**, 122977.
- He, G.Q., Kong, Q., Chen, Q.H., Ruan, H. 2005. Batch and fed-batch production of butyric acid by *Clostridium butyricum* ZJUCB. *J Zhejiang Univ Sci B*, **6**(11), 1076-1080.
- He, M., Sun, Y., Zou, D., Yuan, H., Zhu, B., Li, X., Pang, Y. 2012. Influence of Temperature on Hydrolysis Acidification of Food Waste. *Procedia Environmental Sciences*, **16**, 85-94.

- Horiuchi, J.I., Shimizu, T., Tada, K., Kanno, T., Kobayashi, M. 2002. Selective production of organic acids in anaerobic acid reactor by pH control. *Bioresource Technology*, **82**, 209-213.
- Hunter, S.M., Blanco, E., Borrion, A. 2021. Expanding the anaerobic digestion map: A review of intermediates in the digestion of food waste. *Sci Total Environ*, **767**, 144265.
- Hussain, A., Dubey, S.K. 2017. Specific methanogenic activity test for anaerobic degradation of influents. *Applied Water Science*, **7**, 535-542.
- Jang, Y.-S., Im, J.A., Choi, S.Y., Lee, J.I., Lee, S.Y. 2014. Metabolic engineering of *Clostridium acetobutylicum* for butyric acid production with high butyric acid selectivity. *Metabolic Engineering*, **23**, 165-174.
- Jiang, J., Zhang, Y., Li, K., Wang, Q., Gong, C., Li, M. 2013. Volatile fatty acids production from food waste: effects of pH, temperature, and organic loading rate. *Bioresour Technol*, **143**, 525-530.
- Jiang, L., Fu, H., Yang, H.K., Xu, W., Wang, J., Yang, S.T. 2018. Butyric acid: Applications and recent advances in its bioproduction. *Biotechnol Adv*, **36**(8), 2101-2117.
- Jiang, Y., McAdam, E., Zhang, Y., Heaven, S., Banks, C., Longhurst, P. 2019. Ammonia inhibition and toxicity in anaerobic digestion: A critical review. *Journal of Water Process Engineering*, **32**, 100899.
- Jin, Y., Lin, Y., Wang, P., Jin, R., Gao, M., Wang, Q., Chang, T.C., Ma, H. 2019. Volatile fatty acids production from saccharification residue from food waste ethanol fermentation: Effect of pH and microbial community. *Bioresour Technol*, **292**, 121957.
- Junicke, H., van Loosdrecht, M.C., Kleerebezem, R. 2016. Kinetic and thermodynamic control of butyrate conversion in non-defined methanogenic communities. *Appl Microbiol Biotechnol*, **100**(2), 915-925.
- Kanehisa, M., Furumichi, M., Tanabe, M., Sato, Y., Morishima, K. 2017. KEGG: new perspectives on genomes, pathways, diseases and drugs. *Nucleic Acids Res*, **45**(D1), D353-D361.
- Kelbert, M., Machado, T.O., Araújo, P.H.H., Sayer, C., de Oliveira, D., Maziero, P., Simons, K.E., Carciofi, B.A.M. 2024. Perspectives on biotechnological production of butyric acid from lignocellulosic biomass. *Renewable and Sustainable Energy Reviews*, **202**, 114717.

- Khan, M.A., Ngo, H.H., Guo, W., Chang, S.W., Nguyen, D.D., Varjani, S., Liu, Y., Deng, L., Cheng, C. 2019. Selective production of volatile fatty acids at different pH in an anaerobic membrane bioreactor. *Bioresour Technol*, **283**, 120-128.
- Khan, M.A., Ngo, H.H., Guo, W.S., Liu, Y., Nghiem, L.D., Hai, F.I., Deng, L.J., Wang, J., Wu, Y. 2016. Optimization of process parameters for production of volatile fatty acid, biohydrogen and methane from anaerobic digestion. *Bioresour Technol*, **219**, 738-748.
- Khatami, K., Atasoy, M., Ludtke, M., Baresel, C., Eyice, O., Cetecioglu, Z. 2021. Bioconversion of food waste to volatile fatty acids: Impact of microbial community, pH and retention time. *Chemosphere*, **275**, 129981.
- Kim, M., Kim, K.Y., Lee, K.M., Youn, S.H., Lee, S.M., Woo, H.M., Oh, M.K., Um, Y. 2016. Butyric acid production from softwood hydrolysate by acetate-consuming *Clostridium* sp. S1 with high butyric acid yield and selectivity. *Bioresour Technol*, **218**, 1208-1214.
- Kim, S.-H., Han, S.-K., Shin, H.-S. 2006. Effect of substrate concentration on hydrogen production and 16S rDNA-based analysis of the microbial community in a continuous fermenter. *Process Biochemistry*, **41**(1), 199-207.
- Kong, X., Wei, Y., Xu, S., Liu, J., Li, H., Liu, Y., Yu, S. 2016. Inhibiting excessive acidification using zero-valent iron in anaerobic digestion of food waste at high organic load rates. *Bioresour Technol*, **211**, 65-71.
- Kong, X., Yu, S., Fang, W., Liu, J., Li, H. 2018a. Enhancing syntrophic associations among *Clostridium butyricum*, *Syntrophomonas* and two types of methanogen by zero valent iron in an anaerobic assay with a high organic loading. *Bioresour Technol*, **257**, 181-191.
- Kong, X., Yu, S., Xu, S., Fang, W., Liu, J., Li, H. 2018b. Effect of Fe(0) addition on volatile fatty acids evolution on anaerobic digestion at high organic loading rates. *Waste Manag*, **71**, 719-727.
- Kumanowska, E., Urunuela Saldana, M., Zielonka, S., Oechsner, H. 2017. Two-stage anaerobic digestion of sugar beet silage: The effect of the pH-value on process parameters and process efficiency. *Bioresour Technol*, **245**(Pt A), 876-883.
- Labib, F., Ferguson, J.F., Benjamin, M.M., Merigh, M., Ricker, N.L. 1992. Anaerobic butyrate degradation in a fluidized-bed reactor: effects of increased concentrations of hydrogen and acetate. *Environmental science & technology*, **26**(2), 369-376.

- Lee, K.M., Kim, K.-Y., Choi, O., Woo, H.M., Kim, Y., Han, S.O., Sang, B.-I., Um, Y. 2015. In situ detoxification of lignocellulosic hydrolysate using a surfactant for butyric acid production by *Clostridium tyrobutyricum* ATCC 25755. *Process Biochemistry*, **50**(4), 630-635.
- Li, B.Y., Xia, Z.Y., Gou, M., Sun, Z.Y., Huang, Y.L., Jiao, S.B., Dai, W.Y., Tang, Y.Q. 2022a. Production of volatile fatty acid from fruit waste by anaerobic digestion at high organic loading rates: Performance and microbial community characteristics. *Bioresour Technol*, **346**, 126648.
- Li, C., He, P., Hao, L., Lü, F., Shao, L., Zhang, H. 2022b. Diverse acetate-oxidizing syntrophs contributing to biogas production from food waste in full-scale anaerobic digesters in China. *Renewable Energy*, **193**, 240-250.
- Li, D., Chen, L., Liu, X., Mei, Z., Ren, H., Cao, Q., Yan, Z. 2017. Instability mechanisms and early warning indicators for mesophilic anaerobic digestion of vegetable waste. *Bioresour Technol*, **245**(Pt A), 90-97.
- Li, J., Sun, D., Wu, S., Yang, W., Xiong, L., Zhang, W., Hua, M., Pan, B. 2024. Long-term and multiscale assessment of methanogenesis enhancement mechanisms in magnetite nanoparticle-mediated anaerobic digestion reactor. *Environ Res*, **262**(Pt 2), 119958.
- Li, Q., Liu, Y., Yang, X., Zhang, J., Lu, B., Chen, R. 2020a. Kinetic and thermodynamic effects of temperature on methanogenic degradation of acetate, propionate, butyrate and valerate. *Chemical Engineering Journal*, **396**.
- Li, W., Liu, Y., Wu, B., Gu, L., Deng, R. 2022c. Upgrade the high-load anaerobic digestion and relieve acid stress through the strategy of side-stream micro-aeration: biochemical performances, microbial response and intrinsic mechanisms. *Water Res*, **221**, 118850.
- Li, Y., Achinas, S., Zhao, J., Geurkink, B., Krooneman, J., Willem Euverink, G.J. 2020b. Co-digestion of cow and sheep manure: Performance evaluation and relative microbial activity. *Renewable Energy*, **153**, 553-563.
- Li, Y., Chen, Z., Peng, Y., Huang, W., Liu, J., Mironov, V., Zhang, S. 2022d. Deeper insights into the effects of substrate to inoculum ratio selection on the relationship of kinetic parameters, microbial communities, and key metabolic pathways during the anaerobic digestion of food waste. *Water Res*, **217**(118440), 118440.
- Li, Y., Li, A.M., Xu, J., Li, W.W., Yu, H.Q. 2013. Formation of soluble microbial products (SMP) by activated sludge at various salinities. *Biodegradation*, **24**(1), 69-78.

- Li, Y., Tang, Y., Xiong, P., Zhang, M., Deng, Q., Liang, D., Zhao, Z., Feng, Y., Zhang, Y. 2020c. High-efficiency methanogenesis via kitchen wastes served as ethanol source to establish direct interspecies electron transfer during anaerobic Co-digestion with waste activated sludge. *Water Research*, **176**, 115763.
- Li, Y., Xu, H., Hua, D., Zhao, B., Mu, H., Jin, F., Meng, G., Fang, X. 2020d. Two-phase anaerobic digestion of lignocellulosic hydrolysate: Focusing on the acidification with different inoculum to substrate ratios and inoculum sources. *Sci Total Environ*, **699**, 134226.
- Lim, J.H., Seo, S.W., Kim, S.Y., Jung, G.Y. 2013. Refactoring redox cofactor regeneration for high-yield biocatalysis of glucose to butyric acid in *Escherichia coli*. *Bioresour Technol*, **135**, 568-573.
- Lim, J.W., Chiam, J.A., Wang, J.Y. 2014. Microbial community structure reveals how microaeration improves fermentation during anaerobic co-digestion of brown water and food waste. *Bioresour Technol*, **171**, 132-138.
- Lin, Q., De Vrieze, J., He, G., Li, X., Li, J. 2016. Temperature regulates methane production through the function centralization of microbial community in anaerobic digestion. *Bioresour Technol*, **216**, 150-158.
- Lindner, J., Zielonka, S., Oechsner, H., Lemmer, A. 2016. Is the continuous two-stage anaerobic digestion process well suited for all substrates? *Bioresour Technol*, **200**, 470-476.
- Liu, C., Liu, D., Qi, Y., Zhang, Y., Liu, X., Zhao, M. 2016. The effect of anaerobic-aerobic and feast-famine cultivation pattern on bacterial diversity during poly-beta-hydroxybutyrate production from domestic sewage sludge. *Environ Sci Pollut Res Int*, **23**(13), 12966-12975.
- Liu, F., Wang, T., Feng, L., Chen, Y. 2025. The mechanisms of pH regulation on promoting volatile fatty acids production from kitchen waste. *J Environ Sci (China)*, **147**, 414-423.
- Liu, H., Wang, J., Liu, X., Fu, B., Chen, J., Yu, H.Q. 2012a. Acidogenic fermentation of proteinaceous sewage sludge: Effect of pH. *Water Res*, **46**(3), 799-807.
- Liu, S., Zhu, N., Li, L.Y. 2012b. The one-stage autothermal thermophilic aerobic digestion for sewage sludge treatment: stabilization process and mechanism. *Bioresour Technol*, **104**, 266-273.

- Liu, T., Malkmes, M.J., Zhu, L., Huang, H., Jiang, L. 2021. Metal-organic frameworks coupling simultaneous saccharification and fermentation for enhanced butyric acid production from rice straw under visible light by *Clostridium tyrobutyricum* CtDeltaack::cat1. *Bioresour Technol*, **332**, 125117.
- Lizama, A.C., Figueiras, C.C., Pedreguera, A.Z., Ruiz Espinoza, J.E. 2019. Enhancing the performance and stability of the anaerobic digestion of sewage sludge by zero valent iron nanoparticles dosage. *Bioresour Technol*, **275**, 352-359.
- Lu, T., Zhang, J., Wei, Y., Shen, P. 2019. Effects of ferric oxide on the microbial community and functioning during anaerobic digestion of swine manure. *Bioresour Technol*, **287**, 121393.
- Lu, Y., Zhang, Q., Wang, X., Zhou, X., Zhu, J. 2020. Effect of pH on volatile fatty acid production from anaerobic digestion of potato peel waste. *Bioresour Technol*, **316**, 123851.
- Lukitawesa, Patinvoh, R.J., Millati, R., Sarvari-Horvath, I., Taherzadeh, M.J. 2020. Factors influencing volatile fatty acids production from food wastes via anaerobic digestion. *Bioengineered*, **11**(1), 39-52.
- Luo, H., Yang, R., Zhao, Y., Wang, Z., Liu, Z., Huang, M., Zeng, Q. 2018. Recent advances and strategies in process and strain engineering for the production of butyric acid by microbial fermentation. *Bioresour Technol*, **253**, 343-354.
- Luo, J., Huang, W., Guo, W., Ge, R., Zhang, Q., Fang, F., Feng, Q., Cao, J., Wu, Y. 2020. Novel strategy to stimulate the food wastes anaerobic fermentation performance by eggshell wastes conditioning and the underlying mechanisms. *Chemical Engineering Journal*, **398**, 125560.
- Lv, N., Cai, G., Pan, X., Li, Y., Wang, R., Li, J., Li, C., Zhu, G. 2022. pH and hydraulic retention time regulation for anaerobic fermentation: Focus on volatile fatty acids production/distribution, microbial community succession and interactive correlation. *Bioresour Technol*, **347**, 126310.
- Ma, H., Chen, X., Liu, H., Liu, H., Fu, B. 2016. Improved volatile fatty acids anaerobic production from waste activated sludge by pH regulation: Alkaline or neutral pH? *Waste Manag*, **48**, 397-403.
- Ma, H., Liu, H., Zhang, L., Yang, M., Fu, B., Liu, H. 2017. Novel insight into the relationship between organic substrate composition and volatile fatty acids distribution in acidogenic co-fermentation. *Biotechnol Biofuels*, **10**, 137.

- Malaviya, A., Jang, Y.-S., Lee, S.Y. 2011. Continuous butanol production with reduced byproducts formation from glycerol by a hyper producing mutant of *Clostridium pasteurianum*. *Applied Microbiology and Biotechnology*, **93**(4), 1485-1494.
- Meng, Q., Liu, S., Guo, Y., Hu, Y., Yu, Z., Bello, A., Wang, Z., Xu, W., Xu, X. 2023. The co-occurrence network patterns and keystone species of microbial communities in cattle manure-corn straw composting. *Environ Sci Pollut Res Int*, **30**(8), 20265-20276.
- Meng, X., Cao, Q., Sun, Y., Huang, S., Liu, X., Li, D. 2022. 16S rRNA genes- and metagenome-based confirmation of syntrophic butyrate-oxidizing methanogenesis enriched in high butyrate loading. *Bioresour Technol*, **345**, 126483.
- Mikkelsen, L.H., Nielsen, P.H. 2001. Quantification of the bond energy of bacteria attached to activated sludge floc surfaces. *Water Science and Technology*, **43**(6), 67-75.
- Molaey, R., Bayrakdar, A., Sürmeli, R.Ö., Çalli, B. 2018. Anaerobic digestion of chicken manure: Mitigating process inhibition at high ammonia concentrations by selenium supplementation. *Biomass and Bioenergy*, **108**, 439-446.
- Montecchio, D., Gazzola, G., Gallipoli, A., Gianico, A., Braguglia, C.M. 2024. Medium chain Fatty acids production from Food Waste via homolactic fermentation and lactate/ethanol elongation: Electron balance and thermodynamic assessment. *Waste Manag*, **177**, 289-297.
- Montero, B., Garcia-Morales, J.L., Sales, D., Solera, R. 2010. Evolution of butyric acid and the methanogenic microbial population in a thermophilic dry anaerobic reactor. *Waste Manag*, **30**(10), 1790-1797.
- Moretto, G., Russo, I., Bolzonella, D., Pavan, P., Majone, M., Valentino, F. 2020. An urban biorefinery for food waste and biological sludge conversion into polyhydroxyalkanoates and biogas. *Water Res*, **170**, 115371.
- Morrison, D.J., Mackay, W. G., Edwards, C. A., Preston, T., Dodson, B., & Weaver, L. T. . 2006. Butyrate production from oligofructose fermentation by the human faecal flora: what is the contribution of extracellular acetate and lactate? *British Journal of Nutrition*, **96**(3), 570-577.
- Moset, V., Cerisuelo, A., Sutaryo, S., Moller, H.B. 2012. Process performance of anaerobic co-digestion of raw and acidified pig slurry. *Water Res*, **46**(16), 5019-5027.
- Motte, J.C., Trably, E., Escudié, R., Hamelin, J., Steyer, J.P., Bernet, N., Dumas, C. 2013. Total solids content: a key parameter of metabolic pathways in dry anaerobic digestion. *Biotechnology for biofuels*, **6**(1), 1-9.

- Mu, L., Wang, Y., Xu, F., Li, J., Tao, J., Sun, Y., Song, Y., Duan, Z., Li, S., Chen, G. 2023. Emerging Strategies for Enhancing Propionate Conversion in Anaerobic Digestion: A Review. *Molecules*, **28**(9), 3883.
- Muller, N., Worm, P., Schink, B., Stams, A.J., Plugge, C.M. 2010. Syntrophic butyrate and propionate oxidation processes: from genomes to reaction mechanisms. *Environ Microbiol Rep*, **2**(4), 489-499.
- Muller, T., Walter, B., Wirtz, A., Burkovski, A. 2006. Ammonium toxicity in bacteria. *Curr Microbiol*, **52**(5), 400-406.
- Nakakubo, R., Møller, H.B., Nielsen, A.M., Matsuda, J. 2008. Ammonia Inhibition of Methanogenesis and Identification of Process Indicators during Anaerobic Digestion. *Environmental Engineering Science*, **25**(10), 1487-1496.
- Nie, E., He, P., Zhang, H., Hao, L., Shao, L., Lü, F. 2021. How does temperature regulate anaerobic digestion? *Renewable and Sustainable Energy Reviews*, **150**, 111453.
- Nielsen, S.S. 2017. *Total carbohydrate by phenol-sulfuric acid method*. Springer, Cham.
- Nikitina, A.A., Kallistova, A.Y., Grouzdev, D.S., Kolganova, T.y.V., Kovalev, A.A., Kovalev, D.A., Panchenko, V., Zekker, I., Nozhevnikova, A.N., Litti, Y.V. 2022. Syntrophic Butyrate-Oxidizing Consortium Mitigates Acetate Inhibition through a Shift from Acetoclastic to Hydrogenotrophic Methanogenesis and Alleviates VFA Stress in Thermophilic Anaerobic Digestion. *Applied Sciences*, **13**(1), 173.
- Ning, X., Huang, Y., Huang, P., Ou, X., Luo, H., Bai, Z., Chen, H., Ge, X., Li, L. 2024. Effect of the inoculum mixing ratio on the anaerobic digestion of food waste: Reactor performance and microbial community. *Environmental Technology & Innovation*, **35**, 103680.
- Oh, H.J., Kim, K.-Y., Lee, K.M., Lee, S.-M., Gong, G., Oh, M.-K., Um, Y. 2019. Butyric acid production with high selectivity coupled with acetic acid consumption in sugar-glycerol mixture fermentation by *Clostridium tyrobutyricum* ATCC25755. *Journal of Industrial and Engineering Chemistry*, **75**, 44-51.
- Paiano, P., Menini, M., Zeppilli, M., Majone, M., Villano, M. 2019. Electro-fermentation and redox mediators enhance glucose conversion into butyric acid with mixed microbial cultures. *Bioelectrochemistry*, **130**, 107333.
- Pan, L., Tian, L., Wang, L. 2024. Multiomics study on co-fermentation of chemically enhanced sludge and waste activated sludge to produce volatile fatty acids under

- different temperatures and pHs. *Journal of Environmental Chemical Engineering*, **12**(4), 113081.
- Pan, X., Zhao, L., Li, C., Angelidaki, I., Lv, N., Ning, J., Cai, G., Zhu, G. 2021. Deep insights into the network of acetate metabolism in anaerobic digestion: focusing on syntrophic acetate oxidation and homoacetogenesis. *Water Res*, **190**, 116774.
- Parsy, A., Ficara, E., Mezzanotte, V., Guerreschi, A., Guyoneaud, R., Monlau, F., Sambusiti, C. 2024. Incorporating saline microalgae biomass in anaerobic digester treating sewage sludge: Impact on performance and microbial populations. *Bioresource Technology*, **397**, 130444.
- Peng, X., Zhang, S., Li, L., Zhao, X., Ma, Y., Shi, D. 2018. Long-term high-solids anaerobic digestion of food waste: Effects of ammonia on process performance and microbial community. *Bioresour Technol*, **262**, 148-158.
- Perez-Esteban, N., Tully, R., Peces, M., Dosta, J., Astals, S. 2025. Consistent acidogenic co-fermentation of waste activated sludge and food waste under thermophilic conditions. *Water Res*, **271**, 122970.
- Petrognani, C., Boon, N., Ganigué, R. 2020. Production of isobutyric acid from methanol by *Clostridium luticellarii*. *Green Chemistry*, **22**(23), 8389-8402.
- Ping, Q., Lu, X., Zheng, M., Li, Y. 2018. Effect of CaO(2) addition on anaerobic digestion of waste activated sludge at different temperatures and the promotion of valuable carbon source production under ambient condition. *Bioresour Technol*, **265**, 247-256.
- Poirier, S., Desmond-Le Quemener, E., Madigou, C., Bouchez, T., Chapleur, O. 2016. Anaerobic digestion of biowaste under extreme ammonia concentration: Identification of key microbial phylotypes. *Bioresour Technol*, **207**, 92-101.
- Pryde, S.E., Duncan, S. H., Hold, G. L., Stewart, C. S., & Flint, H. J. . 2002. The microbiology of butyrate formation in the human colon. *FEMS microbiology letters*, **217**(2), 133-139.
- PubChem. 2024. PubChem Compound Summary Vol. 2024.
<https://www.ncbi.nlm.nih.gov/pccompound/>.
- Qi, S., Wang, Z., Hu, Y., Lei, J., Zhan, X., Stengel, D.B. 2023. Selective enrichment of auto-floating microalgae for wastewater bioremediation and biofuel/bioproduct production. *Algal Research*, **69**, 102911.

- Qiu, S., Zhang, X., Xia, W., Li, Z., Wang, L., Chen, Z., Ge, S. 2023. Effect of extreme pH conditions on methanogenesis: Methanogen metabolism and community structure. *Sci Total Environ*, **877**, 162702.
- Rafieenia, R., Giroto, F., Peng, W., Cossu, R., Pivato, A., Raga, R., Lavagnolo, M.C. 2017. Effect of aerobic pre-treatment on hydrogen and methane production in a two-stage anaerobic digestion process using food waste with different compositions. *Waste Manag*, **59**, 194-199.
- Rafieenia, R., Pivato, A., Schievano, A., Lavagnolo, M.C. 2018. Dark fermentation metabolic models to study strategies for hydrogen consumers inhibition. *Bioresour Technol*, **267**, 445-457.
- Rajagopal, R., Masse, D.I., Singh, G. 2013. A critical review on inhibition of anaerobic digestion process by excess ammonia. *Bioresour Technol*, **143**, 632-641.
- Ramesh, A., Lee, D.J., Hong, S.G. 2006. Soluble microbial products (SMP) and soluble extracellular polymeric substances (EPS) from wastewater sludge. *Appl Microbiol Biotechnol*, **73**(1), 219-225.
- Raposo, F., De la Rubia, M.A., Fernández-Cegrí, V., Borja, R. 2012. Anaerobic digestion of solid organic substrates in batch mode: An overview relating to methane yields and experimental procedures. *Renewable and Sustainable Energy Reviews*, **16**(1), 861-877.
- Rebroš, M., Dolejš, I., Stloukal, R., Rosenberg, M. 2016. Butyric acid production with *Clostridium tyrobutyricum* immobilised to PVA gel. *Process Biochemistry*, **51**(6), 704-708.
- Ritchie, H., Rosado, P., Roser, M. 2023. "Energy", OurWorldInData.org. <https://ourworldindata.org/energy>.
- Roy, C.K., Hoshiko, Y., Toya, S., Maeda, T. 2022. Effect of different concentrations of sodium selenite on anaerobic digestion of waste sewage sludge. *Environmental Technology & Innovation*, **27**, 102403.
- Saini, M., Wang, Z.W., Chiang, C.J., Chao, Y.P. 2014. Metabolic engineering of *Escherichia coli* for production of butyric acid. *J Agric Food Chem*, **62**(19), 4342-4348.
- Sanchez-Ledesma, L.M., Rodríguez-Victoria, J.A., Ramírez-Malule, H. 2024. Effect of Fermentation Time, pH, and Their Interaction on the Production of Volatile Fatty Acids from Cassava Wastewater. *Water*, **16**(11), 1514.

- Santos, L.A.d., Valença, R.B., Silva, L.C.S.d., Holanda, S.H.d.B., Silva, A.F.V.d., Jucá, J.F.T., Santos, A.F.M.S. 2020. Methane generation potential through anaerobic digestion of fruit waste. *Journal of Cleaner Production*, **256**, 120389.
- Shen, L., Cheng, J., Wang, J., Cui, L., Zhang, Y., Liao, W., Liu, Z., Zhou, H., Wu, X., Li, J., Zeng, W. 2022. Comparison of extraction methods for extracellular polymeric substances (EPS) and dynamic characterization of EPS from sessile microorganisms during pyrite bioleaching. *Journal of Environmental Chemical Engineering*, **10**(3), 107922.
- Shi, C., Liu, Y., Wu, Y., Han, D., Ma, J., Li, K., Wang, K., Zhou, Y. 2022. Target and Enhance Ethanol and Butyrate Production from Anaerobic Fermentation via the pH and Organic Loading Rate Combined Strategy. *Appl Biochem Biotechnol*, **194**(12), 6367-6385.
- Shi, X., Wang, S., Wang, Z., Wu, G., Hu, Z., Zhan, X. 2024a. Ammonia-induced constraints on butyrate degradation in anaerobic digestion: Impact of ammonia levels and pH conditions, and recovery behaviour. *International Biodeterioration & Biodegradation*, **193**, 105847.
- Shi, X., Yasuda, S., Wang, Z., Hu, Y., Wu, G., Lens, P., Zhan, X. 2024b. Microbial transitions and degradation pathways driven by butyrate concentration in mesophilic and thermophilic anaerobic digestion under low hydrogen partial pressure. *Bioresour Technol*, **419**, 132012.
- Shin, H.-S., Song, Y.-C. 1995. A Model for Evaluation of Anaerobic Degradation Characteristics of Organic Waste: Focusing on Kinetics, Rate-Limiting Step. *Environmental Technology*, **16**(8), 775-784.
- Siriwongrungson, V., Zeng, R.J., Angelidaki, I. 2007. Homoacetogenesis as the alternative pathway for H₂ sink during thermophilic anaerobic degradation of butyrate under suppressed methanogenesis. *Water Res*, **41**(18), 4204-4210.
- Sitthi, S., Hatamoto, M., Watari, T., Yamaguchi, T. 2022. Accelerating anaerobic propionate degradation and studying microbial community using modified polyvinyl alcohol beads during anaerobic digestion. *Bioresour Technol*, **17**, 100907.
- Spirito, C.M., Richter, H., Rabaey, K., Stams, A.J., Angenent, L.T. 2014. Chain elongation in anaerobic reactor microbiomes to recover resources from waste. *Curr Opin Biotechnol*, **27**, 115-122.

- Stavropoulos, K.P., Kopsahelis, A., Zafiri, C., Kornaros, M. 2016. Effect of pH on Continuous Biohydrogen Production from End-of-Life Dairy Products (EoL-DPs) via Dark Fermentation. *Waste and Biomass Valorization*, **7**(4), 753-764.
- Stein, U.H., Wimmer, B., Ortner, M., Fuchs, W., Bochmann, G. 2017. Maximizing the production of butyric acid from food waste as a precursor for ABE-fermentation. *Sci Total Environ*, **598**, 993-1000.
- Sterling Jr, M.C., Lacey, R.E., Engler, C.R., Ricke, S.C. 2001. Effects of ammonia nitrogen on H₂ and CH₄ production during anaerobic digestion of dairy cattle manure. *Bioresource technology*, **77**(1), 9-18.
- Strazzeria, G., Battista, F., Garcia, N.H., Frison, N., Bolzonella, D. 2018. Volatile fatty acids production from food wastes for biorefinery platforms: A review. *J Environ Manage*, **226**, 278-288.
- Su, L., Shen, Y., Zhang, W., Gao, T., Shang, Z., Wang, M. 2017. Cofactor engineering to regulate NAD(+)/NADH ratio with its application to phytosterols biotransformation. *Microb Cell Fact*, **16**(1), 182.
- Suo, Y., Liao, Z., Qu, C., Fu, H., Wang, J. 2019. Metabolic engineering of *Clostridium tyrobutyricum* for enhanced butyric acid production from undetoxified corncob acid hydrolysate. *Bioresource Technology*, **271**, 266-273.
- Tang, F., Tian, J., Zhu, N., Lin, Y., Zheng, H., Xu, Z., Liu, W. 2022. Dry anaerobic digestion of ammoniated straw: Performance and microbial characteristics. *Bioresour Technol*, **351**, 126952.
- Tang, J., Yang, H., Pu, Y., Hu, Y., Huang, J., Jin, N., He, X., Wang, X.C. 2023. Caproic acid production from food waste using indigenous microbiota: Performance and mechanisms. *Bioresour Technol*, **387**, 129687.
- Tang, Y., Dai, X., Dong, B., Guo, Y., Dai, L. 2020. Humification in extracellular polymeric substances (EPS) dominates methane release and EPS reconstruction during the sludge stabilization of high-solid anaerobic digestion. *Water Res*, **175**, 115686.
- Tian, T., Qiao, S., Yu, C., Tian, Y., Yang, Y., Zhou, J. 2017. Distinct and diverse anaerobic respiration of methanogenic community in response to MnO(2) nanoparticles in anaerobic digester sludge. *Water Res*, **123**, 206-215.
- Tisocco, S., Beausang, C., Zhan, X., Crosson, P. 2024. Integration of anaerobic co-digestion of grass silage and cattle slurry within a livestock farming system in Ireland:

- Quantification of greenhouse gas emission reduction and nutrient flow. *Resources, Conservation and Recycling*, **206**, 107650.
- Tiwari, B.R., Rouissi, T., Brar, S.K., Surampalli, R.Y. 2021. Critical insights into psychrophilic anaerobic digestion: Novel strategies for improving biogas production. *Waste Manag*, **131**, 513-526.
- Vázquez-Fernández, A., Suárez-Ojeda, M.E., Carrera, J. 2022. Review about bioproduction of Volatile Fatty Acids from wastes and wastewaters: Influence of operating conditions and organic composition of the substrate. *Journal of Environmental Chemical Engineering*, **10**(3), 107917.
- Venkata Mohan, S., Nikhil, G.N., Chiranjeevi, P., Nagendranatha Reddy, C., Rohit, M.V., Kumar, A.N., Sarkar, O. 2016. Waste biorefinery models towards sustainable circular bioeconomy: Critical review and future perspectives. *Bioresour Technol*, **215**, 2-12.
- Villar, E., Farrant, G.K., Follows, M., Garczarek, L., Speich, S., Audic, S. 2015. Environmental characteristics of Agulhas rings affect interocean plankton transport. *Science*, **248**(6237), 1261447.
- Vital, M., Howe, A.C., Tiedje, J.M. 2014. Revealing the bacterial butyrate synthesis pathways by analyzing (meta)genomic data. *mBio*, **5**(2), e00889.
- Vital, M., Karch, A., Pieper, D.H. 2017. Colonic butyrate-producing communities in humans: an overview using omics data. *mSystems*, **2**(6), 10-28.
- Wang, C., Nakakoji, S., Ng, T.C.A., Zhu, P., Tsukada, R., Tatara, M., Ng, H.Y. 2023a. Acclimatizing waste activated sludge in a thermophilic anaerobic fixed-bed biofilm reactor to maximize biogas production for food waste treatment at high organic loading rates. *Water Res*, **242**, 120299.
- Wang, F., Hidaka, T., Tsuno, H., Tsubota, J. 2012. Co-digestion of polylactide and kitchen garbage in hyperthermophilic and thermophilic continuous anaerobic process. *Bioresour Technol*, **112**, 67-74.
- Wang, K., Yin, J., Shen, D., Li, N. 2014. Anaerobic digestion of food waste for volatile fatty acids (VFAs) production with different types of inoculum: effect of pH. *Bioresour Technol*, **161**, 395-401.
- Wang, L., Chauliac, D., Moritz, B.E., Zhang, G., Ingram, L.O., Shanmugam, K.T. 2019. Metabolic engineering of *Escherichia coli* for the production of butyric acid at high titer and productivity. *Biotechnol Biofuels*, **12**, 62.

- Wang, M., Chen, H., Chang, S. 2024. Investigation of volatile fatty acids production in biological hydrolysis of waste activated sludge via microbial community network and fermentation pathway analyses. *Journal of Environmental Chemical Engineering*, **12**(2), 112056.
- Wang, N., Yuan, T., Ko, J.H., Shi, X., Xu, Q. 2020a. Enhanced syntrophic metabolism of propionate and butyrate via nickel-containing activated carbon during anaerobic digestion. *Journal of Material Cycles and Waste Management*, **22**(5), 1529-1538.
- Wang, Q., Jiang, J., Zhang, Y., Li, K. 2015. Effect of initial total solids concentration on volatile fatty acid production from food waste during anaerobic acidification. *Environ Technol*, **36**(13-16), 1884-1891.
- Wang, Q., Kuninobu, M., Ogawa, H.I., Kato, Y. 1999. Degradation of volatile fatty acids in highly efficient anaerobic digestion. *Biomass and Bioenergy*, **16**(6), 407-416.
- Wang, Q., Zhang, G., Chen, L., Yang, N., Wu, Y., Fang, W., Zhang, R., Wang, X., Fu, C., Zhang, P. 2023b. Volatile fatty acid production in anaerobic fermentation of food waste saccharified residue: Effect of substrate concentration. *Waste Manag*, **164**, 29-36.
- Wang, S., Hu, Y., Hu, Z., Wu, W., Wang, Z., Jiang, Y., Zhan, X. 2021a. Improved reduction of antibiotic resistance genes and mobile genetic elements from biowastes in dry anaerobic co-digestion. *Waste Manag*, **126**, 152-162.
- Wang, S., Ruan, Y., Zhou, W., Li, Z., Wu, J., Liu, D. 2018. Net energy analysis of small-scale biogas self-supply anaerobic digestion system operated at psychrophilic to thermophilic conditions. *Journal of Cleaner Production*, **174**, 226-236.
- Wang, X., Chen, T., Gao, C., Xie, Y., Zhang, A. 2022a. Use of extracellular polymeric substances as natural redox mediators to enhance denitrification performance by accelerating electron transfer and carbon source metabolism. *Bioresour Technol*, **345**, 126522.
- Wang, Y., Zhang, Y., Wang, J., Meng, L. 2009. Effects of volatile fatty acid concentrations on methane yield and methanogenic bacteria. *Biomass and Bioenergy*, **33**(5), 848-853.
- Wang, Z., Hu, Y., Wang, S., Wu, G., Zhan, X. 2023c. A critical review on dry anaerobic digestion of organic waste: Characteristics, operational conditions, and improvement strategies. *Renewable and Sustainable Energy Reviews*, **176**, 113208.

- Wang, Z., Jiang, Y., Wang, S., Zhang, Y., Hu, Y., Hu, Z.H., Wu, G., Zhan, X. 2020b. Impact of total solids content on anaerobic co-digestion of pig manure and food waste: Insights into shifting of the methanogenic pathway. *Waste Manag*, **114**, 96-106.
- Wang, Z., Wang, S., Hu, Y., Du, B., Meng, J., Wu, G., Liu, H., Zhan, X. 2022b. Distinguishing responses of acetoclastic and hydrogenotrophic methanogens to ammonia stress in mesophilic mixed cultures. *Water Res*, **224**, 119029.
- Wang, Z., Wang, T., Si, B., Watson, J., Zhang, Y. 2021b. Accelerating anaerobic digestion for methane production: Potential role of direct interspecies electron transfer. *Renewable and Sustainable Energy Reviews*, **145**, 111069.
- Wu, D., Li, L., Zhen, F., Liu, H., Xiao, F., Sun, Y., Peng, X., Li, Y., Wang, X. 2022. Thermodynamics of volatile fatty acid degradation during anaerobic digestion under organic overload stress: The potential to better identify process stability. *Water Res*, **214**, 118187.
- Wu, Q., Bao, X., Guo, W., Wang, B., Li, Y., Luo, H., Wang, H., Ren, N. 2019. Medium chain carboxylic acids production from waste biomass: Current advances and perspectives. *Biotechnol Adv*, **37**(5), 599-615.
- Wu, W.-M., Jain, M.K., Hickey, R.F., Zeikus, J.G. 2000. Perturbation of syntrophic isobutyrate and butyrate degradation with formate and hydrogen. *Biotechnology and Bioengineering*, **52**(3), 404-411.
- Xie, L., Wei, X., Zhou, X., Meng, D., Zhou, R., Zhang, Y.P.J., Xu, S., You, C. 2018. Conversion of d-glucose to l-lactate via pyruvate by an optimized cell-free enzymatic biosystem containing minimized reactions. *Synth Syst Biotechnol*, **3**(3), 204-210.
- Xing, T., Wang, Z., Zhen, F., Liu, H., Wo, D., Li, L., Guo, Y., Kong, X., Sun, Y. 2022. Initial pH-driven production of volatile fatty acid from hybrid Pennisetum. *Bioresour Technol*, **347**, 126426.
- Xu, H., Gong, S., Sun, Y., Ma, H., Zheng, M., Wang, K. 2015. High-rate hydrogenotrophic methanogenesis for biogas upgrading: the role of anaerobic granules. *Environ Technol*, **36**(1-4), 529-537.
- Xu, S.Y., Karthikeyan, O.P., Selvam, A., Wong, J.W. 2012. Effect of inoculum to substrate ratio on the hydrolysis and acidification of food waste in leach bed reactor. *Bioresour Technol*, **126**, 425-430.

- Xu, Y., Meng, X., Song, Y., Lv, X., Sun, Y. 2023. Effects of different concentrations of butyrate on microbial community construction and metabolic pathways in anaerobic digestion. *Bioresour Technol*, **377**, 128845.
- Yadav, M., Joshi, C., Paritosh, K., Thakur, J., Pareek, N., Masakapalli, S.K., Vivekanand, V. 2022. Reprint of Organic waste conversion through anaerobic digestion: A critical insight into the metabolic pathways and microbial interactions. *Metab Eng*, **71**, 62-76.
- Yang, K., Yu, Y., Hwang, S. 2003. Selective optimization in thermophilic acidogenesis of cheese-whey wastewater to acetic and butyric acids: partial acidification and methanation. *Water Research*, **37**(10), 2467-2477.
- Yang, Y., Liu, C., Zhao, W., Mazarji, M., Ren, L., Liu, C., Pan, J., Yan, B. 2024. Anaerobic propionic acid production via succinate pathway at extremely low pH. *Chemical Engineering Journal*, **486**, 150190.
- Yellezuome, D., Zhu, X., Wang, Z., Liu, R. 2022. Mitigation of ammonia inhibition in anaerobic digestion of nitrogen-rich substrates for biogas production by ammonia stripping: A review. *Renewable and Sustainable Energy Reviews*, **157**, 112043.
- Yenigün, O., Demirel, B. 2013. Ammonia inhibition in anaerobic digestion: A review. *Process Biochemistry*, **48**(5-6), 901-911.
- Yi, Y., Wang, H., Chen, Y., Gou, M., Xia, Z., Hu, B., Nie, Y., Tang, Y. 2020. Identification of Novel Butyrate- and Acetate-Oxidizing Bacteria in Butyrate-Fed Mesophilic Anaerobic Chemostats by DNA-Based Stable Isotope Probing. *Microb Ecol*, **79**(2), 285-298.
- Yin, D.M., Mahboubi, A., Wainaina, S., Qiao, W., Taherzadeh, M.J. 2021. The effect of mono- and multiple fermentation parameters on volatile fatty acids (VFAs) production from chicken manure via anaerobic digestion. *Bioresour Technol*, **330**, 124992.
- Yin, J., Yu, X., Wang, K., Shen, D. 2016. Acidogenic fermentation of the main substrates of food waste to produce volatile fatty acids. *International Journal of Hydrogen Energy*, **41**(46), 21713-21720.
- Yin, Q., Yang, S., Wang, Z., Xing, L., Wu, G. 2018. Clarifying electron transfer and metagenomic analysis of microbial community in the methane production process with the addition of ferrous oxide. *Chemical Engineering Journal*, **333**, 216-225.
- Yin, Y., Zhang, Z., Yang, K., Gu, P., Liu, S., Jia, Y., Zhang, Z., Wang, T., Yin, J., Miao, H. 2022. Deeper insight into the effect of salinity on the relationship of enzymatic

- activity, microbial community and key metabolic pathway during the anaerobic digestion of high strength organic wastewater. *Bioresour Technol*, **363**, 127978.
- Yu, H.Q., Fang, H.H. 2003. Acidogenesis of gelatin-rich wastewater in an upflow anaerobic reactor: influence of pH and temperature. *Water research*, **37**(1), 55-66.
- Yu, H.Q., Fang, H.H.P. 2002. Acidogenesis of dairy wastewater at various pH levels. *Water Science and Technology*, **42**(10), 201-206.
- Yu, P., Tu, W., Wu, M., Zhang, Z., Wang, H. 2021. Pilot-scale fermentation of urban food waste for volatile fatty acids production: The importance of pH. *Bioresour Technol*, **332**, 125116.
- Zeller, G., Tap, J., Voigt, A.Y., Sunagawa, S., Kultima, J.R., Costea, P.I., Amiot, A., Bohm, J., Brunetti, F., Habermann, N., Hercog, R., Koch, M., Luciani, A., Mende, D.R., Schneider, M.A., Schrotz-King, P., Tournigand, C., Tran Van Nhieu, J., Yamada, T., Zimmermann, J., Benes, V., Kloor, M., Ulrich, C.M., von Knebel Doeberitz, M., Sobhani, I., Bork, P. 2014. Potential of fecal microbiota for early-stage detection of colorectal cancer. *Mol Syst Biol*, **10**(11), 766.
- Zeng, Y., Liu, H., Chen, W., Li, H., Dong, H., Wu, H., Xu, H., Sun, D., Liu, X., Li, P., Qiu, B., Dang, Y. 2024. Riboflavin-loaded carbon cloth aids the anaerobic digestion of cow dung by promoting direct interspecies electron transfer. *Environ Res*, **241**, 117660.
- Zhang, C., Yang, H., Yang, F., Ma, Y. 2009. Current progress on butyric acid production by fermentation. *Curr Microbiol*, **59**(6), 656-63.
- Zhang, L., Loh, K.C., Kuroki, A., Dai, Y., Tong, Y.W. 2021a. Microbial biodiesel production from industrial organic wastes by oleaginous microorganisms: Current status and prospects. *J Hazard Mater*, **402**, 123543.
- Zhang, L., Loh, K.C., Sarvanantharajah, S., Tong, Y.W., Wang, C.H., Dai, Y. 2019. Mesophilic and thermophilic anaerobic digestion of soybean curd residue for methane production: Characterizing bacterial and methanogen communities and their correlations with organic loading rate and operating temperature. *Bioresour Technol*, **288**, 121597.
- Zhang, Q., Lu, Y., Zhou, X., Wang, X., Zhu, J. 2020. Effect of different vegetable wastes on the performance of volatile fatty acids production by anaerobic fermentation. *Sci Total Environ*, **748**, 142390.

- Zhang, W., Heaven, S., Banks, C.J. 2017. Thermophilic Digestion of Food Waste by Dilution: Ammonia Limit Values and Energy Considerations. *Energy & Fuels*, **31**(10), 10890-10900.
- Zhang, Y., Jiang, Y., Wang, S., Wang, Z., Liu, Y., Hu, Z., Zhan, X. 2021b. Environmental sustainability assessment of pig manure mono- and co-digestion and dynamic land application of the digestate. *Renewable and Sustainable Energy Reviews*, **137**, 112043.
- Zhang, Y., Jing, Z., Feng, Y., Chen, S., Li, Y., Han, Y., Feng, L., Pan, J., Mazarji, M., Zhou, H., Wang, X., Xu, C. 2023a. Using automated machine learning techniques to explore key factors in anaerobic digestion: At the environmental factor, microorganisms and system levels. *Chemical Engineering Journal*, **475**, 146069.
- Zhang, Y., Li, C., Yuan, Z., Wang, R., Angelidaki, I., Zhu, G. 2023b. Syntrophy mechanism, microbial population, and process optimization for volatile fatty acids metabolism in anaerobic digestion. *Chemical Engineering Journal*, **452**, 139137.
- Zhang, Y., Li, J., Meng, J., Wang, X. 2021c. A cathodic electro-fermentation system for enhancing butyric acid production from rice straw with a mixed culture. *Sci Total Environ*, **767**, 145011.
- Zhao, W., Yan, B., Ren, Z.J., Wang, S., Zhang, Y., Jiang, H. 2022. Highly selective butyric acid production by coupled acidogenesis and ion substitution electrodialysis. *Water Res*, **226**, 119228.
- Zheng, M., Zheng, M., Wu, Y., Ma, H., Wang, K. 2015. Effect of pH on types of acidogenic fermentation of fruit and vegetable wastes. *Biotechnology and Bioprocess Engineering*, **20**(2), 298-303.
- Zhou, M., Yan, B., Wong, J.W.C., Zhang, Y. 2018. Enhanced volatile fatty acids production from anaerobic fermentation of food waste: A mini-review focusing on acidogenic metabolic pathways. *Bioresour Technol*, **248**(Pt A), 68-78.
- Zhu, Y., Yang, S.T. 2003. Adaptation of *Clostridium tyrobutyricum* for enhanced tolerance to butyric acid in a fibrous-bed bioreactor. *Biotechnol Prog*, **19**(2), 365-372.
- Zhu, Y., Yang, S.T. 2004. Effect of pH on metabolic pathway shift in fermentation of xylose by *Clostridium tyrobutyricum*. *J Biotechnol*, **110**(2), 143-57.
- Ziels, R.M., Nobu, M.K., Sousa, D.Z. 2019. Elucidating Syntrophic Butyrate-Degrading Populations in Anaerobic Digesters Using Stable-Isotope-Informed Genome-Resolved Metagenomics. *mSystems*, **4**(4), e00159-19.

Zigová, J.Š.E. 2000. Advances in biotechnological production of butyric acid. *Journal of Industrial Microbiology & Biotechnology*, **24**, 153-160.